BEHAVIORS OF POLYLACTIDE BIOCOMPOSITES REINFORCED WITH MICROCRYSTALLINE CELLULOSE

A THESIS SUBMITTED TO
THE GRADUATE SCHOOL OF NATURAL AND APPLIED SCIENCES
OF
MIDDLE EAST TECHNICAL UNIVERSITY

BY

BERK DOĞU

IN PARTIAL FULFILLMENT OF THE REQUIREMENTS
FOR
THE DEGREE OF MASTER OF SCIENCE
IN
METALLURGICAL AND MATERIALS ENGINEERING

AUGUST 2015

Approval of the thesis:

BEHAVIORS OF POLYLACTIDE BIOCOMPOSITES REINFORCED WITH MICROCRYSTALLINE CELLULOSE

submitted by **BERK DOĞU** in partial fulfillment of the requirements for the degree of **Master of Science in Metallurgical and Materials Engineering Department, Middle East Technical University** by,

Prof. Dr. Gülbin Dural Ünver
Dean, Graduate School of **Natural and Applied Sciences** _____

Prof. Dr. C. Hakan Gür
Head of Department, **Metallurgical and Materials Eng.** _____

Prof. Dr. Cevdet Kaynak
Supervisor, **Metallurgical and Materials Eng. Dept.** _____

Examining Committee Members:

Prof. Dr. Tayfur Öztürk
Metallurgical and Materials Engineering Dept., METU _____

Prof. Dr. Cevdet Kaynak
Metallurgical and Materials Engineering Dept., METU _____

Prof. Dr. C. Hakan Gür
Metallurgical and Materials Engineering Dept., METU _____

Assoc. Prof. Dr. Y. Eren Kalay
Metallurgical and Materials Engineering Dept., METU _____

Assist. Prof. Dr. Kazım Tur
Metallurgical and Materials Eng. Dept., Atılım University _____

DATE: 07.08.2015

I hereby declare that all information in this document has been obtained and presented in accordance with academic rules and ethical conduct. I also declare that, as required by these rules and conduct, I have fully cited and referenced all material and results that are not original to this work.

Name, Last Name : Berk Doğu

Signature :

ABSTRACT

BEHAVIORS OF POLYLACTIDE BIOCOMPOSITES REINFORCED WITH MICROCRYSTALLINE CELLULOSE

Doğu, Berk
M. S., Department of Metallurgical and Materials Engineering
Supervisor: Prof. Dr. Cevdet Kaynak
August 2015, 90 pages

The purpose of the first part of this thesis was to investigate the effects of microcrystalline cellulose (MCC) content on the properties of polylactide (PLA) biocomposites; including the influences of maleic anhydride (MA) grafted PLA copolymer (PLA-g-MA) compatibilization. PLA/MCC biocomposites were produced by industrially compatible production techniques, i.e. twin-screw extrusion melt-mixing for compounding and injection molding for shaping of bulk specimens. SEM analysis and mechanical tests indicated that use of 3 wt% MCC resulted in very uniform distribution and consequently improved properties especially in terms of ductility and toughness. For instance, compared to neat PLA, the increases in the values of %strain at break and fracture toughness were 78% and 31%, respectively. After MA compatibilization, these increases became as much as 82% and 55%, respectively. Moreover, DSC and TGA indicated that use of MCC resulted in no significant changes in the transition temperatures and thermal degradation temperatures of PLA.

The purpose of the second part of this thesis was to reveal effects of accelerated weathering in neat PLA and its 3 wt% MCC biocomposite. Weathering conditions were applied via consecutive steps of UV irradiation and humidity in accordance with ISO 4892-3 standards for 200 hours. Various characterization techniques and mechanical tests indicated that photolysis, photo-oxidation and hydrolysis were the main degradation mechanisms leading to significant decrease in the molecular weight of PLA via main chain scission. Consequently, except elastic modulus other mechanical properties; strength, ductility and fracture toughness of PLA and PLA/MCC decreased substantially. However, after comparing the mechanical properties of the neat PLA and PLA/MCC biocomposite specimens having 200 h of accelerated weathering, it was concluded that; for the outdoor applications use of PLA/MCC biocomposite (with only 3 wt% MCC) was extremely beneficial compared to using neat PLA.

Keywords: Polylactide, Microcrystalline Cellulose, Biocomposite, Maleic Anhydride, Interfacial Compatibilization, Accelerated Weathering

ÖZ

MİKROKRİSTAL SELÜLOZ TAKVİYELİ POLİLAKTİT
BİYOKOMPOZİTLERİN DAVRANIŞLARI

Doğu, Berk
Yüksek Lisans, Metalürji ve Malzeme Mühendisliği Bölümü
Tez Yöneticisi: Prof. Dr. Cevdet Kaynak
Ağustos 2015, 90 sayfa

Bu tez çalışmasının birinci bölümünün amacı mikrokristal selüloz (MCC) miktarının polilaktit (PLA) biyokompozitlerinin özellikleri üzerindeki etkisini incelemektir. Bu bölüm maleik anhidrat (MA) ile graft edlmiş PLA kopolimer (PLA-g-MA) uyumlaştırmasının etkilerini de içermektedir. PLA/MCC biyokompozitleri endüstriyel teknikler ile uyumlu yöntemler ile üretilmiştir. Kompaundlama için çift vidalı ekstrüder ile eriyik karıştırma tekniği, numunelerin şekillendirilmesi için de enjeksiyon kalıplama tekniği kullanılmıştır. SEM analizi ve mekanik testler ağırlıkça %3 MCC kullanımının oldukça homojen bir dağılıma ve bunun sonucu olarak da özellikle süneklik ve tokluk değerleri olmak üzere mekanik özelliklerde iyileşmelere neden olduğunu göstermiştir. Örneğin, saf PLA ile karşılaştırıldığında, kırılmadaki %uzama ve kırılma tokluğu değerlerindeki artışlar sırasıyla %78 ve %31 oranlarındadır. MA uyumlaştırmasından sonra, bu artışlar %82 ve %55 oranlarına ulaşmıştır. Ayrıca, DSC ve TGA analizleri MCC kullanımının PLA'nın ısıl dönüşüm ve ısıl bozunum sıcaklıklarında önemli değişimlere neden olmadığını da göstermiştir.

Bu çalışmanın ikinci bölümünün amacı ise hızlandırılmış atmosferik yaşlandırmanın saf PLA ve onun ağırlıkça %3 MCC biyokompozit numuneleri üzerindeki etkilerini araştırmaktır. Atmosferik yaşlandırma koşulları, ISO 4892-3 standartları ile uyumlu olan ardışık UV radyasyonu ve nem döngüleri ile 200 saat boyunca uygulanmıştır. Çeşitli karakterizasyon teknikleri ve mekanik testler temel bozunum mekanizmalarının fotoliz, foto-oksidasyon ve hidroliz olduğunu; ve bu mekanizmaların ana zincir yapısındaki kesilmeler nedeniyle PLA'nın molekül ağırlığında önemli azalmalara yol açtığını göstermiştir. Bunun sonucunda, PLA ve PLA/MCC biyokompozit numunelerinin elastik modül dışındaki diğer mekanik özellikleri; mukavemet, süneklik ve kırılma tokluğu değerleri oldukça azalmıştır. Ancak, 200 saat hızlandırılmış atmosferik yaşlandırmaya maruz kalan PLA ve PLA/MCC numunelerinin mekanik özellikleri karşılaştırıldığında, atmosferik koşullara maruz kalan uygulamalar için, yalnızca %3 MCC içeren PLA/MCC biyokompozit kullanımının saf PLA kullanımına göre oldukça yararlı olduğu sonucuna varılmıştır.

Anahtar Kelimeler: Polilaktit, Mikrokristal Selüloz, Biyokompozit, Maleik Anhidrat, Arayüzey Uyumlaştırması, Hızlandırılmış Atmosferik Yaşlandırma

to my lovely family

ACKNOWLEDGEMENTS

I would like to thank to my supervisor Prof. Dr. Cevdet Kaynak for his valuable advice, guidance and patience at each stage of this thesis.

I would like to gratefully acknowledge financial support from METU Scientific Research Fund grant for the Project BAP-03-08-2015-002.

I would like to acknowledge administrative board of the Metallurgical and Materials Engineering Department for supplying all the research facilities required in this dissertation and all the technical staff of the department especially Serkan Yılmaz and Önder Şahin. I would also like to thank to METU Central Laboratory for SLS analyses.

I want to thank my laboratory mates, Ali Rıza Erdoğan, Burcu Sarı, Yelda Meyva and Deniz Varsavaş for their friendship and support.

My special thanks go to Erman Aksüt, İbrahim Kurtulan, Burak Şancı, Merve Yenigün, Seda Özdemir, Irmak Ece Şener, Mertcan Başkan, Lütfi Ağartan and Gökçe Öztürk and my love Özlem Şenöz for helping me get through the hard time, and for all the support and entertainment.

I would like to express my deepest thankfulness to my mother Füsun Doğu, my father Kemal Doğu and my brother Burak Doğu. They have been a constant love and encouragement in each step of my life from childhood to adulthood. This dissertation would certainly be not possible without their support.

TABLE OF CONTENTS

ABSTRACT ..... **vii**
ÖZ ..... **ix**
ACKNOWLEDGEMENTS ..... **xii**
TABLE OF CONTENTS ..... **xiii**
LIST OF TABLES ..... **xv**
LIST OF FIGURES ..... **xvii**
NOMENCLATURE ..... **xix**
CHAPTERS **1**
1. INTRODUCTION **1**
1.1 Polylactide 1
1.2 Cellulose 4
1.3 Polylactide/Natural Fiber Biocomposites 11
1.4 Weathering Behavior of PLA 13
1.5 Literature Survey 18
1.5.1 Studies on the Behavior of PLA/MCC Biocomposites 18
1.5.2 Studies on the Interfacial Compatibilization of the PLA/MCC Biocomposites 19
1.5.3 Studies on the Accelerated Weathering Behavior of PLA based Biocomposites 20
1.6 Purpose of the Study 21
2. EXPERIMENTAL WORK 23
2.1 Materials Used 23
2.2 Production of PLA/MCC Biocomposites 25
2.3 Production of PLA/gMA/MCC Biocomposite 26
2.4 Characterization by FTIR and SEM 27
2.5 Mechanical Tests and Thermal Analyses 27

2.6 Accelerated Weathering of the Neat PLA and its PLA/MCC Biocomposite .. 28
2.7 Analyses for the Changes in the Crystallinity of PLA Matrix 29
2.8 Analyses for the Changes in the Color of the Specimens..... 29
2.9 Analyses for the Changes in the Chemical Structure of the Specimens..... 30
2.10 Analyses for the Changes in the Morphology, Mechanical Properties and Thermal Behavior of Specimens 30
3. RESULTS AND DISCUSSION..... 31
3.1 Effects of MCC Content and MA Compatibilization..... 31
3.1.1 Infrared Spectroscopy of the PLA/MCC Biocomposites..... 31
3.1.2 Fracture Surface Morphology of the PLA/MCC Biocomposites..... 34
3.1.3 Modulus and Strength of the PLA/MCC Biocomposites..... 37
3.1.4 Ductility and Toughness of the PLA/MCC Biocomposites..... 41
3.1.5 Thermal Properties of the PLA/MCC Biocomposites..... 43
3.2 Effects of Accelerated Weathering..... 48
3.2.1 Changes in the Crystallinity..... 48
3.2.2 Changes in the Color..... 51
3.2.3 Changes in the Chemical Structure..... 54
3.2.4 Changes in the Morphology..... 58
3.2.5 Changes in Mechanical Properties..... 61
3.2.6 Changes in Thermal Properties..... 71
4. CONCLUSIONS..... 77
REFERENCES..... 81

LIST OF TABLES

TABLES

Table 1.1 Mechanical properties of crsyalline cellulose [6]……..…….....7

Table 1.2 Thermal properties of crystalline cellulose [6]……7

Table 1.3 Chemical composition of several natural fibers [15]……..……...12

Table 3.1 Tensile Modulus (E), Flexural Modulus (E_{Flex}), Tensile Strength (σ_{TS}) an Flexural Strength (σ_{Flex}) of the Specimens……..……...39

Table 3.2 Tensile Strain at Break (ε_f) and Fracture Toughness (K_{IC} and G_{IC}) of the Specimens……..……....42

Table 3.3 Transition Temperatures (T_g , T_c , T_m), Enthalpies (ΔH_m , ΔH_c) and Crystallinity Percent (X_C) of the Specimens During First Heating……..……...45

Table 3.4 Thermal degradation temperatures ($T_{5\%}$, $T_{10\%}$,$T_{25\%}$) of the specimens at 5, 10 and 25 wt% mass losses and the maximum mass loss temperature (T_{max})…….……..46

Table 3.5 CIELAB color space parameters (L^*, a^*, b^*) and color change difference (ΔE^*) values of the neat PLA and its 3 wt% MCC biocomposite specimens before and after each accelerated weathering period…….……....53

Table 3.6 Tensile Modulus (E), Flexural Modulus (E_{Flex}), Tensile Strength (σ_{TS}) and Flexural Strength (σ_{Flex}) of the neat PLA and its 3 wt% MCC biocomposite specimens before and after each accelerated weathering period…….……...64

Table 3.7 Tensile Strain at Break (ε_f) and Fracture Toughness (K_{IC} and G_{IC}) of the neat PLA and its 3 wt% MCC biocomposite specimens before and after each accelerated weathering period…….……68

Table 3.8 Comparison of the mechanical properties of the PLA-200h and PLA/MCC-200h specimens with benefits of the biocomposite specimen in terms of "Δ benefit" (increase in the values) and "% benefit" (percent increase in the values)…….....70

Table 3.9 Transition temperatures (T_g, T_c, T_m), enthalpies (ΔH_m, ΔH_c) and crystallinity percent (X_C) of the neat PLA and its 3 wt% MCC biocomposite specimens before and after each accelerated weathering period obtained during first heating DSC profile……73
Table 3.10 Thermal degradation temperatures ($T_{5\%}$, $T_{10\%}$,$T_{25\%}$) of the neat PLA and its 3 wt% MCC biocomposite specimens at 5, 10 and 25 wt% mass losses and the maximum mass loss temperature (T_{max}) before and after each accelerated weathering period……..……75

LIST OF FIGURES

FIGURES

Figure 1.1 Chemical structure of PLA [2]……..…..1

Figure 1.2 Stereo forms of lactide [1]…….…2

Figure 1.3 Schematic of PLA productions via prepolymer and lactide [3]….....3

Figure 1.4 The structure of cellulose: 1—4 linkage of β glucose monomers [6].....5

Figure 1.5 Crystal structures of α and β cellulose [7]……....6

Figure 1.6 Hierarchical structure of wood [8]……8

Figure 1.7 Location and extraction of nano crystalline cellulose [9]……9

Figure 1.8 MFC micrographs after high-pressure mechanical treatment (left) and TEMPO-mediated oxidation (right) [11, 12]…….……10

Figure 1.9 Transmission electron microcopy images of cellulose nanocrystals [13, 14]……...11

Figure 1.10 Possible photodegradation reaction of PLA [16]……..…....14

Figure 1.11 Reaction schemes for the photolysis [17]……...15

Figure 1.12 Reaction schemes for the photooxidation[17]……...16

Figure 1.13 Possible hydrolysis reaction of PLA [18]……..17

Figure 2.1 General and closer view SEM images showing the diameter and length ranges of MCC used…….…..24

Figure 2.2 X-ray diffractogram of MCC used.....25

Figure 3.1 ATR-FTIR spectra of PLA and its biocomposites …….32

Figure 3.2 SEM fractographs showing dispersion state of MCCs in PLA matrix…35

Figure 3.3 SEM fractographs showing interfacial morphology between the PLA matrix and MCC fillers……...36

Figure 3.4 Stress-Strain curves of the specimens obtained during tensile and 3-point bending flexural tests……..38

Figure 3.5 Effects of MCC content and MA compatibilization on the mechanical properties of the specimens (note that gMA in the x –axes denotes PLA/gMA/MCC 3 specimens)..... 40

Figure 3.6 First heating DSC thermograms of the specimens ……..44
Figure 3.7 Thermogravimetric curves of the specimens 47
Figure 3.8 X-ray diffractograms of the specimens before and after each accelerated weathering period: (a) neat PLA, (b) PLA/MCC biocomposite 49
Figure 3.9 Photographic images showing slight changes in the color of the neat PLA and its MCC biocomposite specimens after each accelerated weathering period..... 52
Figure 3.10 Drastic decrease in the weight average molecular weight of the PLA matrix after each accelerated weathering period..... 54
Figure 3.11 FTIR-ATR spectra of the specimens before and after each accelerated weathering period: (a) neat PLA, (b) PLA/MCC biocomposite 56
Figure 3.12 SEM images showing fracture surface morphology of the specimens before and after each accelerated weathering period: (a) neat PLA, (b) PLA/MCC biocomposite 59
Figure 3.13 Tensile stress-strain curves of the neat PLA and its MCC biocomposite specimens before and after each accelerated weathering period..... 60
Figure 3.14 Flexural stress-strain curves of the neat PLA and its MCC biocomposite specimens before and after each accelerated weathering period..... 62
Figure 3.15 Effects of each accelerated weathering period on the mechanical properties of the specimens: (a) neat PLA, (b) PLA/MCC biocomposite 64
Figure 3.16 First heating DSC thermograms of the neat PLA and its MCC biocomposite specimens before and after each accelerated weathering period 72
Figure 3.17 Thermogravimetric curves of the neat PLA and its MCC biocomposite specimens before and after each accelerated weathering period..... 76

NOMENCLATURE

2θ	:	XRD diffraction angle
σ_{TS}	:	tensile strength
σ_{Flex}	:	flexural strength
ε_f	:	elongation at break, final strain
ΔH_m	:	melting enthalpy of the specimens
ΔH_c	:	crystallization enthalpy of the specimens
$\Delta H_m°$	:	melting enthalpy of 100% crystalline PLA
E	:	tensile modulus
E_A	:	tensile modulus in axial direction
E_{Flex}	:	flexural modulus
E_T	:	tensile modulus in transverse direction
$G_{ıc}$	:	fracture toughness as critical strain energy release rate
$K_{ıc}$	:	fracture toughness as critical stress intensity factor
$T_{5wt\%}$	:	thermal degradation temperature at 5 wt% mass loss
$T_{10wt\%}$	:	thermal degradation temperature at 10 wt% mass loss
$T_{25wt\%}$	:	thermal degradation temperature at 25 wt% mass loss
T_c	:	cold crystallization temperature
T_g	:	glass transition temperature
T_m	:	melting temperature
T_{max}	:	thermal degradation temperature at maximum mass loss rate
X_c	:	degree of crystallinity
w_{PLA}	:	weight fraction of PLA

ATR-FTIR	**:**	attenuated total reflectance-Fourier transform infrared spectroscopy
DRA	**:**	diffused reflectance analysis
DSC	**:**	differential scanning calorimetry
MA	**:**	maleic anhydride
MCC	**:**	microcrystalline cellulose
MFI	**:**	melt flow index
PLA	**:**	poly(lactic acid) or polylactide
PLLA	**:**	L-enantiomer of polylactide
PDLA	**:**	D-enantiomer of polylactide
PLA-g-MA	**:**	maleic anhydride grafted polylactide
SEM	**:**	scanning electron microscopy
SLS	**:**	static light scattering spectroscopy
TGA	**:**	thermogravimetric analysis
XRD	**:**	X-ray diffraction

CHAPTER 1

INTRODUCTION

1.1 Polylactide

The overall production of most of petroleum-based synthetic polymers is approximately around 140 million tons per year and they remain as a waste in the ecosystem after usage because of their resistances against microbial attacks. Therefore, biopolymers have a vital role for biodegradable replacement. Natural biodegradable biopolymers are produced from renewable resources such as starch, chips or sugarcane. One of the most promising natural biodegradable biopolymer is poly(lactic acid) or simply called as polylactide (PLA) [1]. The chemical structure of PLA with end groups is shown in Figure 1.1.

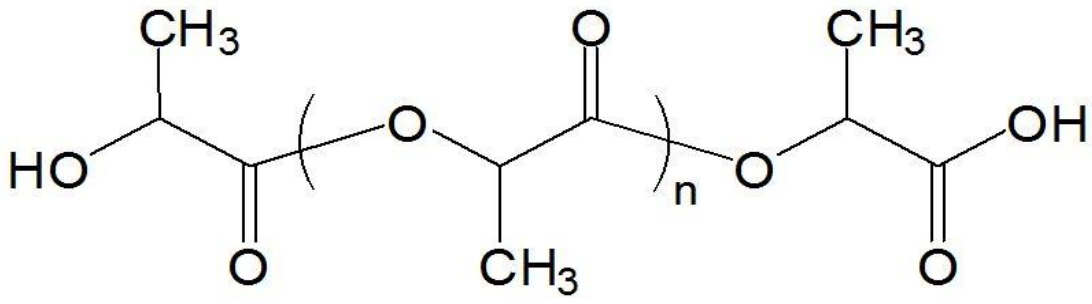

Figure 1.1 Chemical structure of PLA [2]

PLA is an aliphatic polyester having thermoplastic character. Depending on its stereo isomerism, it can be semi-crystalline or amorphous. Figure 1.2 shows three different stereo chemical forms of PLA structure, which are; poly(L-lactic acid) designated as

PLLA, poly(D-lactic acid) designated as PDLA and poly(D-, L-lactic acid) designated as PDLLA. The most common type of PLA with mass production is PLLA, and the second one PDLA has also certain use [3].

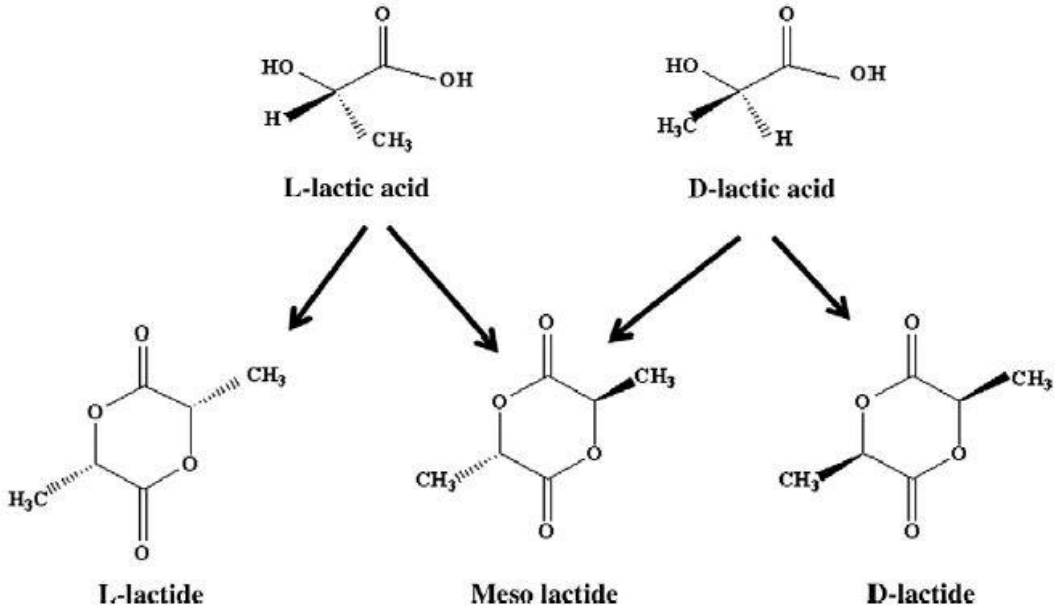

Figure 1.2 Stereo forms of lactide [1]

As shown in Figure 1.3, there are basically two main production routes used for PLA; the first one is the "direct condensation of lactic acid monomers", while the second one is "the ring-opening polymerization of the cyclic lactide dimer". In the former, due to the fact that the water molecule is generated in every step, there occur some difficulties of removing water, which limits the molecular weight of polymer. In the latter route which is more common, high molecular weight PLA is obtained with the use of some metal catalysts such as tin octoate in solution or in the melt, which consequently causes the racemization of PLA.

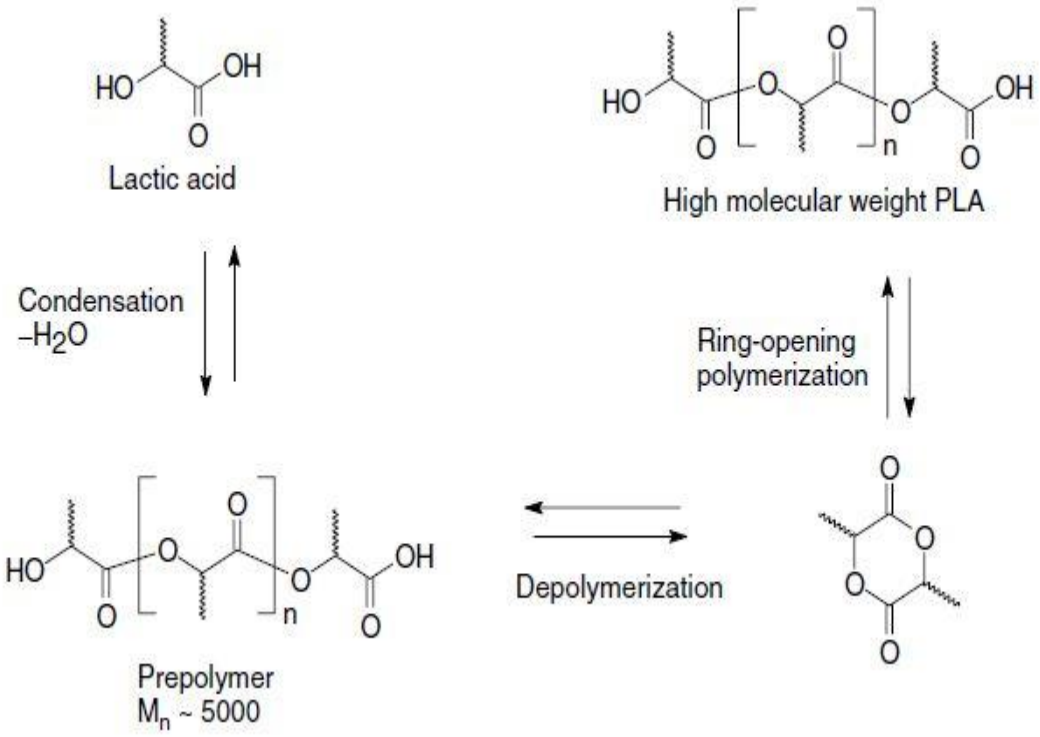

Figure 1.3 Two production routes of PLA [3]

Many properties of high molecular weight PLA such as density, heat capacity, mechanical and rheological properties considerably depend on its transition temperatures of T_g and T_m. Semi-crystalline PLA (mostly found in the market and extensively used by researchers) has a glass transition temperature (T_g) of around 60°C and a melting temperature (T_m) range of 130-230°C, respectively. These transition temperatures (T_g and T_m) strongly depend on optical isomer structure, thermal history and molecular weight [3].

PLA has a wide range of use in today's industry such as medical, food, chemical and textile. Recent technologies and studies have made possible that PLA could be also used in structural components such as automotive parts due to its certain level of strength, stiffness and hardness compared to other low performance biopolymers [1, 3].

One of the main concerns of PLA is its brittleness, which limits the use of PLA in structural applications. In the academia, many approaches have been used for toughening of PLA such as plasticization and blending with elastomeric materials. However, these approaches for high toughness PLA resulted in substantial decreases in the strength and modulus values. Another problem of PLA is its sensitivity to atmospheric conditions such as sunlight and moisture.

Therefore, in the present study, mechanical properties especially ductility and toughness, before and after atmospheric weathering conditions via UV irradiation and moisture will be studied not only for neat PLA, but also for its biocomposite specimens reinforced with microcrystalline cellulose (MCC) fillers.

1.2 Cellulose

(i) Structure and Properties

Cellulose is the most abundant organic compound on Earth, because it is the structural component of the primary cell wall of all plants. It is an organic substance with the general formula of $(C_6H_{10}O_5)_n$. Its chemical structure is composed of thousands of linear chains of β(1→4) linked D-glucose units as shown in Figure 1.4. It can be derived from D-glucose units by condensation via β(1→4) glycosidic covalent bonds holding a carbohydrate molecule to another [4, 5].

Cellulose is odorless, hydrophilic (water loving) due to hydroxyl groups (-OH) in their structures and biodegradable. Unlike starch, cellulose is a straight chain polymer having no coiling or branching, instead it has extended rod-like stiff structure. Since there are many hydroxyl groups on the D-glucose units, hydrogen bond will form between the units and neighboring chains. Hydrogen bond holding the chains together side-by-side results in strong microfibrillar structure such as cell walls having high tensile strength.

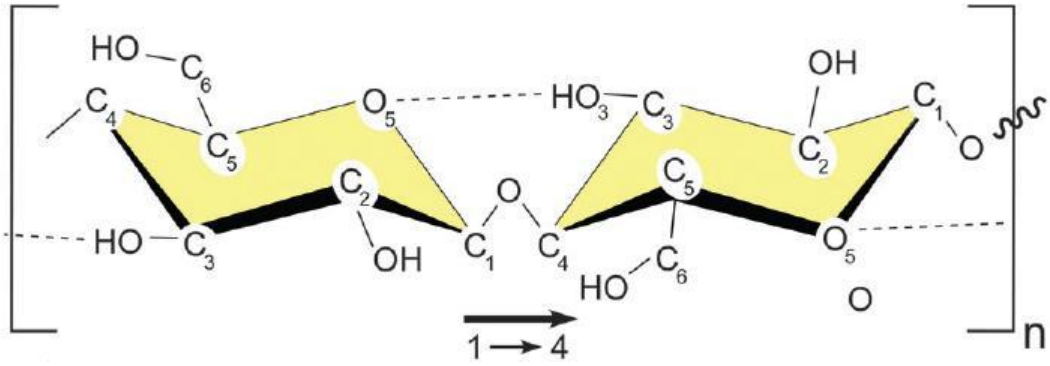

Figure 1.4 The structure of cellulose: β(1-4) linkage of D-glucose monomers [6]

Cellulose can have different crystalline structures (I, II, III and IV). "Cellulose I" crystal structure is the most common one also called as natural cellulose, because it forms from living organisms such as bacteria, algae, trees and plants. It is thermodynamically metastable having two phases; "Iα" with a triclinic structure and "Iβ" with a monoclinic structure. Alpha cellulose (Iα) is found in bacteria and algae, while beta cellulose (Iβ) is present in higher plants. "Cellulose II, III and IV" crystal structures can form via certain processes [6].

The Iα and Iβ crystal structures of cellulose are shown in Figure 1.5. The Iα unit cell within a space group P1 contains one cellulose chain, and the unit-cell parameters are a = 0.672 nm, b = 0.596 nm, c = 1.040 nm, α = 118.08º, β = 114.80º, γ = 80.37º. The Iβ unit cell, space group $P2_1$, contains two cellulose chains, and the unit-cell parameters are a = 0.778 nm, b = 0.820 nm, c = 1.038 nm, γ= 96.51º. Three lattice planes with approximate d-spacings of 0.39 nm, 0.53 nm, and 0.61 nm are shared and correspond to Iα lattice planes (110), (010), and (100), and Iβ lattice planes (200), (110), and ($\overline{1}$ 10), respectively. The main difference between Iα and Iβ is the relative displacement of cellulose sheets (parallel stacking of cellulose chains in one plane) along the (110) and (200) planes (called ‘‘hydrogen bonded’’ planes) in the

chain axis direction. For Iα there is a relative displacement of c/4 between each subsequent hydrogen-bonded plane, while for Iβ the displacement alternates between c/4 and -c/4 [6, 7].

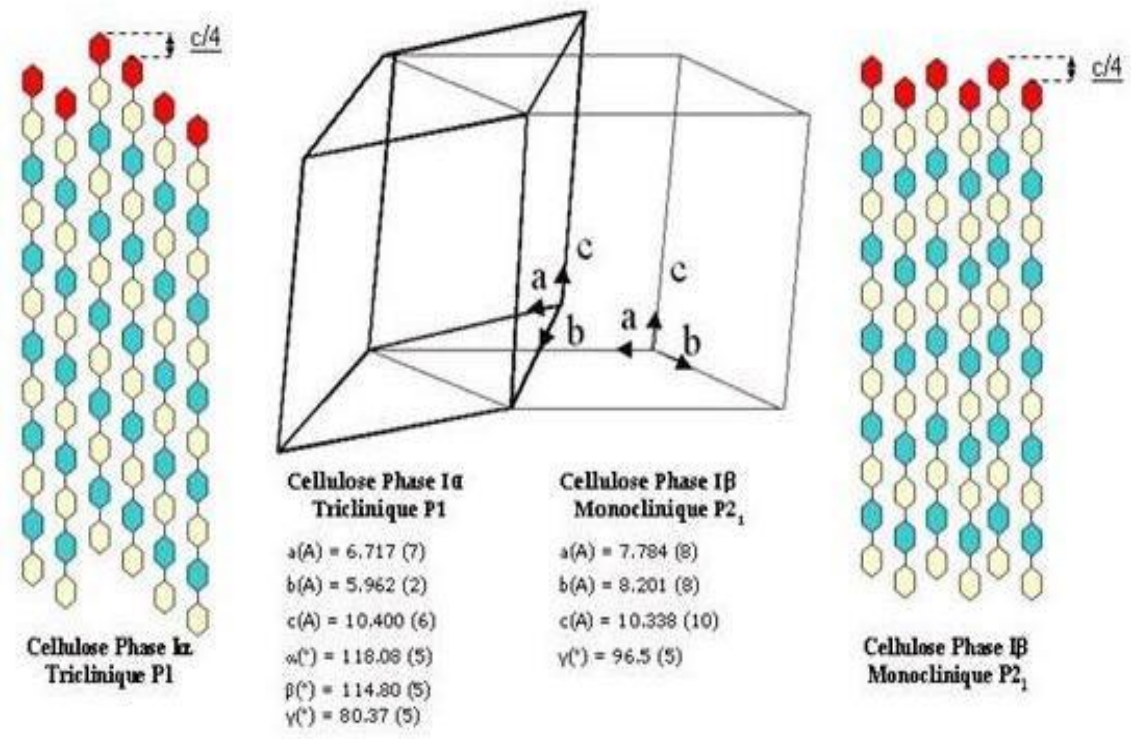

Figure 1.5 α and β phases of Cellulose I crystal structure [7]

Certain mechanical and thermal properties of crystalline cellulose are given in Table 1.1 and 1.2, respectively. These properties are affected by several factors such as percent crystallinity, anisotropy and defects.

Table 1.1 Mechanical properties of crystalline cellulose [6]

	ρ (g/cm^3)	σ_f (GPa)	E_A (GPa)	E_T (GPa)
Crystalline cellulose	1.6	7.5-7.7	110-220	10-50

ρ: density, σ_f : tensile strength, E_A :elastic modulus in axial direction, E_T :elastic modulus in transverse direction

Table 1.2 Thermal properties of crystalline cellulose [6]

	T_g (^{o}C)	T_m (^{o}C)	T_d (^{o}C)
Crystalline cellulose	170-190	250-300	350-400

T_g: glass transition temperature, T_m: melting temperature, T_d: thermal degradation temperature

The use of cellulose in the industry is remarkable including the applications of barrier films, transparent films, antimicrobial films, flexible displays, reinforcing fillers for polymers, biomedical implants, drug delivery, fibers and textiles, separation membranes, batteries, super capacitors etc. [6].

(ii) Macro, Micro and Nano Scales of Cellulose

As stated above, cellulose is the main structural material in plants; therefore, the route for micro and nano scales starts with the plants. Figure 1.6 shows the hierarchical structure of wood. Cellulose is a macromolecule composed of thousands of microfibrils. However, microfibrils cause aggregation during the use of cellulose in the preparation of composites, which weakens the properties of composites especially mechanical ones.

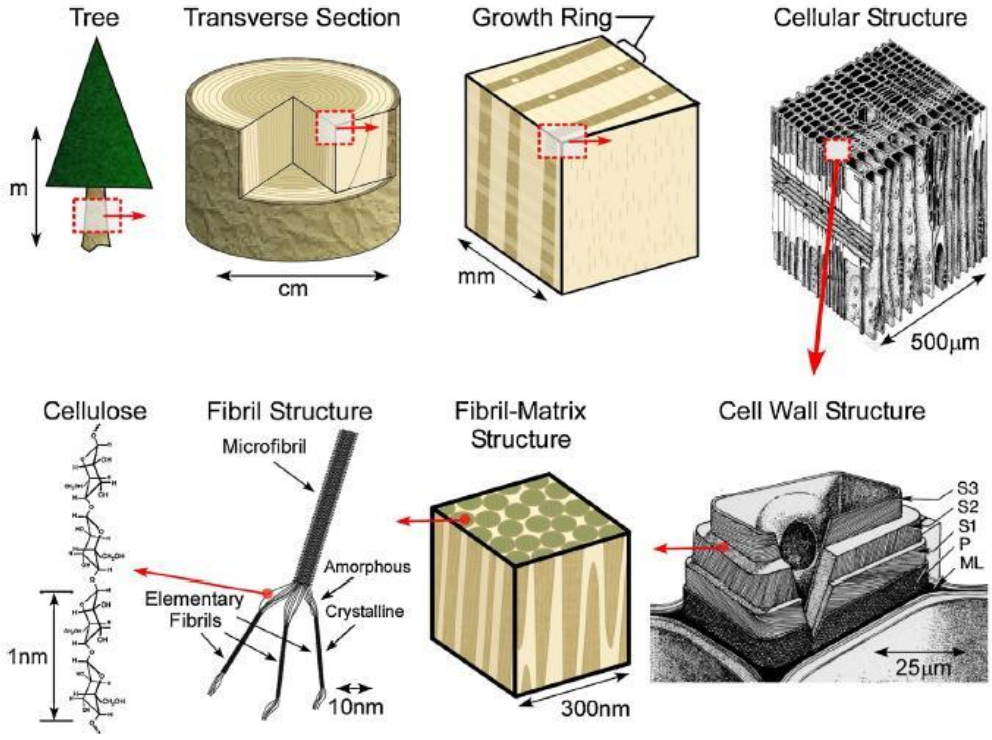

Figure 1.6 Hierarchical structure of wood [8]

As shown in Figure 1.7, a single cellulose microfibril structure is composed of inner "crystalline cellulose" region, outer "hemicellulose amorphous" region, and the "paracrystalline cellulose" region in between.

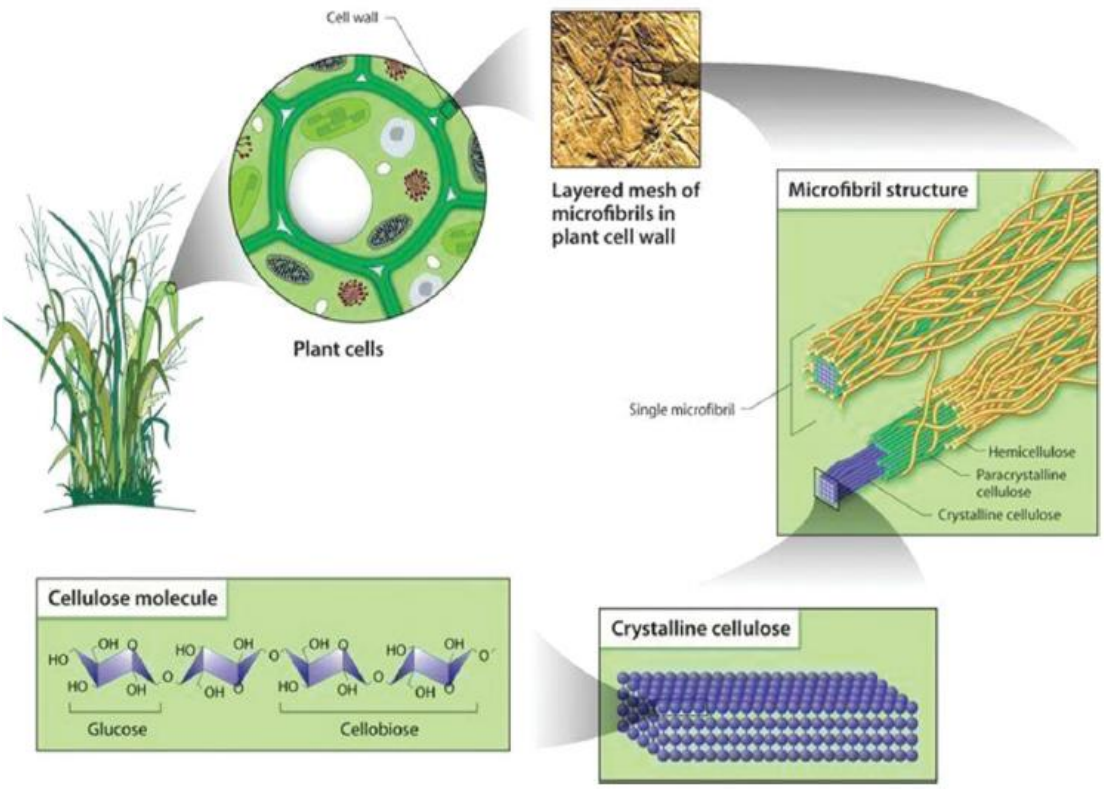

Figure 1.7 Location and extraction of nano crystalline cellulose [9]

To go over from macro to micro and nano cellulose, there are mainly two steps. The first step is purification and homogenization pretreatments. This step particularly depends on the source of cellulose. That is different pretreatments will be required, for example for wood, plant, algae and bacteria. Pretreatments for wood and plant basically include the complete or partial removal of matrix materials such as hemicellulose and lignin. Details of these procedures are discussed in the literature [6, 8, 9]. The second step involves the separation of purified cellulose into micro and nano cellulose. Basically, three techniques are used for this step: mechanical treatment, acid hydrolysis and enzymatic hydrolysis [6, 8, 9].These techniques can be used separately, though in practice to obtain the desired structure, these techniques are used in sequence or in combination.

In the mechanical technique (the most widely used one) via high-pressure homogenizers, grinders, refiners, etc., shear forces are applied to cause transverse cleavage along the longitudinal axis of the cellulose microfibrillar structure. This structure is called "microfibrillated cellulose" (MFC) having 50-70 % crystallinity, 10-100 nm diameter range and 0.5-10 µm length range. In order to obtain thinner cellulose microfibrils, some subsequent chemical treatments can be achieved such as 2,2,6,6-tetramethylpiperidine-1-oxyl (TEMPO)-mediated oxidation, the introduction of charged polyelectrolytes through carboxymethylation [6,10]. Figure 1.8 shows the micrographs of disintegrated microfibrils after high-pressure mechanical treatment and TEMPO-mediated oxidation.

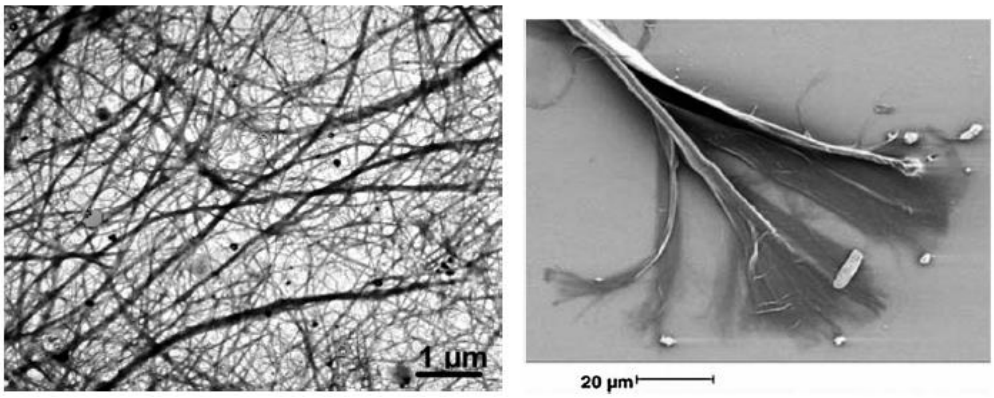

Figure 1.8 MFC micrographs after high-pressure mechanical treatment (left) and the subsequent TEMPO-mediated oxidation (right) [11, 12]

Second technique used by academia and industries is acid hydrolysis. In this technique, amorphous regions of the cellulose microfibrils are eliminated by introducing acid attacks. The most widely used acids are hydro-chloric acid (HCl) and sulfuric acid (H_2SO_4). The main mechanism underlying this method is that hydronium ions (H_3O^+) coming from the dissolution of the acid in water penetrate cellulose microfibrils in the amorphous regions so that hydrolytic cleavage of the glycosidic bonds can occur leading to the release of crystalline regions. Subsequent mechanical treatment like ultrasonication can be applied to remove amorphous

regions further. “Microcrystalline cellulose” (MCC) structure is obtained by this technique having 80-85 % crystallinity and particle size range of 10-50 μm.

“Cellulose nanocrystals” (CNC) are rod-like or whisker shaped particles remained after acid hydrolysis of MCC or MFC as shown in Figure 1.9. They have a diameter range of 3-5 nm and a length range of 50-500 nm.

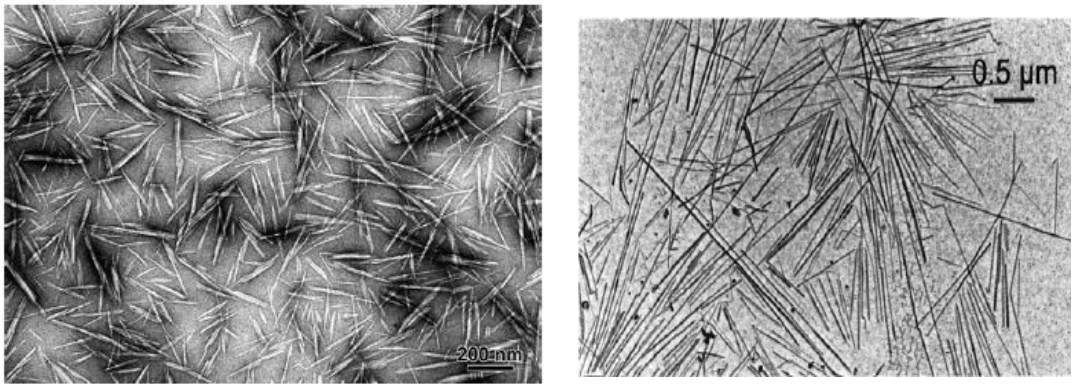

Figure 1.9 TEM images of cellulose nano crystals [13, 14]

1.3 Polylactide/Natural Fiber Biocomposites

The use of natural fibers in polylactide matrix biocomposites has been increasing due to their rather high specific strength and modulus, low cost and ease of processing. Some of these studies will be discussed in the Section 1.5 Literature Survey.

As reviewed in the literature [15], natural fibers can be classified into six basic groups: bast fibers (hemp, jute, kenaf, flax and ramie), leaf fibers (abaca, pineapple and sisal), seed fibers (cotton, coir and kapok), core fibers (kenaf, jute and hemp), grass and reed fibers (wheat, corn and rice) and all other types (wood and roots). Natural fibers are composed of basically three constituents: cellulose, hemicellulose and lignin. Chemical compositions of several natural fibers are tabulated in Table 1.3.

Table 1.3 Chemical compositions of several natural fibers [15]

Fiber	Cellulose (wt%)	Hemicellulose (wt%)	Lignin (wt%)	Waxes (wt%)
Bagasse	55.2	16.8	25.3	–
Bamboo	26–43	30	21–31	–
Flax	71	18.6–20.6	2.2	1.5
Kenaf	72	20.3	9	–
Jute	61–71	14–20	12–13	0.5
Hemp	68	15	10	0.8
Ramie	68.6–76.2	13–16	0.6–0.7	0.3
Abaca	56–63	20–25	7–9	3
Sisal	65	12	9.9	2
Coir	32–43	0.15–0.25	40–45	–
Oil palm	65	–	29	–
Pineapple	81	–	12.7	–
Curaua	73.6	9.9	7.5	–
Wheat straw	38–45	15–31	12–20	–
Rice husk	35–45	19–25	20	14–17
Rice straw	41–57	33	8–19	8–38

The major problem of natural fibers is their hydrophilicity, i.e. their affinity to moisture. Especially amorphous regions of the fiber structure are very susceptible to water absorption, thus it would be worse with the lower cellulose crystallinity and the higher void content of the fibers. Moisture content will decrease the mechanical properties of fibers considerably. Apart from their hydrophilic nature, other shortcomings of natural fibers include their susceptibility to UV irradiation, temperature and fire.

Just like many other thermoplastic polymer matrix composites, PLA/Natural Fiber biocomposite can be compounded by two techniques; melt-mixing or solution mixing. Shaping can be achieved also by conventional methods such as injection molding and compression molding.

Although such composites offer greater advantages over other polymer composites, it is known that there is a compatibility problem between PLA matrix and natural fibers. The weakness of interfacial adhesion between the two constituents is due to the hydrophilic character of natural fibers and hydrophobic character of PLA. This

interfacial adhesion problem is especially solved by modifying the surfaces of natural fibers with physical and chemical methods. Calendaring, corona and plasma treatments are common examples for physical methods, while chemical methods are silanization, alkaline treatment, acetylation, maleated coupling and enzyme treatments [15].

1.4 Weathering Behavior of PLA

Polymeric components when used in the atmospheric conditions (i.e. outdoor applications) they are exposed to basically three types of degradation; "photodegradation" due to sunlight, "hydrolytic degradation" due to humidity, and "biodegradation" due to microorganisms in the soil and water. Weathering tests are used to investigate the effects of the first and the second one, i.e. the effects of UV irradiation and moisture.

For the PLA structure, it was first discussed that [16] the basic photodegradation mechanism of UV irradiation is the main chain scission by absorption of photons. This type of reaction given in Figure 1.10 is defined as Norrish II type photo cleavage. Then, it was indicated that [17] photodegradation reaction might proceed with two possibilities, the first one is "photolysis" reaction and the second one is "photooxidation" reaction.

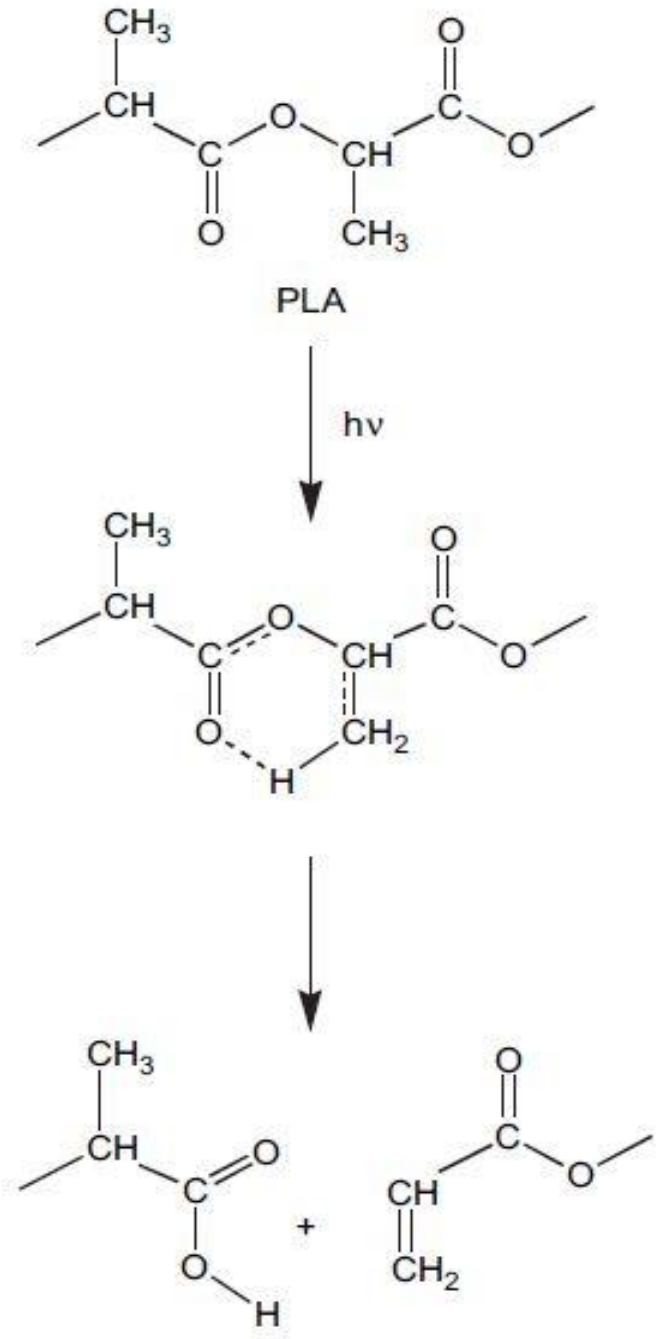

Figure 1.10 Possible photodegradation reaction of PLA [16]

Photolysis mechanism, as shown in Figure 1.11, leads to the breakage of the C-O backbone bonds, resulting in decreases in molecular weight.

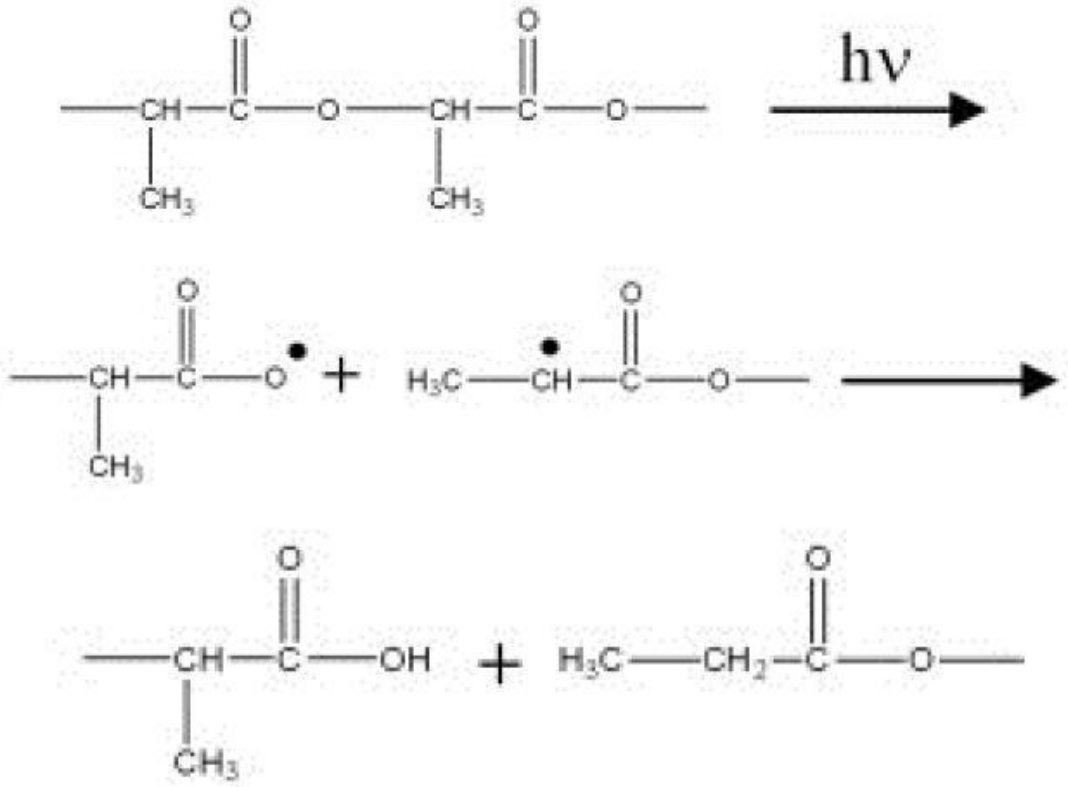

Figure 1.11 Possible photolysis reaction of PLA [17]

Photooxidation mechanism, as shown in Figure 1.12, leads to the formation of a hydroperoxide derivative and its subsequent degradation to compounds containing a carboxylic acid and diketone end groups. Furthermore, the photolysis of the diketone may lead to the cleavage of the C-C bond between the two carbonyl groups, resulting in two carbonyl radicals. This radical pair leads to formation of several photodecomposed products.

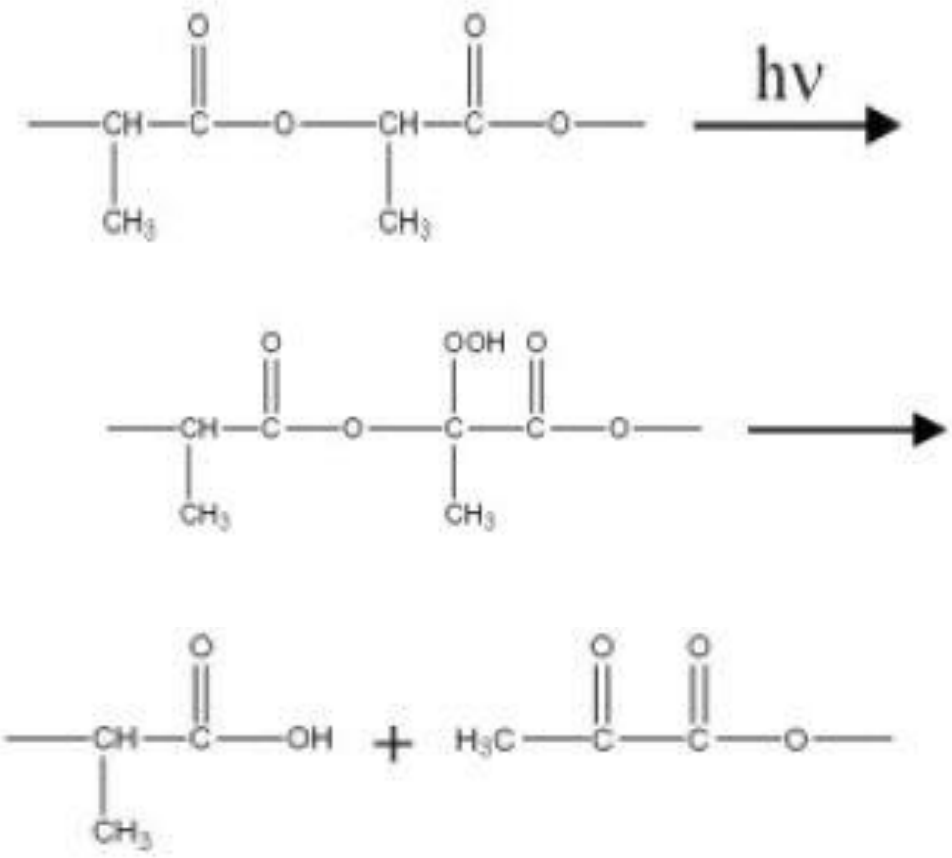

Figure 1.12 Possible photooxidation reaction of PLA [17]

In the PLA structure, moisture leads to plasticization and swelling. However, above 30^{o}C, detrimental hydrolytic degradation becomes significant. This degradation mechanism is defined as "hydrolysis". As shown in Figure 1.13, hydrolysis of PLA backbone occurs through its ester bond. In this reaction, formation of lactic acid oligomers from chain scission lead to higher amount of carboxylic acid end groups and further catalyze the degradation reaction [18].

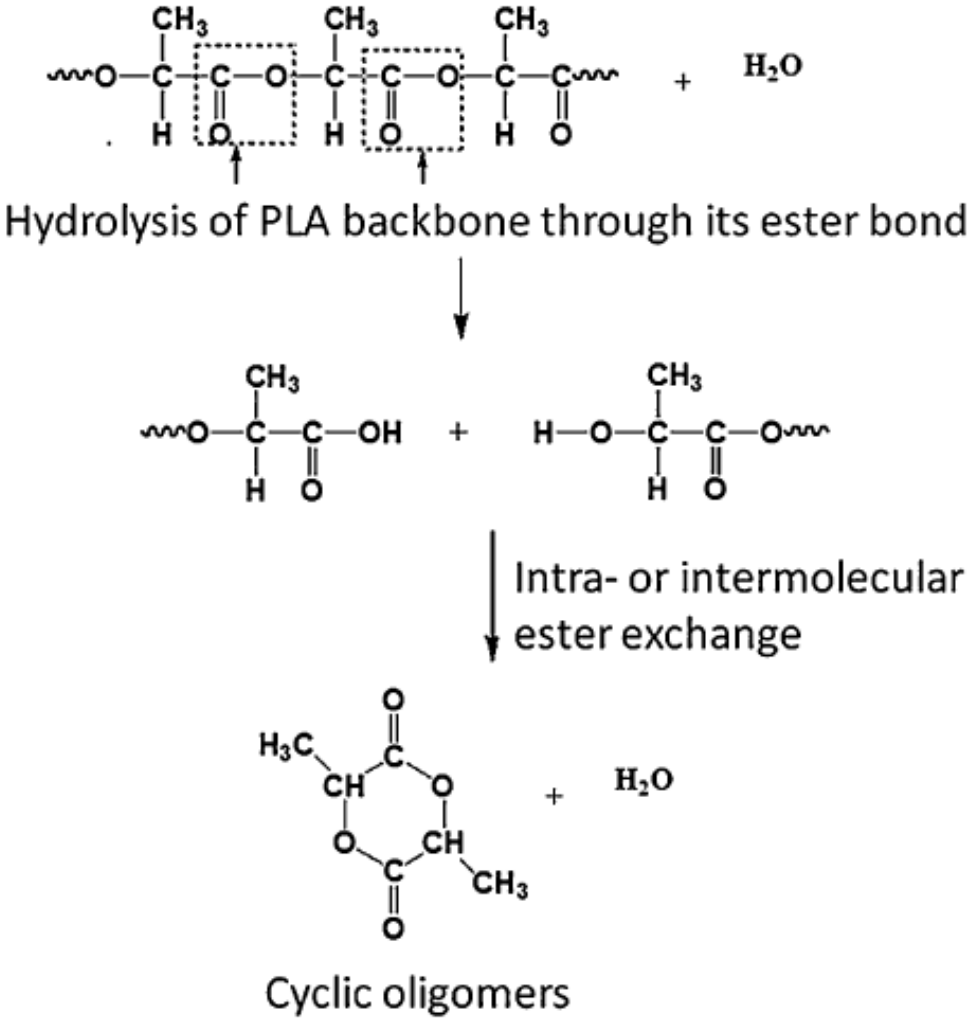

Figure 1.13 Possible hydrolysis reaction of PLA [18]

During weathering, crystallinity amount of PLA might increase due to two reasons. One reason is that, UV irradiation and outdoor temperature might reach to the cold crystallization start temperature of PLA, which is around 70°C. Another reason could be much higher mobility of the short chains of PLA occurred due to chain scissions. This crystallization mechanism is named as "cleavage-induced" crystallization.

1.5 Literature Survey

1.5.1 Studies on the Behavior of PLA/MCC Biocomposites

Poly(L-lactic acid), shortly polylactide (PLA), is a thermoplastic aliphatic polyester which can be synthesized from renewable sources such as starch and sugar beet. Its high biodegradability and biocompatibility with certain level of modulus and strength values made PLA to be used in several applications especially in the food packaging and biomedical sectors. For the other sectors such as automotive industry, inherent brittleness of PLA is today still one of the significant shortcomings.

There have been several studies to overcome brittleness problem of PLA. These studies especially concentrated on the blending of PLA with elastomeric materials such as synthetic and natural rubbers [19-22] and thermoplastic polyurethane elastomers [23-25]. However, these researchers basically reported that although there were significant improvements in the ductility and toughness values, these blends sacrificed their strength and modulus values.

Another group of studies in the literature to improve mechanical properties of biopolymer PLA is the "biocomposite" approach, i.e. reinforcing of PLA with cellulose-based natural fibers. Examples of these fibers include kenaf [26-30], flax [31-34], bamboo [35-38], hemp [39, 40] and jute [27, 41]. It was revealed that these PLA/natural fiber biocomposites might have not only improved mechanical properties, but also improved thermal properties.

Cellulose is an organic polysaccharide made up of several thousands of linear chains linked end to end. Cellulose chains are aggregated to form microfibrils and these microfibrils again aggregate further to form "cellulose macrofibers". Therefore, natural fibers used in those studies above [26-41] were considered as "cellulose microfibers". As discussed by Pandey et al. [42] in detail, in the structure of cellulose

microfibers, there are both “crystalline” and “amorphous” cellulose regions. Amorphous regions which weaken cellulose macrofiber’s properties can be eliminated by using a proper “acid attack” treatment so that the “crystalline regions” can be separated. Then, these crystallites can grow in size since they can move freely. In the literature, that structure is generally called as “microcrystalline cellulose” (MCC).

In literature, there are very limited number of studies [43, 44] using microcrystalline cellulose (MCC) as reinforcement in PLA matrix biocomposites. One of them was conducted by Mathew et al. [43] investigating the effects of MCC on the mechanical properties of PLA. They used melt-mixing method with four different MCC amounts; 10, 15, 20 and 25 wt%. They indicated that addition of MCC decreased tensile strength and % elongation at break values of PLA by 23-27% and 21-29%, respectively. The only improvement was in the value of elastic modulus of PLA by 14-39 %.

Mohamad Haafiz et al. [44] used solution-mixing method to produce film specimens with 1, 3, 5 wt% MCC. They revealed that there were no improvement in the tensile strength and % elongation at break values of PLA; while there were certain improvements in the values of elastic modulus and thermal degradation temperatures.

1.5.2 Studies on the Interfacial Compatibilization of the PLA/MCC Biocomposites

In order to achieve improved engineering performance for the PLA/MCC biocomposites, the interfacial interactions between the matrix and the reinforcement should be improved. In this respect, there is again very limited number of studies [45, 46] in the literature.

In the first one, Xiao et al. [45] used a surface modification technique by grafting of L-lactic acid oligomers on the surfaces of MCC. Then, they compared the properties

of PLA biocomposites with 30 wt% grafted and ungrafted MCC. It was seen that grafted MCC resulted in 50% increase in tensile strength, 100% increase in % elongation at break, as well as 12% increase in crystallinity amount of PLA.

In the latter, Mukherjee et al. [46] used surface acetylation technique by replacing the hydroxyl groups present on the surfaces of MCC with acetyl groups. They revealed that surface-treated MCC could be uniformly distributed in the PLA matrix leading to better thermal properties such as storage modulus. However, no mechanical tests were conducted.

1.5.3 Studies on the Accelerated Weathering Behavior of PLA based Biocomposites

It is known that the biopolymer polylactide (PLA), chemically knowns as poly(L-lactic acid), has been an alternative polymeric material to petroleum-based traditional polymers not only in the food packaging and biomedical items, but also in certain engineering applications such as household appliances and automotive components.

Despite the comparable mechanical properties of PLA with those of industrial polyolefins, sensitivity of PLA against atmospheric conditions such as UV irradiation of sunlight, moisture and temperature; the use of PLA for outdoor applications could be problematic. Thus, weathering behavior of PLA and PLA-based blends and composites should be thoroughly explored.

Unfortunately, there is still limited number of studies. Some of these studies investigated weathering behavior of neat PLA [16, 17, 47-51], blends of PLA with other biopolymers such as polyhydroxyalkanoate [52], or with other elastomeric polymers such as poly(ethylene-vinyl-acetate) [53]; and also biocomposites of PLA filled with keratin [54], tannin [55], wheat starch [56], rice starch [57], rice hulls [58], lignin [59], hemp-fiber [60], and eucalyptus wood fiber [61].

Although some of these researchers conducted accelerated weathering (both UV and moisture) conditions, many of them used only UV irradiation either naturally or artificially. These studies related to UV irradiation [17, 47, 52, 53] indicated that "photolysis" and/or "photo-oxidation" are the degradation mechanisms leading to "main chain scission" in certain chemical bonds of the PLA structure.

Another group of studies investigated only influences of moisture and/or immersion in fresh or seawater. They [51, 58] revealed that apart from the effects of "swelling" and "plasticization", the main degradation mechanism of "hydrolysis" in this case could also lead to decreased molecular weight of PLA via chain scission.

Weathering studies of PLA-based blends and biocomposites demonstrated that depending on the amount, structure and chemical interaction with the filler material, weathering behavior of PLA matrix either remains unchanged or affected beneficially or detrimentally.

1.6 Purpose of the Study

In the literature, since strength and modulus of PLA/MCC biocomposites were determined especially under tensile loading and no fracture toughness data were reported, the main purpose of the first part of this thesis is to investigate effects of MCC content on the fracture toughness of PLA biocomposites produced by industrially compatible production techniques, i.e. twin-screw extrusion melt-mixing for compounding and injection molding for shaping of bulk specimens. Moreover, apart from thermal properties, strength and elastic modulus values were determined not only under tensile loading, but also under bending loading.

Another missing point in the literature is, to the best of our knowledge, having no maleic anhydride interfacial compatibilization study reported yet. Thus, another purpose of the first part of this thesis is to explore influences of using maleic

anhydride grafted PLA copolymer compatibilization on the toughness and other properties of PLA/MCC biocomposites.

In the literature, there are certain number of studies [43-46] investigating the effects of microcrystalline cellulose (MCC) on the mechanical and thermal properties of PLA under normal conditions. However, to the best of our knowledge, there are no PLA/MCC studies exploring the effects of weathering, even only under UV irradiation or only moisture. Therefore, the purpose of the second part of this thesis is to investigate accelerated weathering (both UV and moisture) behavior of neat PLA and PLA/MCC biocomposites by comparing their mechanical and thermal properties under increasing accelerated weathering periods.

CHAPTER 2

EXPERIMENTAL WORK

2.1 Materials Used

(i) Matrix Polymer (PLA)

In the thesis, commercial L-lactic acid type polylactide (PLA) supplied from NaturePlast (France) with an extrusion grade (PLE 001) was used as the matrix material. According to its technical data sheet, it has a melting temperature range of 145°-155°C, degradation temperature range of 240°-250°C, while the melt flow index range at 190°C under 2.16 kg is 2-8 g/10 min, as well as a density of 1.25 g/cm^3. Moreover, weight average molecular weight of this PLA was determined by using the static light scattering (SLS) spectroscopy technique via Malvern CGS-3 giving the result of 375 600 g/mol.

(ii) Reinforcement (MCC)

Microcrystalline cellulose (MCC) used as the reinforcement filler in this study was also a commercial product (Sigma-Aldrich, product no: 310697) in the form of white powder. SEM studies, given in Figure 2.1, revealed that the diameter and length of the MCC filler used were between 12-15 μm and 35-50 μm, respectively.

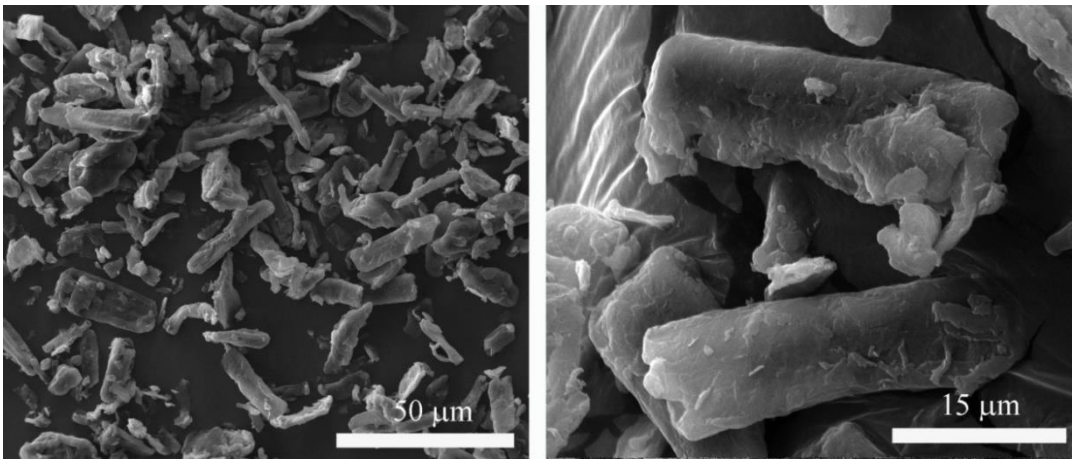

Figure 2.1 General and closer view SEM images showing the diameter and length ranges of MCC used

X-ray diffractogram of MCC used in this study is given in Figure 2.2. Three 2θ reflections at 15.1^{o}, 16.1^{o} and 22.3^{o} correspond to (110), ($\bar{1}$10) and (200) planes, respectively, while 2θ reflection at 18.5^{o} represents the amorphous phase of cellulose.

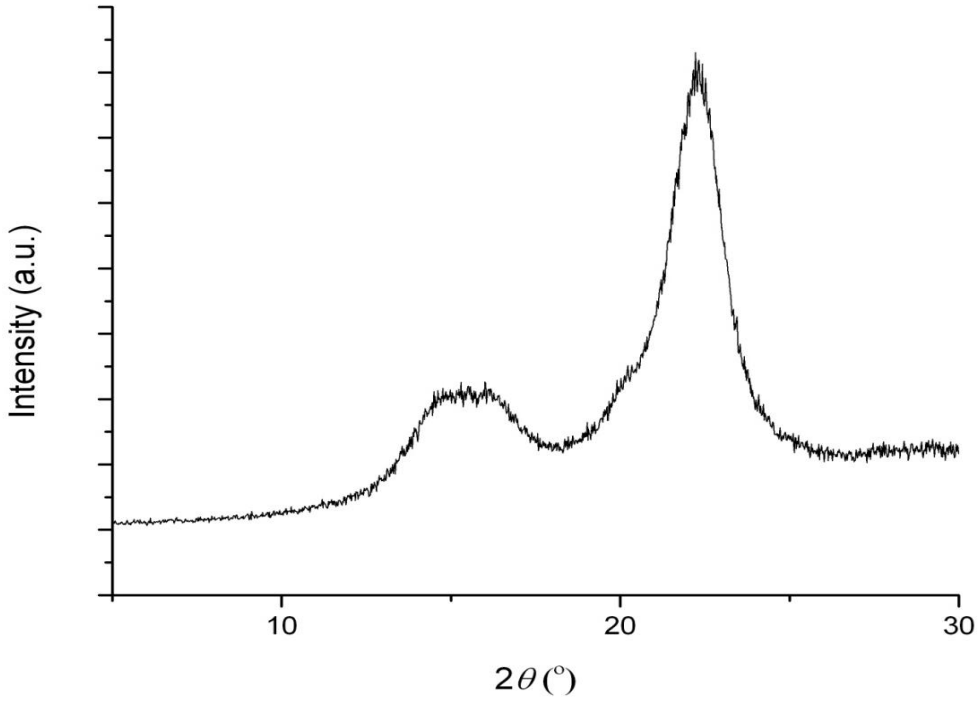

Figure 2.2 X-ray diffractogram of MCC used

(iii) Compatibilizing Agent (MA)

Maleic anhydride (MA) (Sigma-Aldrich, purity 99%) used for grafting of PLA has molecular weight of 98.06 g/mol, melting temperature range of 51-56°C and boiling temperature of 200°C. Initiator used for MA grafting reaction was dicumyl peroxide (DCP) (Sigma-Aldrich, purity 99%) with melting temperature of 39°C.

2.2 Production of PLA/MCC Biocomposites

PLA/MCC biocomposites were produced by two industrially compatible steps; i.e. "twin-screw extrusion melt-compounding" and "injection molding melt-shaping" with laboratory size equipment.

In the first step, PLA granules and MCC powders were pre-dried for 15 hours and 3 hours, respectively; in a vacuum oven at 60°C, and then pre-mixed manually. This mixture was melt compounded via Rondol Microlab 300 laboratory size (D=10 and L/D=20) twin-screw extruder. Typical temperature profile from feeder to die used were 115°-170°-180°-175°-150°C while the typical screw speed used was 50 rpm throughout the compounding stage; followed by four-blade cutting of the continuous strands into pellets of 2-3 mm.

In the second step, prior to shaping pellets were again allowed to re-dry for 15 hours in a vacuum oven at 60°C. Standard sized specimens required for testing and analyses were melt-shaped via laboratory scale DSM Xplore Micro injection molder. Typical barrel and mold temperatures used were 190°C and 35°C, respectively; while the melting time in the barrel was approximately 7 minutes, with the subsequent three-step pressure-time profile determined as 14 bar for 3 s, 12 bar for 5 s, and 12 bar for 5 s.

In the first part of this thesis, PLA biocomposites were produced with the loadings of 1, 3, 5 and 7 wt% MCC. These biocomposites were designated by using the format of "PLA/MCC *x*", where *x* denotes wt% of MCC used.

2.3 Production of PLA/gMA/MCC Biocomposite

Interfacial compatibilization was applied only for the PLA/MCC 3 biocomposite, as would be discussed in "Results and Discussion" section.

Effects of interfacial compatibilization was conducted by using the maleic anhydride (MA) grafted PLA copolymer, i.e. PLA-g-MA. For this purpose, different amounts of the copolymer was compounded with the PLA/MCC 3 composition, and it was revealed that use of 3 wt% PLA-g-MA copolymer resulted in optimum properties. Thus, only this composition was evaluated. For simplicity, PLA-g-MA copolymer

was designated as “gMA” in this thesis. Therefore, that specimen having interfacial compatibilization was designated as “PLA/gMA/MCC 3”.

Note that PLA-g-MA copolymer was produced by using the reactive extrusion technique via twin-screw melt mixing of PLA and 2 wt% maleic anhydride (MA) including 0.5 wt% dicumyl peroxide (DCP) as the free radical initiator. By using the titration method, the amount of grafted MA on PLA was found as 1.18%. Details of these procedures are explained in our former study [61] thoroughly.

2.4 Characterization by FTIR and SEM

In order to reveal possible interfacial interactions between PLA, MA and MCC fillers, “Fourier transform-infrared (FTIR) spectroscopy” was used. At least 32 scans were signal-averaged by the “attenuated total reflectance (ATR)” unit of Bruker ALPHA IR spectrometer in the wavenumber range of 400 to 4000 $cm^{-1}$with a resolution of 4 cm^{-1}.

Morphological analysis in terms of distribution of MCC in PLA matrix and the interface between them were carried out for the gold sputtered fracture surface of fracture toughness specimens under FEI Nova Nano 430 scanning electron microscope (SEM).

2.5 Mechanical Tests and Thermal Analyses

K_{IC} and G_{IC} fracture toughness tests were conducted for single-edge-notched-bending specimens according to ISO 13586 standards under Instron 5565A system. Notches and pre-cracks on these specimens were created by Ceast Notchvis system as defined in the standard. Apart from toughness tests; tension and flexural tests were also carried out to determine other mechanical properties of the specimens. Tension tests

were applied according to ISO 527-2 standard, while flexural tests in terms of three-point bending were applied according to ISO 178 standard. These tests were carried out under 5 kN Instron 5565A universal testing system. For each specimen group, these tests were repeated 5 times; and mechanical properties were determined as the average values including their standard deviations.

The first thermal analysis to determine transition temperatures and enthalpies of each specimen was differential scanning calorimetry (DSC) analyses. The heating profile used for the materials was -80° to 220°C with 10°C/min rate under SII X-DSC 700 Exstar system. The second analysis for the determination of the thermal degradation temperatures of each specimen was thermogravimetric analyses (TGA). This time the heating profile was 30° to 550°C under SII TG/DTA 7300 Exstar system.

2.6 Accelerated Weathering of the Neat PLA and its PLA/MCC Biocomposite

As would be discussed in the "Results and Discussion" section of the first part of this thesis, it was revealed that use of 3 wt% MCC resulted in the best optimum mechanical properties. Therefore, in the second part of this thesis, influences of accelerated weathering were explored for the PLA/MCC biocomposites having only 3 wt% MCC.

In order to investigate the weathering behavior of neat PLA and its 3 wt% MCC biocomposite, an *accelerated weathering tester* (Q-LAB Model QUV/se) was used. The weathering conditions were in accordance with the Cycle-C of the SAE J2020, ASTM G154-05 and ISO 4892-3 standards. Fluorescent lamps (UVB-313) with 0.49 W/m^2 irradiance (at 310 nm) were used with cycles of 8 h UV irradiation at 70°C, followed by 4 h dark condensation at 50°C. These consecutive cycles were applied to the specimens attached to the test panels without any interruption. Effects of accelerated weathering were investigated for four periods: 50, 100, 150 and 200 h.

Specimens for each period were designated as PLA/MCC-*x*h, where *x* denotes the accelerated weathering period.

Effects of each period of accelerated weathering on the behavior of the neat PLA and its 3 wt% MCC biocomposite specimens were investigated by comparing the changes in the results of the following tests and analyses conducted.

2.7 Analyses for the Changes in the Crystallinity of PLA Matrix

For the effects of each accelerated weathering period on the changes in the crystallinity of the neat PLA and the matrix of 3 wt% MCC biocomposite specimens, X-ray diffraction (XRD) analyses were performed. Measurements were conducted by Bruker D8 Advance A25 X-ray diffractometer with monochromatic CuK_{α} radiation. The anode voltage and current were set at 40 kV and 40 mA, respectively. Diffraction angle 2θ was scanned from 5 to 30^{o} at a scanning rate of 2^{o}/min.

2.8 Analyses for the Changes in the Color of the Specimens

Color changes after each accelerated weathering period were observed both visually and quantitatively. Visual observation was done by photographing the images of the weathered specimens and comparing their color with the unweathered one.

The quantitative analysis for the color change was conducted by determining the CIELAB color space parameters *(L*, a*, b*)* of the specimens before and after each accelerated weathering period. For this purpose *diffused reflectance analysis* (DRA) was utilized via DRA unit of Agilent Cary 60 UV-vis spectrophotometer in accordance with CIE 1976 standards.

2.9 Analyses for the Changes in the Chemical Structure of the Specimens

The first analysis was to observe the decreases in the molecular weight of PLA matrix after each accelerated weathering period. For this purpose, *static light scattering* (SLS) spectrometry (Malvern CGS-3) was conducted to determine the weight-average molecular weight (M_w) of the specimens by using the results of Guiner plots of four different concentrations of PLA samples dissolved in chloroform.

The second analysis was ATR-FTIR to observe the changes in the chemical bonds of the specimens after each accelerated weathering period. Spectra were taken via the same system mentioned in Section 2.4 above.

2.10 Analyses for the Changes in the Morphology, Mechanical Properties and Thermal Behavior of Specimens

In order to compare changes in the fracture surface morphology, tensile and flexural modulus, tensile and flexural strength, ductility, fracture toughness, transition and thermal degradation temperatures of the neat PLA and its 3 wt% MCC biocomposite specimens before and after each accelerated weathering period, SEM observations, mechanical tests and thermal analyses mentioned in the above Sections 2.4 and 2.5 were performed.

CHAPTER 3

RESULTS AND DISCUSSION

As stated before, since this thesis has two different parts; their results are presented and discussed successively in the following two subsections.

3.1 Effects of MCC Content and MA Compatibilization

3.1.1 Infrared Spectroscopy of the PLA/MCC Biocomposites

ATR-FTIR spectra (Figure 3.1) of the specimens were obtained in order to compare the chemical structure of neat PLA with its biocomposites of 3 wt% MCC including the one having MA compatibilization. Figure 3.1 shows that neat PLA spectrum has all the characteristic IR band assignments as discussed in the literature [62-64]. These bands basically include C-C stretching at 867 cm^{-1}, C-O stretching peaks at 1079, 1126, 1181 and 1264 cm^{-1}, C-H deformation peaks at 1377 and 1452 cm^{-1}, C=O ester carbonyl groups at 1748 cm^{-1}, and C-H stretching at 2853 and 2924 cm^{-1}.

It is known that IR spectroscopy can be successfully used to characterize chemical interaction between the matrix and the filler in composite materials. When these two components are completely immiscible, then there would be no appreciable changes in the IR spectrum of their composite, i.e. characteristic peaks of the matrix and the filler would remain the same. However, when there is hydrogen bonding or other polar interactions between the matrix and the filler, then there would be a certain level of compatibility. These distinct chemical interactions between the matrix and the filler consequently might lead to the changes in the IR spectrum of their composite, usually in the form band shifting and broadening.

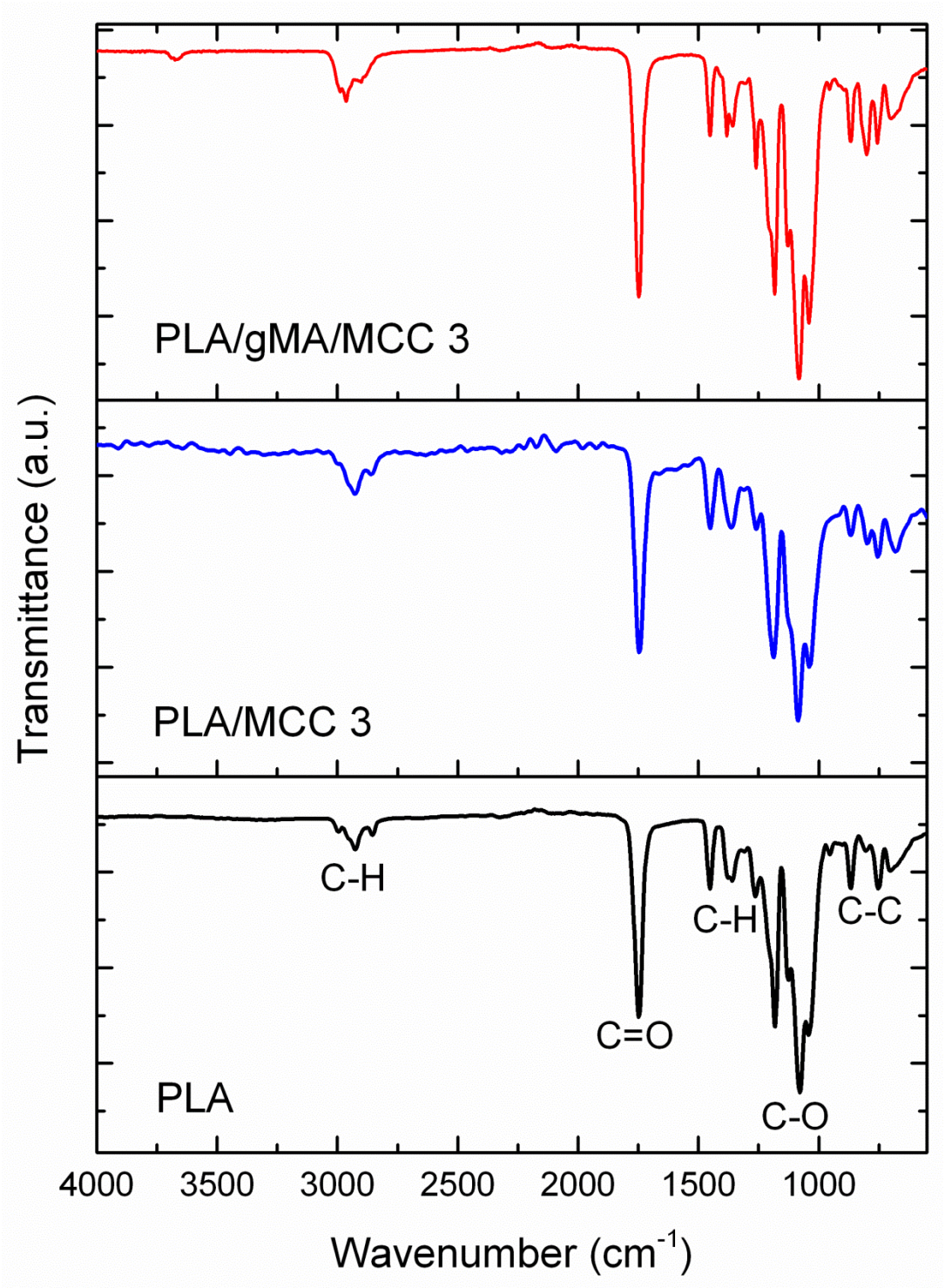

Figure 3.1 ATR-FTIR spectra of PLA and its biocomposites

Figure 3.1 shows that when 3 wt% MCC was incorporated into PLA matrix, IR spectrum of this biocomposite does not change, i.e. there is no appearance of new IR peaks. One reason for this result is the use of low amount of filler and the similarity of the IR spectrum of PLA and cellulose. Another reason for the absence of new peak could be due to having only physical interaction between PLA and MCC surfaces rather than having a chemical interaction.

On the other hand, it is known that there is the possibility of hydrogen bond formation between the surfaces of cellulose (i.e. hydroxyl groups) and the functional groups of PLA structure (i.e. carbonyl groups of the backbone, hydroxyl and carboxyl groups of the chain terminals). In the literature [64], it is discussed that this chemical interaction is especially attributed to the broadening and/or shifting of the C=O peak at 1756-1760 cm^{-1}, i.e. the interaction between the O-H of cellulose surfaces and C=O of PLA backbones. It is seen in Figure 3.1 that, there is very slight broadening and shifting of this peak from 1748 to 1745 cm^{-1} in the IR spectrum of PLA/MCC 3 biocomposite specimen.

In this study, in order to improve interfacial hydrogen bond interaction between PLA and cellulose, maleic anhydride (MA) copolymer compatibilization was used. Typical IR bands reported [62, 65] for the MA structure are cyclic C=C stretching band at 1590 cm^{-1}, asymmetric and symmetric C=O stretching at 1774 cm^{-1} and 1850 cm^{-1} , respectively. It is stated in the literature [66, 67] that hydrogen bond type chemical interaction could also occur between the hydrogen of the hydroxyl groups of the cellulose surfaces and the oxygen of the carbonyl groups of the MA structure. This interaction is attributed to the shift of the C=O of MA at around 1774 cm^{-1}. Figure 3.1 shows that this shift was overlapped by the C=O of PLA between 1720-1785 cm^{-1}.

3.1.2 Fracture Surface Morphology of the PLA/MCC Biocomposites

Properties of the composites are strongly dependent on the uniform distribution of the fillers. Therefore, SEM examination of the biocomposites were first performed by the lower magnification (Figure 3.2) of the fracture surfaces of the specimens taken from their fracture toughness tests in order to investigate the level of distribution of MCC in PLA matrix.

Figure 3.2 shows that there was no significant distribution problem in the specimens with 1 and 3 wt% MCC contents, while there was slight level of agglomeration with 5 and 7 wt% MCC. It is also seen in Figure 3.2 that due to the improved interaction via MA grafted copolymer compatibilization, the distribution of 3 wt% MCC particles was better than the specimen without compatibilization.

SEM fractographs were also taken at a higher magnification, as given in Figure 3.3, to reveal the interfacial interactions between the PLA matrix and MCC surfaces. These images simply indicate that in the specimen without compatibilization MCCs were usually “debonded” and “pulled-out” from the PLA matrix. On the other hand, in the specimen with MA copolymer compatibilization, certain level of interfacial interaction was evident by the adherence of the PLA fibrils on the surfaces of MCC fillers. Therefore, SEM images of the specimen PLA/gMA/MCC 3 had the lowest level of debonding and pull-out.

As discussed in the IR spectroscopy section above, the level of hydrogen bond between the PLA matrix chains and the crystalline cellulose chains on the surfaces of MCC structure becomes much stronger via the functional anhydride group of MA copolymer compatibilization. Therefore, as will be given in the following section, PLA/gMA/MCC 3 specimen obtained the highest mechanical properties.

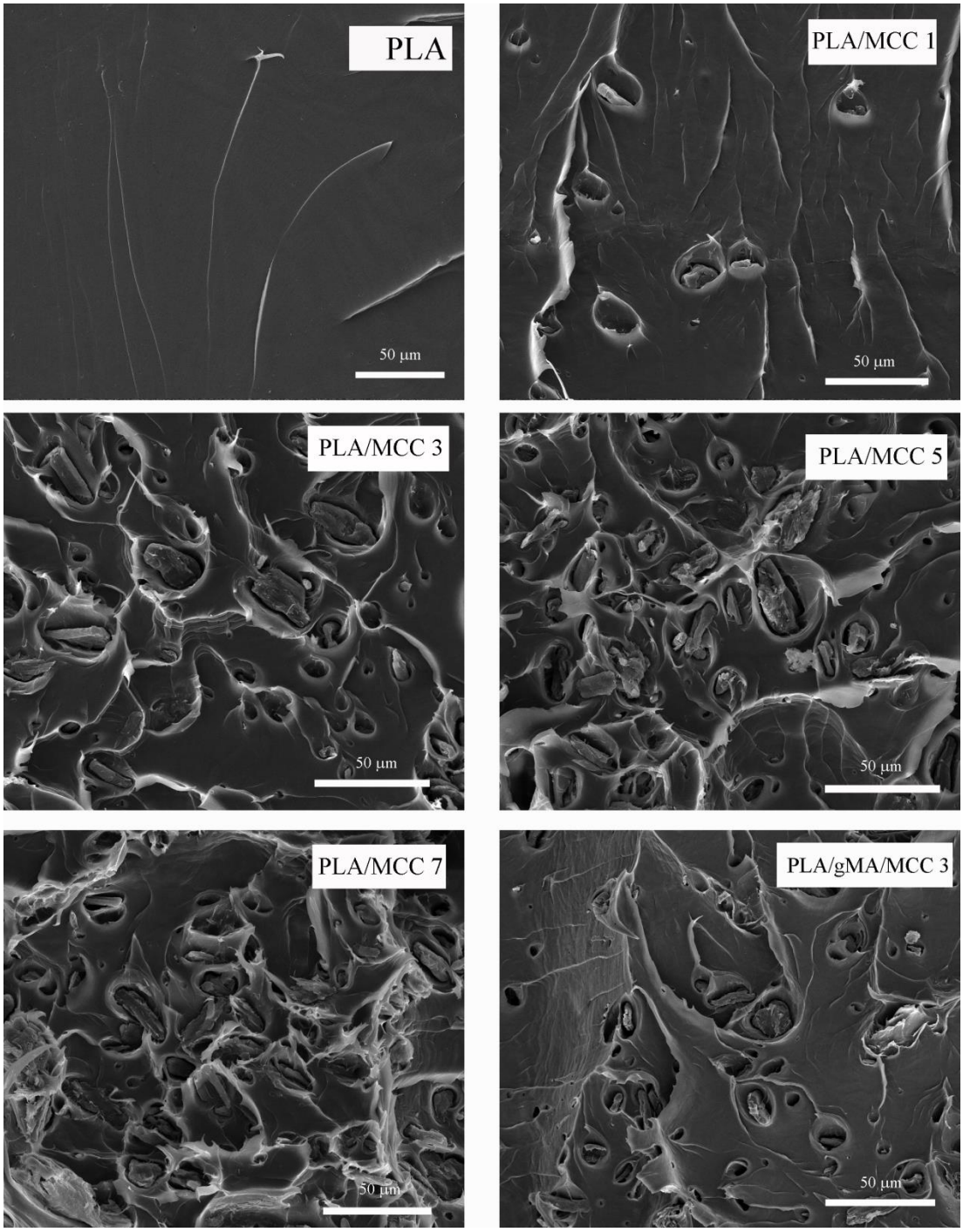

Figure 3.2 SEM fractographs showing dispersion state of MCCs in PLA matrix

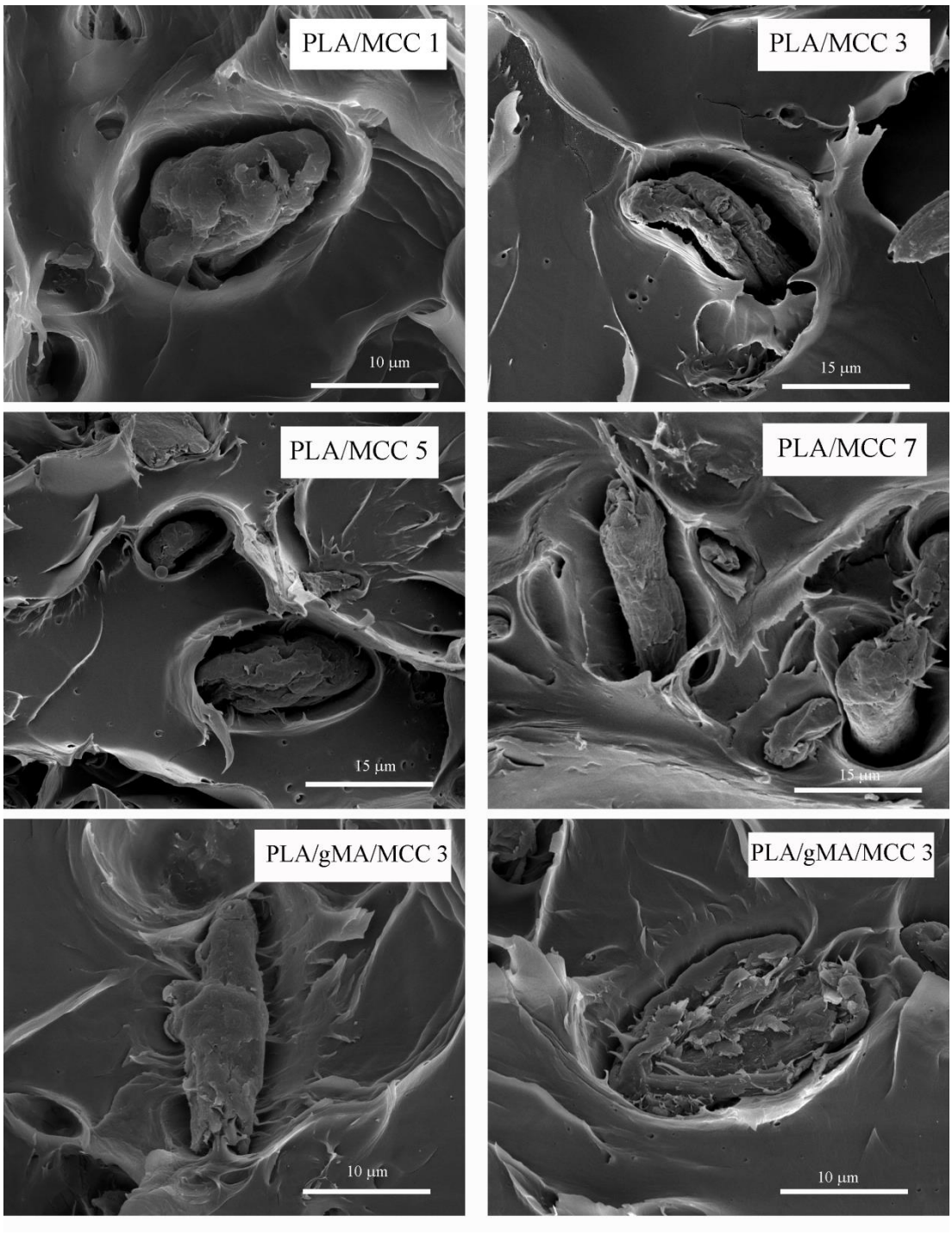

Figure 3.3 SEM fractographs showing interfacial morphology between the PLA matrix and MCC fillers

3.1.3 Modulus and Strength of the PLA/MCC Biocomposites

Effects of MCC content and MA compatibilization on the strength and modulus of PLA was investigated by tension tests and also by three-point bending tests. Figure 3.4 gives "tensile stress-strain" curves and "flexural stress-strain" curves of the specimens separately, while Table 3.1 tabulates values of "Tensile Modulus (E)" and "Tensile Strength (σ_{TS})" determined by tension tests; and values of "Flexural Modulus (E_{Flex})" and "Flexural Strength (σ_{Flex})" determined by bending tests. Furthermore, influences of different amount of MCC and MA compatibilization on the modulus and strength values of the biocomposites are also evaluated in Figures 3.5. Note that the data for the PLA/gMA/MCC 3 specimen in the x-axes of the Figure 3.5 was simply designated as "gMA".

It is known that elastic modulus and strength of the composite materials basically depend on the decrease in the mobility of the macromolecular chain structure of the matrix polymer, and the degree of the load transfer from the matrix to the rigid and strong filler material. Of course for these strengthening mechanisms to operate a sufficient degree of interfacial bonding between the matrix and the filler would be necessary.

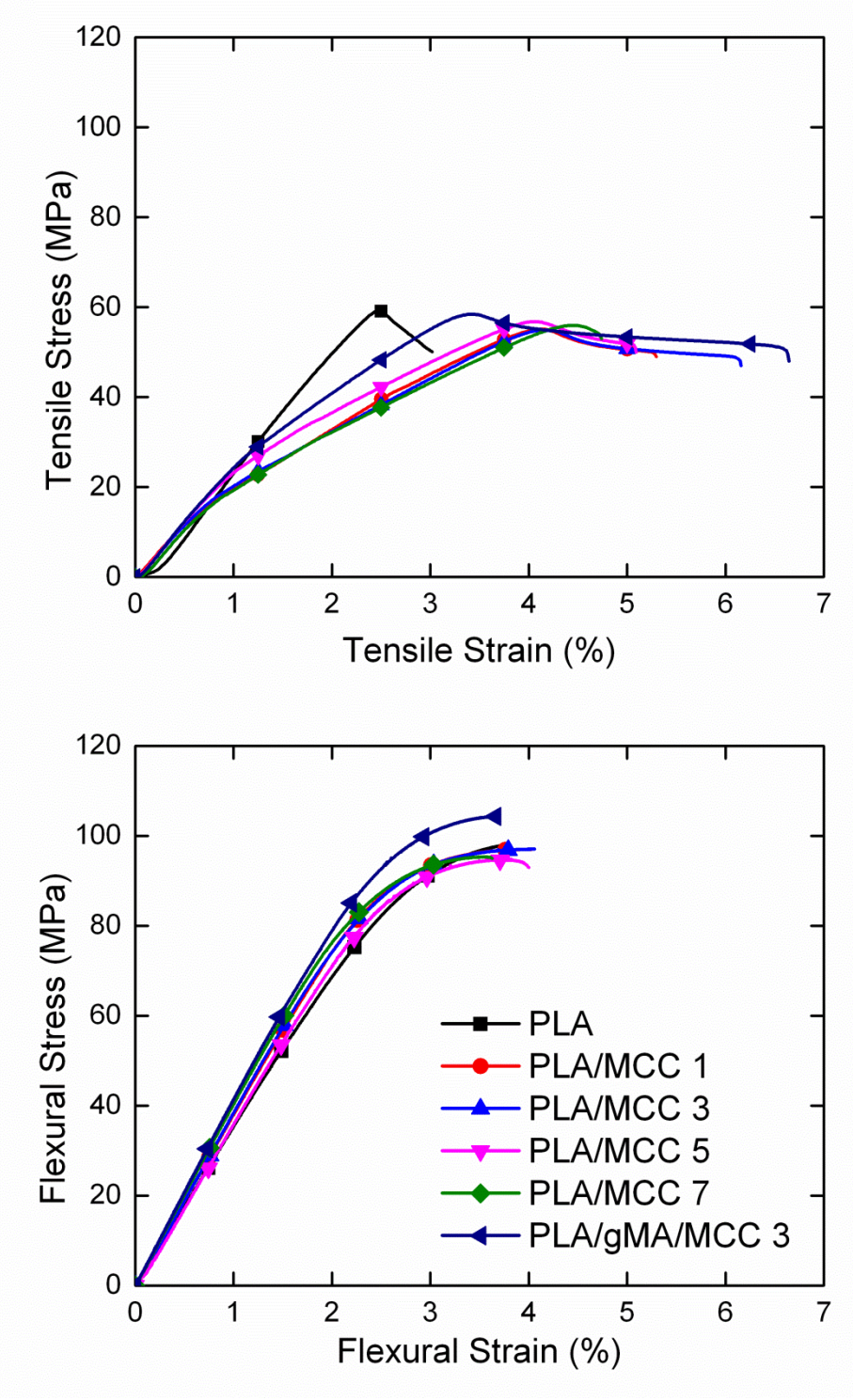

Figure 3.4 Stress-Strain curves of the specimens obtained during tensile and 3-point bending flexural tests

Table 3.1 Tensile Modulus (E), Flexural Modulus (E_{Flex}), Tensile Strength (σ_{TS}) and Flexural Strength (σ_{Flex}) of the Specimens

Specimens	E **(GPa)**	E_{Flex} **(GPa)**	σ_{TS} **(MPa)**	σ_{Flex} **(MPa)**
PLA	2.85±0.08	3.60±0.07	58.6±1.4	97.9±1.3
PLA/MCC 1	2.57±0.08	3.90±0.03	54.6±0.6	97.7±1.2
PLA/MCC 3	2.72±0.04	4.02±0.10	57.5±2.0	98.3±0.8
PLA/MCC 5	2.68±0.08	3.93±0.20	56.5±1.7	95.7±2.2
PLA/MCC 7	2.62±0.10	3.82±0.04	55.7±0.6	94.6±0.6
PLA/gMA/MCC 3	2.86±0.08	4.22±0.03	58.8±0.5	104.5±0.8

Under tensile loading, Figures 3.4, 3.5 and Table 3.1 show that modulus and strength of PLA decrease slightly with the incorporation of MCC fillers. Because, due to the weaker interaction between the polylactide chains and the crystalline cellulose chains, tensile loading leads to higher level of separation between the matrix and the filler. On the other hand, after maleic anhydride compatibilization, Table 3.1 indicates that the decreases in the tensile modulus and strength *(E* and σ_{TS}*)* are recovered, i.e. values of E and σ_{TS} of the neat PLA specimen are almost equal to the values of the PLA/gMA/MCC 3 specimen.

Under flexural loading, Figures 3.4, 3.5 and Table 3.1 reveal that modulus and strength values of the PLA/MCC biocomposites could be higher than that of the neat PLA. Because, during flexural 3-point bending tests, lower half of the cross-section of the bar specimen is under tension, while upper half of the cross-section is exposed to compressive forces. Therefore, in the compressive side of the specimen, separation at the interface would be hindered, leading to better load transfer mechanism from the matrix to the filler.

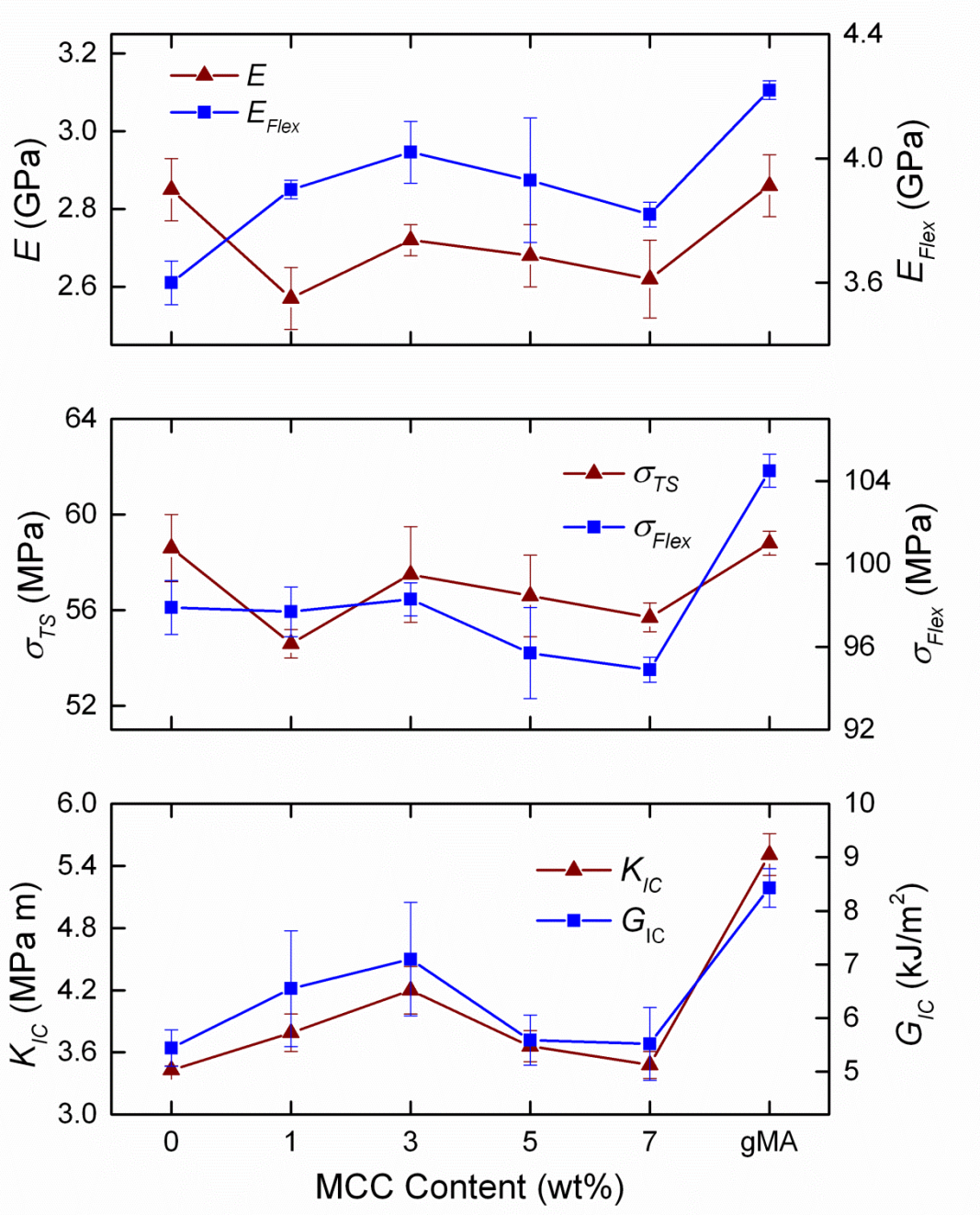

Figure 3.5 Effects of MCC content and MA Compatibilization on the mechanical properties of the specimens (note that gMA in the *x*-axes denotes PLA/gMA/MCC 3 specimen)

It is seen in Figure 3.5 and Table 3.1 that flexural modulus (E_{Flex}) of all PLA/MCC biocomposites is higher than that of the neat PLA. Since the specimen with 3 wt% MCC has the most uniform distribution in the matrix, the increase in the E_{Flex} value is 12% in the PLA/MCC 3 specimen. After MA compatibilization, due to the increased level of hydrogen bonding between the polylactide chains and the crystalline cellulose chains, the increase in E_{Flex} becomes 17% in the PLA/gMA/MCC 3 specimen.

Flexural strength (σ_{Flex}) of the neat PLA was kept in the specimens with 1 wt% and 3 wt% MCC contents, but slightly decreased in the biocomposites with 5 wt% and 7 wt% MCC due to the certain level of agglomeration. However, MA compatibilization increased σ_{Flex} of PLA from 97.9 MPa to 104.5 MPa, i.e. an increase of 7%.

3.1.4 Ductility and Toughness of the PLA/MCC Biocomposites

In tension tests apart from modulus and strength values another measurement is the amount of plastic strain formed until fracture, i.e. "% strain at break". That measurement is considered as "ductility" of materials which represents the total amount of permanent plastic deformation occurred up to fracture of the specimen. Figure 3.4 shows that tensile stress-strain curve of neat PLA specimen is very linear with very little amount of plastic strain. On the other hand, when MCC particles were added the stress-strain curves become non-linear possessing large amounts of plastic strain.

In this study ductility values of the specimens were determined as % final strain at break (ε_f) from their tensile stress-strain curves. Figure 3.4 and Table 3.2 show that ductility of all PLA/MCC biocomposites are much higher than for the neat PLA. The best improvement is again with 3 wt% MCC, increasing the ε_f value from 3.48% up

to 6.03%, i.e. an increase of 73%. After MA compatibilization, that increase reaches to 82%.

Table 3.2 Tensile Strain at Break (ε_f) and Fracture Toughness (K_{IC} and G_{IC}) of the Specimens

Specimens	ε_f **(%)**	K_{IC} **(MPa$\sqrt{m}$)**	G_{IC} **(kJ/m^2)**
PLA	3.48±0.25	3.43±0.04	5.44±0.34
PLA/MCC 1	5.47±1.30	3.79±0.06	6.55±0.23
PLA/MCC 3	6.03±1.70	4.20±0.14	7.10±0.18
PLA/MCC 5	5.17±0.93	3.66±0.08	5.59±0.38
PLA/MCC 7	4.93±0.54	3.48±0.13	5.52±0.52
PLA/gMA/MCC 3	6.33±0.98	4.92±0.20	8.43±0.36

Since the most significant deficiency of the biopolymer PLA is its inherent brittleness, toughness is the key property to be improved for many engineering applications. Therefore, in this research, influences of MCC content and MA compatibilization on the toughness of PLA were studied by "Fracture Toughness" tests. Because, fracture toughness is the most important toughness parameter required in structural engineering applications. This test basically measures ability of the materials to resist initiation and propagation of cracks. In this study, fracture toughness tests were evaluated in terms of "Critical Stress Intensity Factor (K_{IC})" and "Critical Strain Energy Release Rate (G_{IC})" values.

Figure 3.5 and Table 3.2 indicate that fracture toughness values of the PLA/MCC biocomposites are better than the values of the neat PLA. Because, rather weaker interfacial attraction between the matrix and the filler leads to improved efficiency of the basic composite toughening mechanisms of "debonding" and "pull-out" leading to lower crack propagation rate. Due to its uniform distribution, again PLA/MCC 3 specimen had the highest improvements; compared to neat PLA the increases in the values of K_{IC} and G_{IC} were 22% and 31%, respectively.

After MA compatibilization, i.e. better interfacial attraction, another composite toughening mechanism defined as "crack bowing" or "crack deflection" at the MCC particle also become operative leading to decreased crack growth rate. Therefore, for the PLA/gMA/MCC 3 specimen, the increases in K_{IC} and G_{IC} values become as much as 43% and 55%, respectively.

3.1.5 Thermal Properties of the PLA/MCC Biocomposites

Thermal properties of the biocomposites were first investigated by conducting DSC analyses. Figure 3.6 shows first heating thermograms of the specimens, while Table 3.3 tabulates important transition temperatures: "glass transition, crystallization, melting" (T_g, T_c , T_m), "enthalpies of melting and crystallization" (ΔH_m and ΔH_c), and also "percent crystallinity" (X_C) of the specimens obtained by using the following relation:

$$X_C = \frac{\Delta H_m - \Delta H_c}{w_{PLA} \Delta H_m^{\circ}} 100 \qquad (3.1)$$

In this relation, ΔH_m° represents melting enthalpy of 100% crystalline PLA determined as 93 J/g in the literature [67], while w_{PLA} represents weight fraction of the matrix PLA.

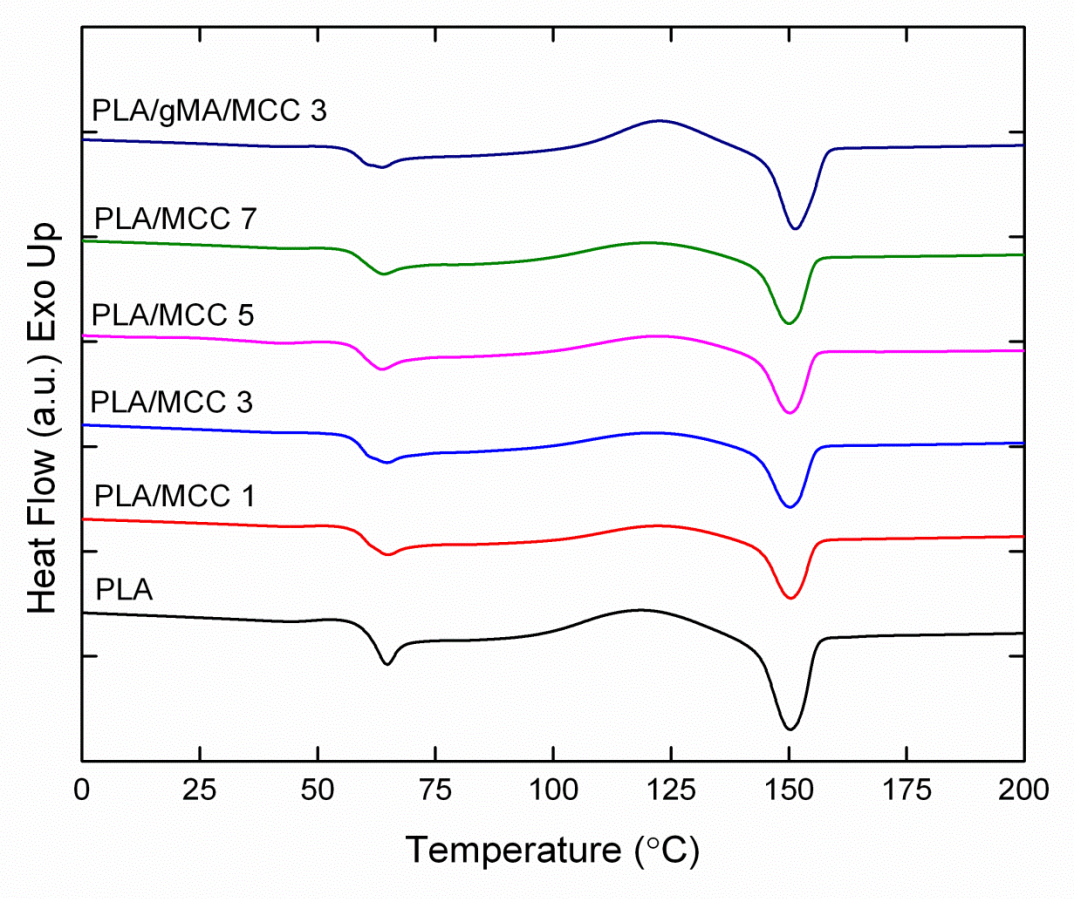

Figure 3.6 First heating DSC thermograms of the specimens

Table 3.3 indicates that MCC content and MA compatibilization have almost no influence on the glass transition, cold crystallization and melting temperatures of the PLA matrix. T_g of the matrix and biocomposites appear at 64-65^{o}C, while values of T_c are in the range of 120-123^{o}C and T_m are at around 150-151^{o}C.

Table 3.3 Transition Temperatures (T_g , T_c , T_m), Enthalpies (ΔH_m , ΔH_c) and Crystallinity Percent (X_C) of the Specimens During First Heating

Specimens	T_g **(°C)**	T_c **(°C)**	T_m **(°C)**	ΔH_m **(J/g)**	ΔH_c **(J/g)**	X_C **(%)**
PLA	65	120	151	16.2	1.2	16.1
PLA/MCC 1	65	122	151	15.3	0.7	15.8
PLA/MCC 3	65	124	151	15.8	0.9	16.5
PLA/MCC 5	64	123	150	15.6	1.1	16.4
PLA/MCC 7	64	122	150	15.9	1.4	16.7
PLA/gMA/MCC 3	64	123	151	18.9	0.6	20.3

Similarly, the crystallinity amount of the matrix and the biocomposites were around 16%. The only significant difference was the higher crystallinity percent (i.e. 20%) in the biocomposite specimen having MA compatibilization. Because, after the improvement of the interfacial bonding between the matrix and the filler, MCC particles could act as nucleation agents leading to higher level of the crystallization of the PLA matrix.

Thermal degradation behavior of the biocomposites were also investigated by thermogravimetric analysis (TGA) as given in Figure 3.7, while thermal degradation temperatures determined were tabulated in Table 3.4. In this table, $T_{5\%}$, $T_{10\%}$ and $T_{25\%}$ represent thermal degradation temperatures of the biocomposites at 5, 10 and 25 wt% mass losses, while T_{max} represents the temperature at maximum mass loss. It is seen that since polylactide and cellulose have similar thermal degradation ranges, there was no significant change in the thermal degradation temperatures of the PLA/MCC biocomposites.

Table 3.4 Thermal degradation temperatures ($T_{5\%}$, $T_{10\%}$,$T_{25\%}$) of the specimens at 5, 10 and 25 wt% mass losses and the maximum mass loss temperature (T_{max})

Specimens	$T_{5\%}$ **(°C)**	$T_{10\%}$ **(°C)**	$T_{25\%}$ **(°C)**	T_{max} **(°C)**
PLA	330	340	352	367
PLA/MCC 1	326	337	350	366
PLA/MCC 3	332	342	353	366
PLA/MCC 5	331	340	351	363
PLA/MCC 7	329	338	349	362
PLA/gMA/MCC 3	331	341	352	366

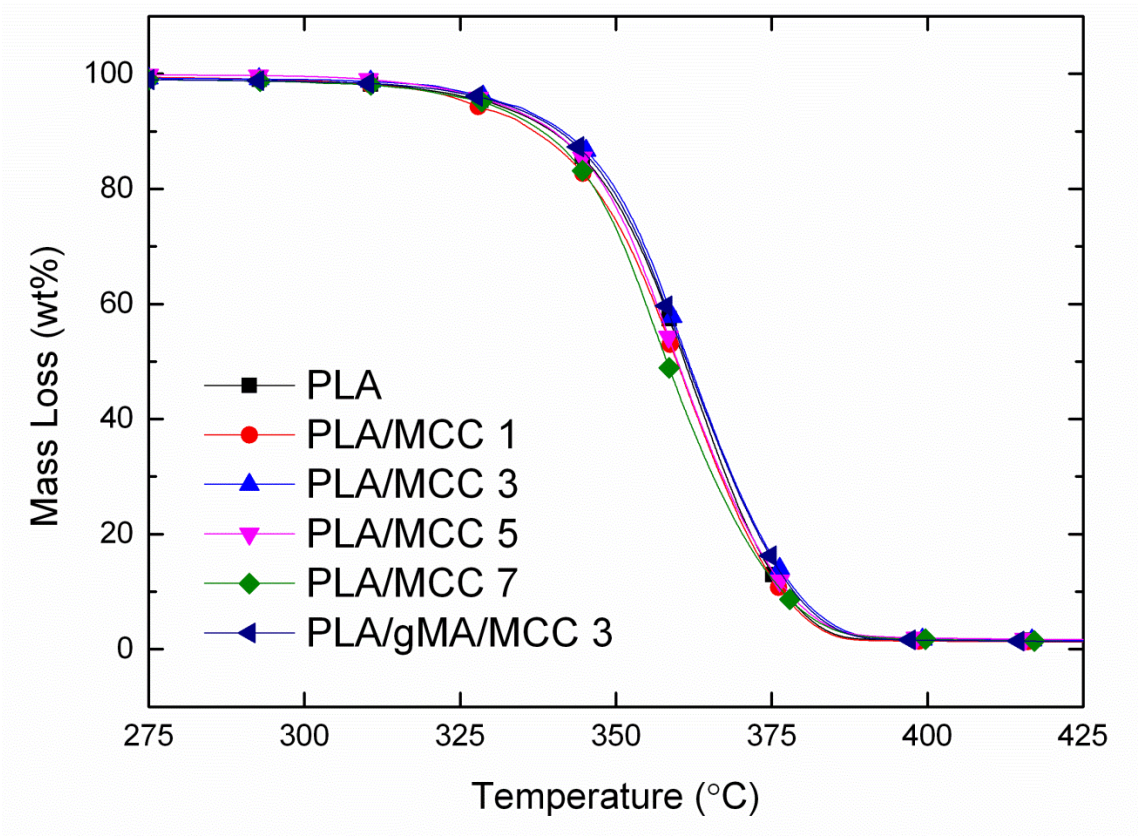

Figure 3.7 Thermogravimetric curves of the specimens

3.2 Effects of Accelerated Weathering

Consequences of each accelerated weathering period on the neat PLA and its 3 wt% MCC biocomposite specimens were investigated by comparing the changes in the crystallinity, color, molecular weight, chemical structure, mechanical properties and thermal behavior of the specimens as discussed successively in the following sections.

3.2.1 Changes in the Crystallinity

It is known that [68-70] the most stable crystal structure of PLA is orthorhombic α phase giving X-ray diffraction peaks at two different 2θ locations of 16.3^{o} and 18.7^{o} from (110)/(200) and (203) planes, respectively.

The bottom curves in Figure 3.8(a) and (b) are the X-ray diffractograms of the injection molded neat PLA and its 3 wt% MCC biocomposite specimens, respectively. It is seen that these curves have no sharp crystallization peaks, they have only very broad halo representing the amorphous structure of PLA. Because, PLA has very slow crystallization rate; thus, due to the very fast cooling rate during injection molding, macromolecular chains of PLA have no sufficient time to crystallize.

On the other hand, after each accelerated weathering period, Figure 3.8(a) and (b) show that all X-ray diffractograms have very sharp peaks of α crystal phase at the 2θ locations of 16.3^{o} and 18.7^{o}. Because, UV irradiation cycles of accelerated weathering take place at 70^{o}C for 8 h, which provides sufficient energy and time for the PLA chains to crystallize.

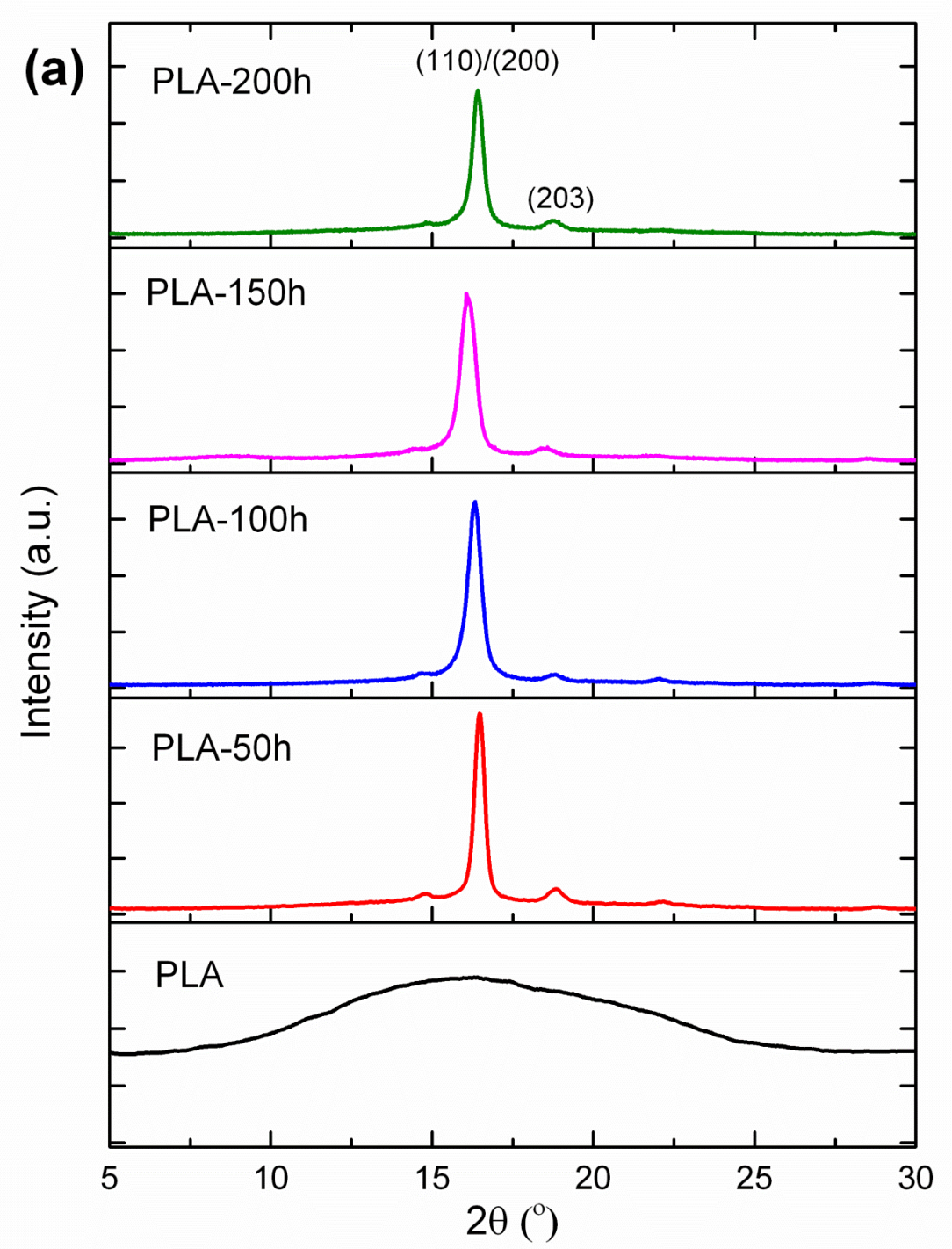

Figure 3.8 X-ray diffractograms of the specimens before and after each accelerated weathering period: (a) neat PLA, (b) PLA/MCC biocomposite

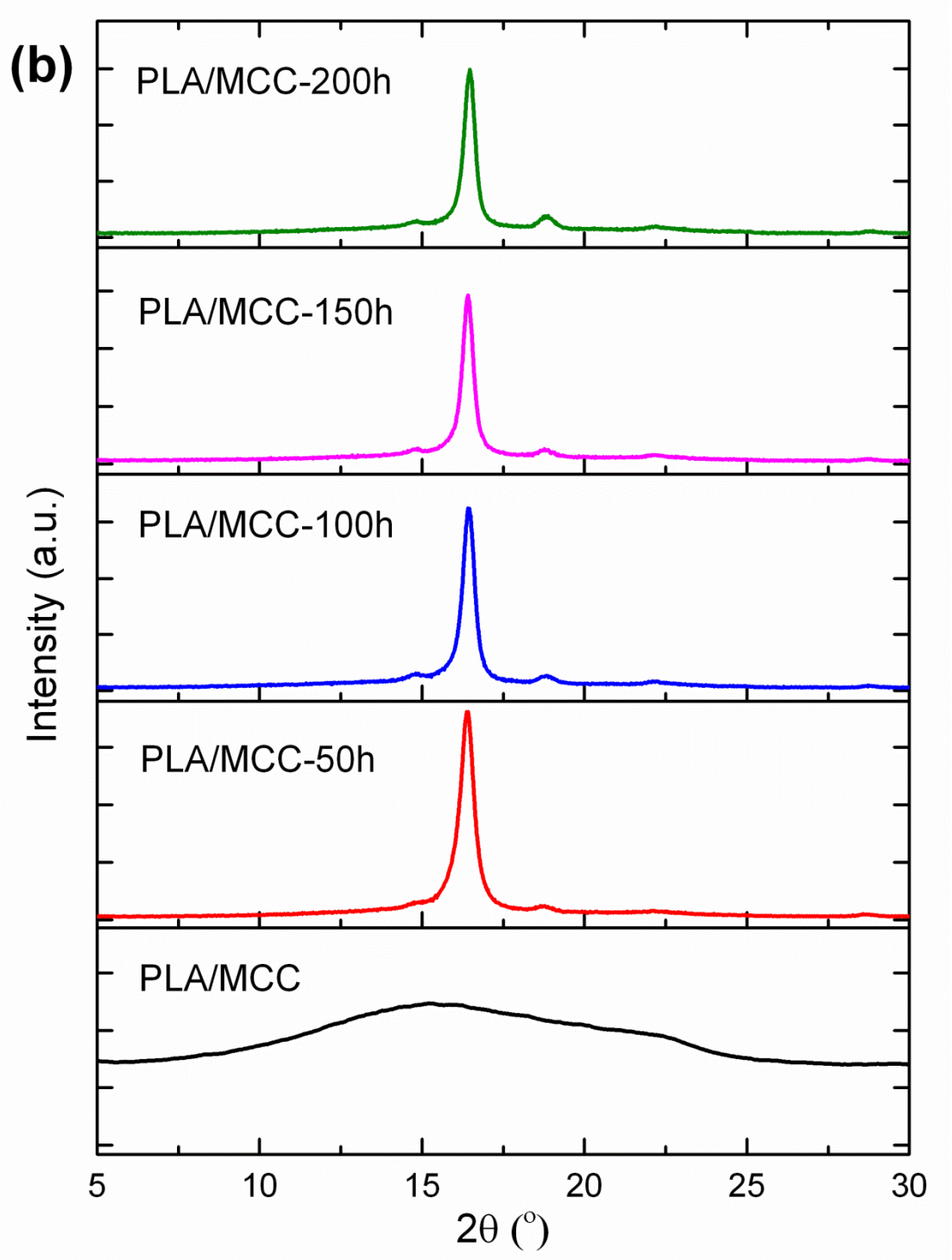

Figure 3.8 (Continued)

3.2.2 Changes in the Color

Color change is a significant problem in the outdoor use of polymeric components. Changes in the color was first evaluated by comparing the photographic images of the neat PLA and its 3 wt% MCC biocomposite specimens after each accelerated weathering period. Figure 3.9 show that neat PLA specimen looks colorless, i.e. very transparent due to the high degree of amorphous structure. Because, as discussed in the above section, very fast cooling rate of injection molding will not allow PLA chains to have conformational ability for crystallization.

Figure 3.9 also shows that after only 50 h accelerated weathering; the color of the neat PLA specimen became white due to the certain level of cold crystallization process occurred during weathering. It can be seen that there was no significant change in the white color of the PLA specimens after weathering periods of 100 h, 150 h and 200 h.

When 3 wt% MCC was added into PLA matrix, Figure 3.9 shows that biocomposite specimen has a kind of glossy creamy color. After each accelerated weathering period, the slight changes in the color of this PLA/MCC specimen was especially in the form of loss of glossy character.

Secondly, a quantitative color change evaluation was conducted by comparing the CIELAB color space parameters L^*, a^*, b^* and the total color difference parameter ΔE^* of the specimens before and after each accelerated weathering period. Table 3.5 tabulates these data determined by diffused reflectance analysis (DRA).

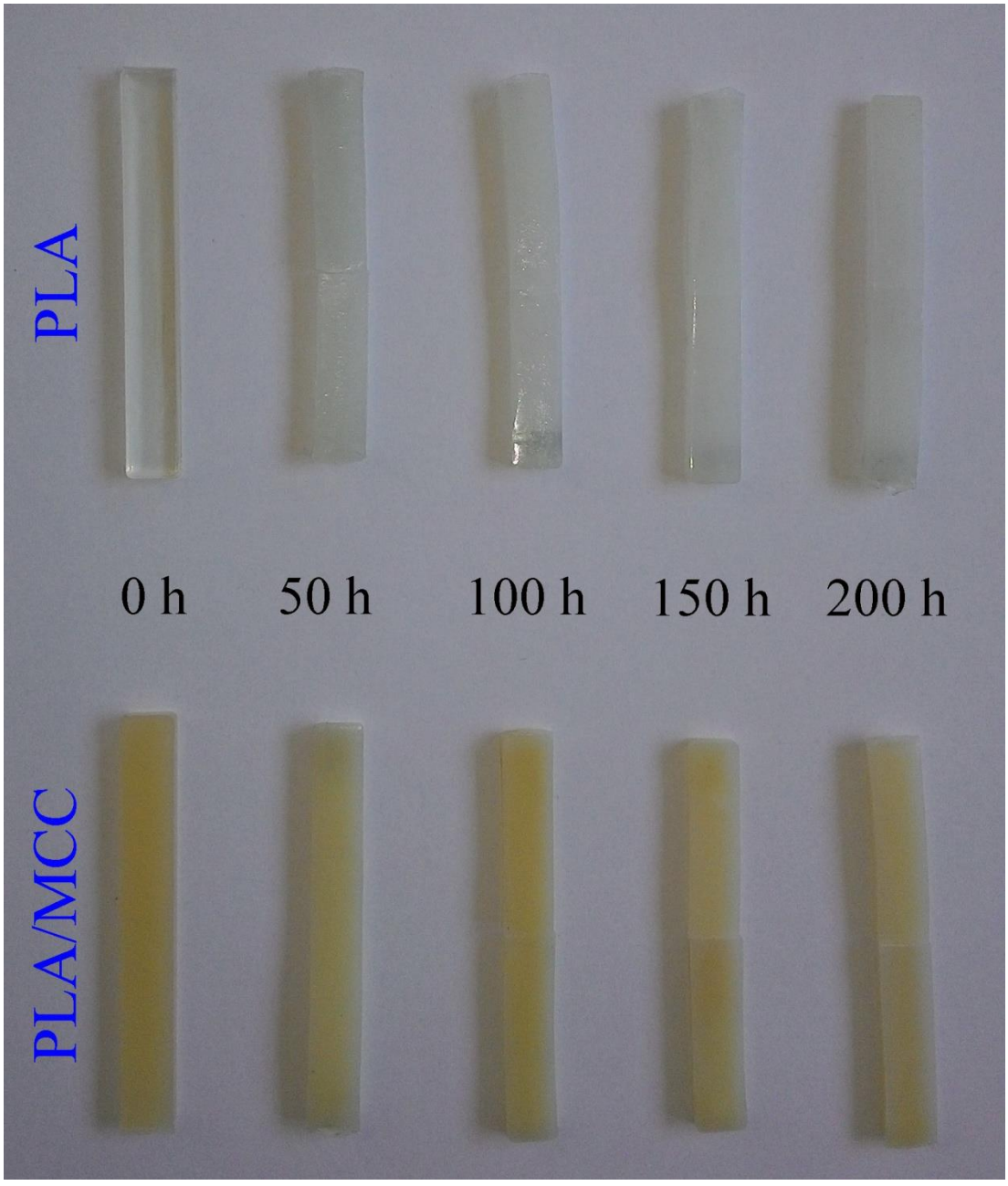

Figure 3.9 Photographic images showing slight changes in the color of the neat PLA and its MCC biocomposite specimens after each accelerated weathering period

Table 3.5 indicates that changes in the color parameters (especially L^* and consequently ΔE^*) take place between the unweathered specimens and 50 h accelerated weathering specimens. Further accelerated weathering periods resulted in only very slight changes in these color parameters. Thus, it can be said that visual color changes in Figure 3.9 are in accordance with the quantitative color parameters given in Table 3.5

Table 3.5 CIELAB color space parameters (L^*, a^*, b^*) and color change difference (ΔE^*) values of the neat PLA and its 3 wt% MCC biocomposite specimens before and after each accelerated weathering period

Specimens	**L***	**a***	**b***	**ΔE***
PLA	16.71	-0.31	-0.64	
PLA-50h	22.49	-0.48	-3.26	6.34
PLA-100h	23.22	-0.29	-3.05	6.94
PLA-150h	22.41	-0.37	-3.71	6.47
PLA-200h	22.38	-0.24	-3.93	6.55
PLA/MCC	26.53	-0.65	-0.16	
PLA/MCC-50h	35.31	-0.71	-1.10	8.84
PLA/MCC-100h	37.92	-0.82	-0.95	11.42
PLA/MCC-150h	38.96	-0.71	-1.76	12.53
PLA/MCC-200h	39.52	-0.65	-1.64	13.08

3.2.3 Changes in the Chemical Structure

Before IR spectroscopy, static light scattering (SLS) spectrometry was used to determine the level of chain scission in the PLA matrix after each accelerated weathering period. Figure 3.10 reveals drastic decrease in the weight average molecular weight (M_w) of the PLA matrix due to the chemical degradation via photolysis and hydrolysis. It is seen in Figure 3.10 that M_w of unweathered PLA matrix ($3.7x10^5$) decreases to $1.3x10^5$ after 100 h accelerated weathering, and drops down to $0.8x10^5$ after 200 h. As will be discussed in the following sections later, these drastic drops in M_w of PLA matrix after each accelerated weathering period resulted in certain level of reductions in the mechanical properties of the specimens.

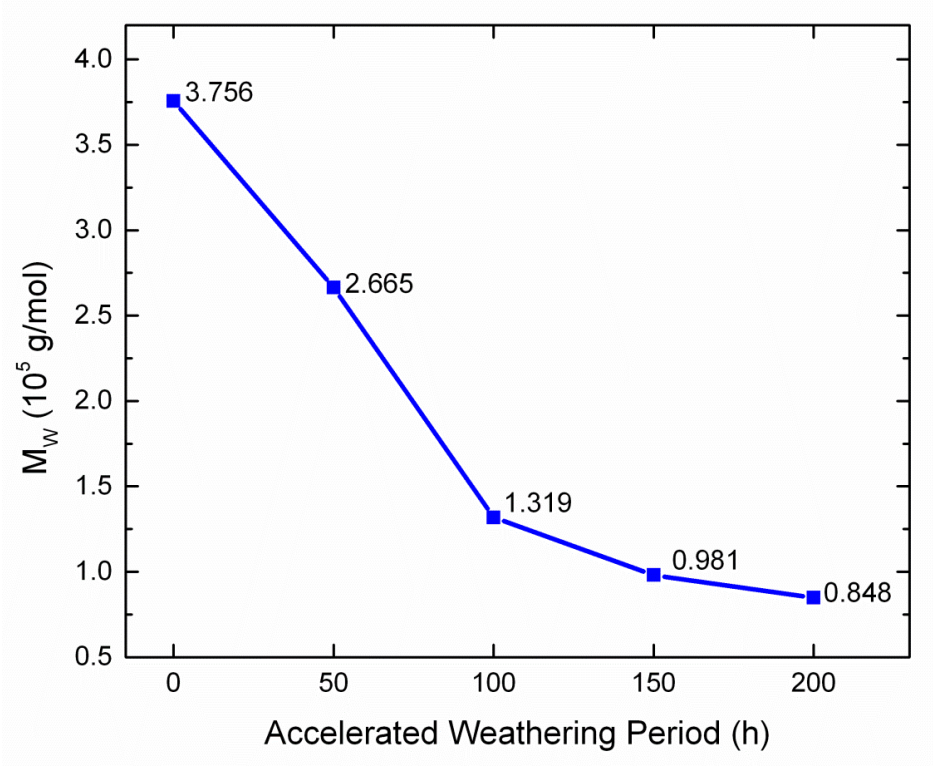

Figure 3.10 Drastic decrease in the weight average molecular weight of the PLA matrix after each accelerated weathering period

Then, changes in the chemical structure of the neat PLA and its 3 wt% MCC biocomposite specimens after each accelerated weathering period were compared by ATR-FTIR analyses as shown in Figure 3.11(a) and (b), respectively. It is known that PLA structure is identified basically by five characteristic IR bands [16, 47, 49, 57]; which were all in accordance with the IR bands observed in this study. These are: C-C stretching at 867 cm^{-1}, C-O stretching peaks at 1079, 1126, 1181 and 1264 cm^{-1}, C-H deformation peaks at 1377 and 1452 cm^{-1}, C=O ester carbonyl groups at 1748 cm^{-1}, and C-H stretching at 2853, 2924 cm^{-1}.

It has been discussed that the main degradation mechanism of UV irradiation is known as "photolysis" leading to "chain scission" especially in the C-O and C-C bonds of the PLA ester backbone structure by absorption of a photon [16, 47, 48]. Therefore, after weathering, intensities of these IR bands are decreased as seen in Figure 3.11.

Apart from photolysis, another consequence of UV irradiation discussed is the "photo-oxidation" that might result in first organic peroxide formation and then their subsequent degradation into carboxylic acid and ketone end groups having C=O bonds [16, 47, 48]. Therefore after weathering, it is discussed that intensity of that IR band either increase or shift to lower wavenumbers. Figure 3.11 indicates that especially after 200 h of accelerated weathering, there is substantial increase in the intensity of C=O bond, and also shifting from 1748 cm^{-1} to 1729 cm^{-1}. Moreover, it is also discussed that, C-O stretching peaks might also shift to lower wavenumbers. Figure 3.11 reveals that these C-O shifts observed after 200 h were from1079 to 1064 cm^{-1}, from 1181 to 1158 cm^{-1}, and from 1264 to 1258 cm^{-1}.

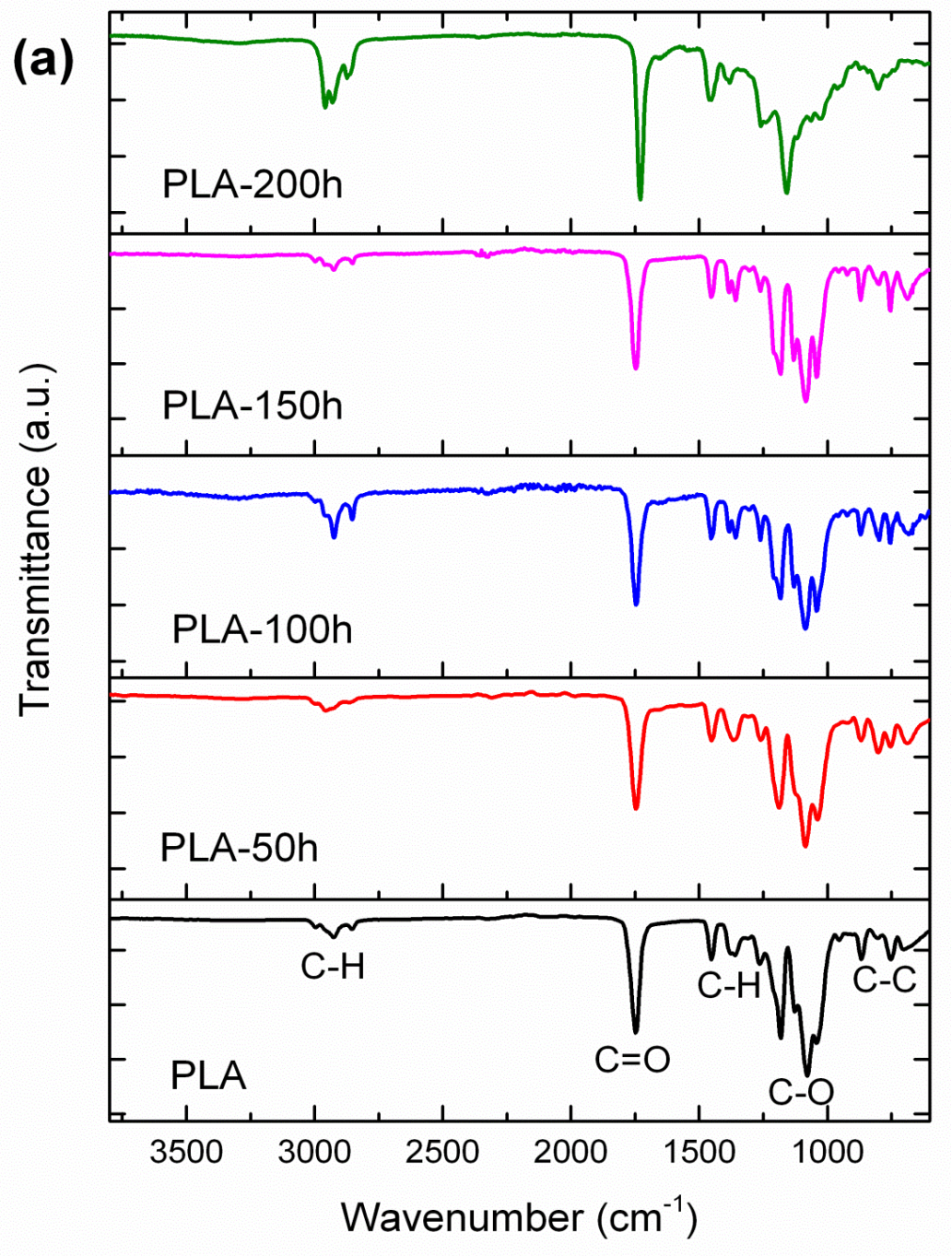

Figure 3.11 ATR-FTIR spectra of the specimens before and after each accelerated weathering period: (a) neat PLA, (b) PLA/MCC biocomposite

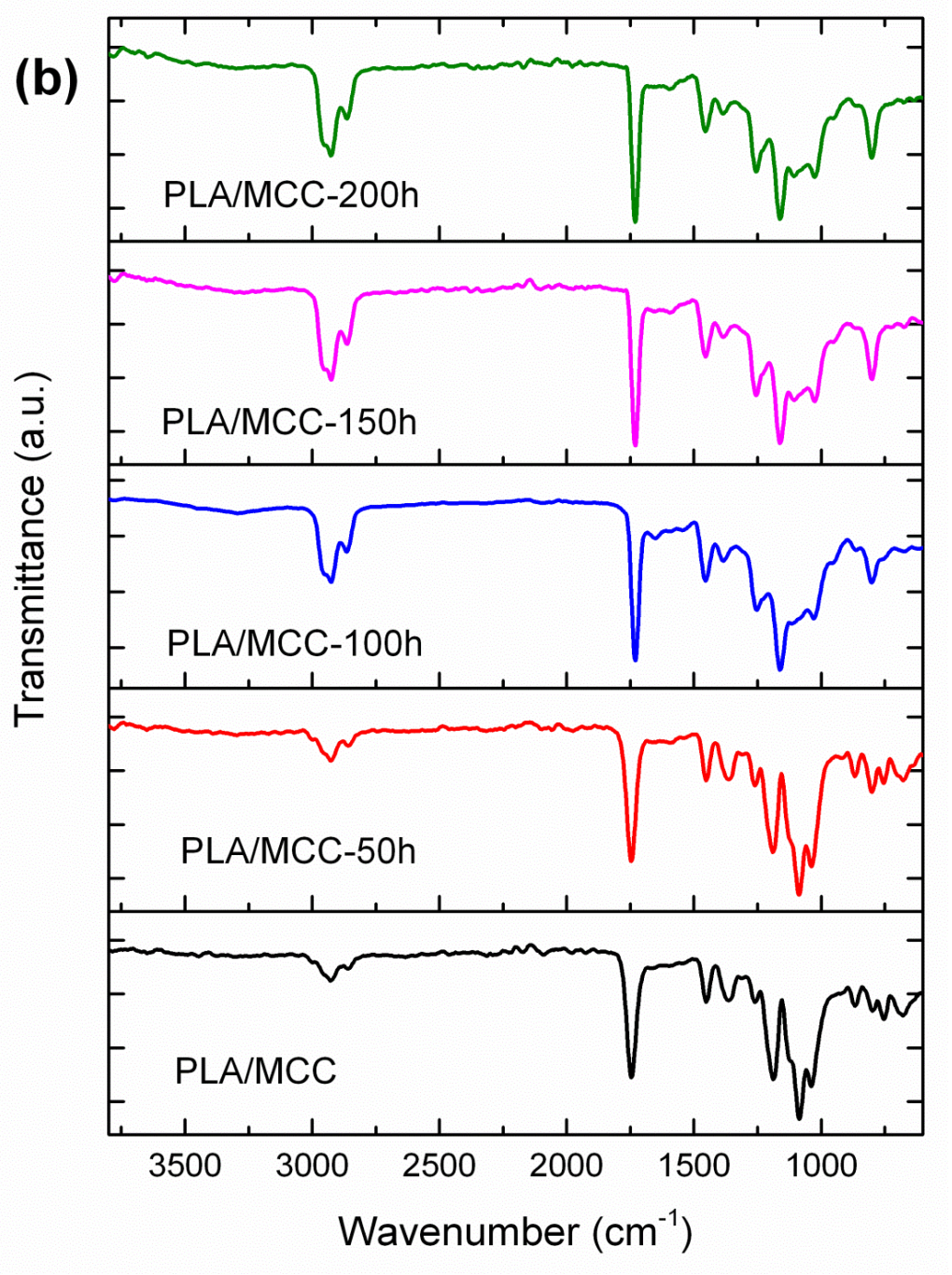

Figure 3.11 (Continued)

Besides UV radiation at 70^{o}C, another important step during accelerated weathering tests was the humidity (condensation) steps at 50^{o}C. Apart from swelling and plasticization, the main degradation mechanism of humidity is defined as "hydrolysis". It is known that hydrolysis also contributes to main chain scission especially in the C-O bonds of the ester structure of PLA [47, 49, 57]. It was also indicated that, just like photo-oxidation, hydrolysis might also lead to formation of carboxylic acid and ketone end groups. Therefore, changes in the IR spectrum of the specimens due to hydrolysis would be very similar to the changes discussed above.

3.2.4 Changes in the Morphology

Changes in the fracture surface morphology of the specimens were evaluated by comparing the SEM images of the fracture surface of fracture toughness test specimens before and after each accelerated weathering period as given in Figure 3.12. It is seen in Figure 3.12(a) that neat PLA specimen before weathering has very smooth brittle surface while Figure 3.12(b) shows that PLA/MCC biocomposite specimen before weathering has rather ductile fracture surface with randomly distributed MCC particles.

Due to severe chemical degradation in the structure of the specimens, Figure 3.12 indicates that during each period of accelerated weathering there are extensive number of deep dimples, cleavages and cracking on the fracture surface of the specimens.

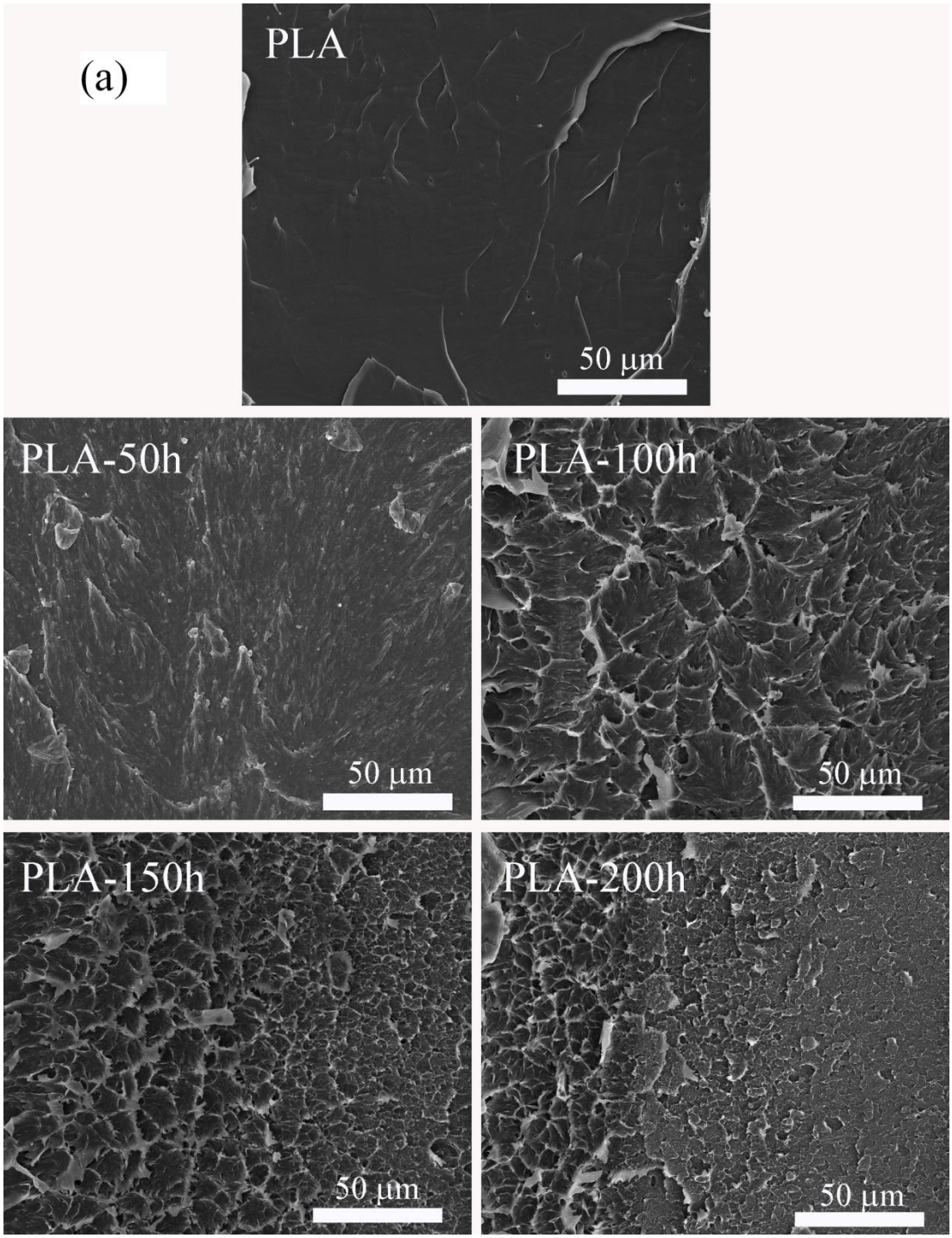

Figure 3.12 SEM images showing fracture surface morphology of the specimens before and after each accelerated weathering period: (a) neat PLA, (b) PLA/MCC biocomposite

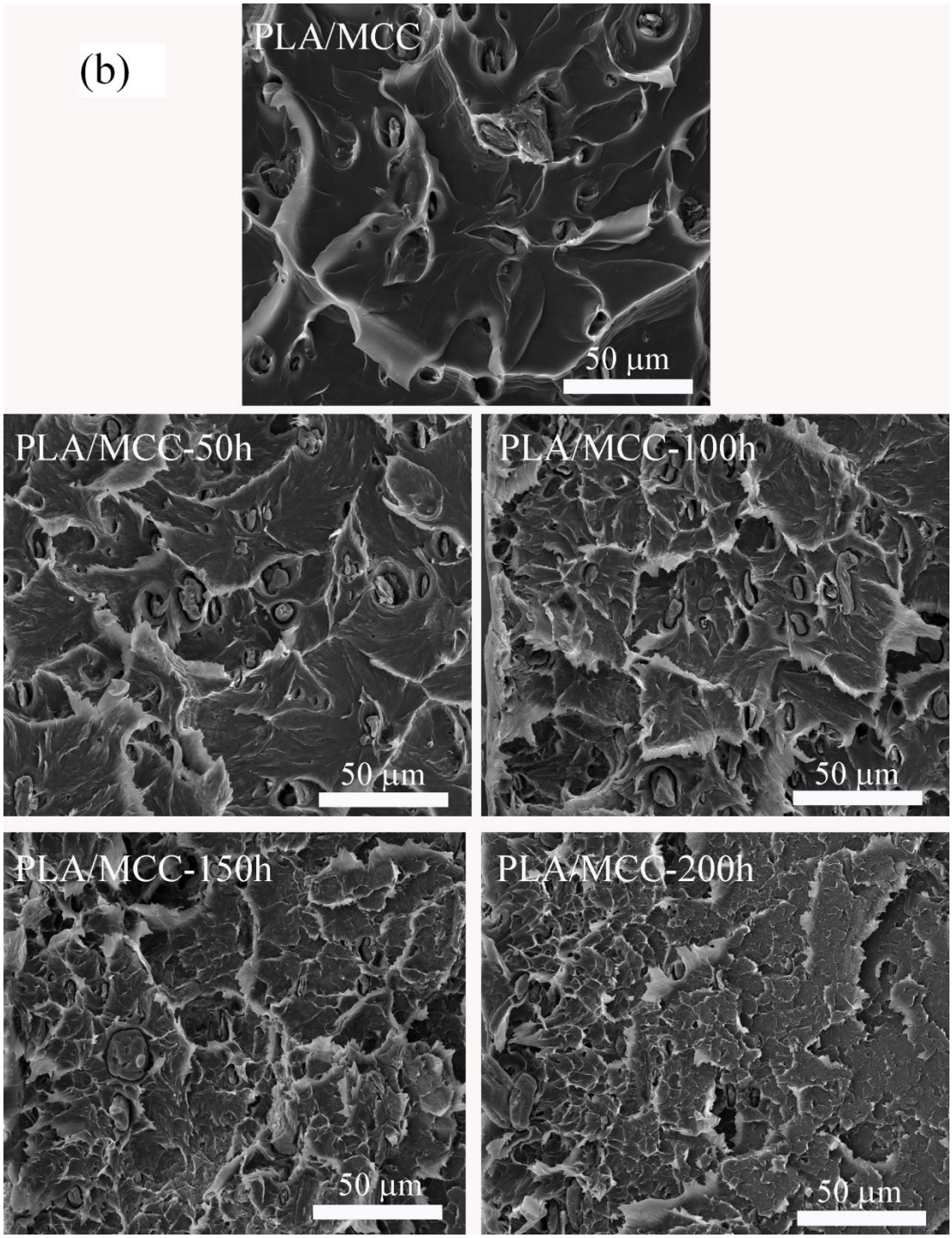

Figure 3.12 (Continued)

3.2.5 Changes in Mechanical Properties

Changes in modulus and strength of the neat PLA and its 3 wt% MCC biocomposite specimens was investigated by tension tests and also by three point bending tests. Figure 3.13 and 3.14 give "tensile stress-strain" and "flexural stress-strain" curves, respectively, while Table 3.6 tabulates values of "Tensile Modulus (E)" and "Tensile Strength (σ_{TS})" determined by tension tests; and values of "Flexural Modulus (E_{Flex})" and "Flexural Strength (σ_{Flex})" determined by bending tests. Furthermore, influences of accelerated weathering periods on the modulus and strength values of the specimens are also evaluated in Figure 3.15.

Table 3.6 and Figure 3.15 indicate that elastic modulus (both E and E_{Flex}) values of neat PLA and its 3 wt% MCC biocomposite increase after 50 h of accelerated weathering. For instance, the increase in E_{Flex} values for neat PLA is 27%, while it is 14% for the PLA/MCC biocomposite. As discussed above, the reason for these increases is the increased crystallinity of the PLA matrix. Because, unweathered injection molded PLA structure is mainly amorphous. During weathering, UV irradiation cycles at 70^{o}C resulted in cold crystallization of PLA chains.

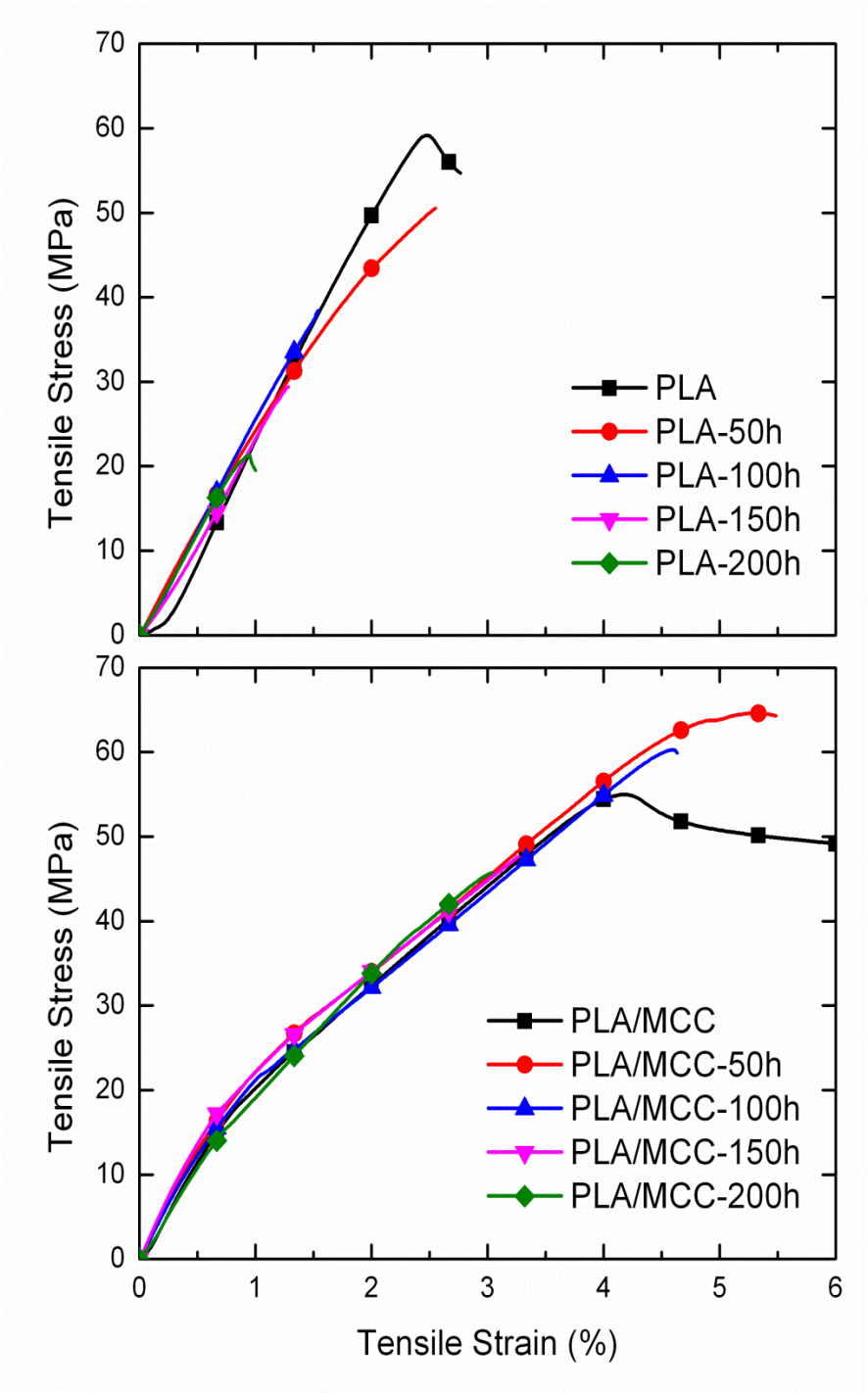

Figure 3.13 Tensile stress-strain curves of the neat PLA and its MCC biocomposite specimens before and after each accelerated weathering period

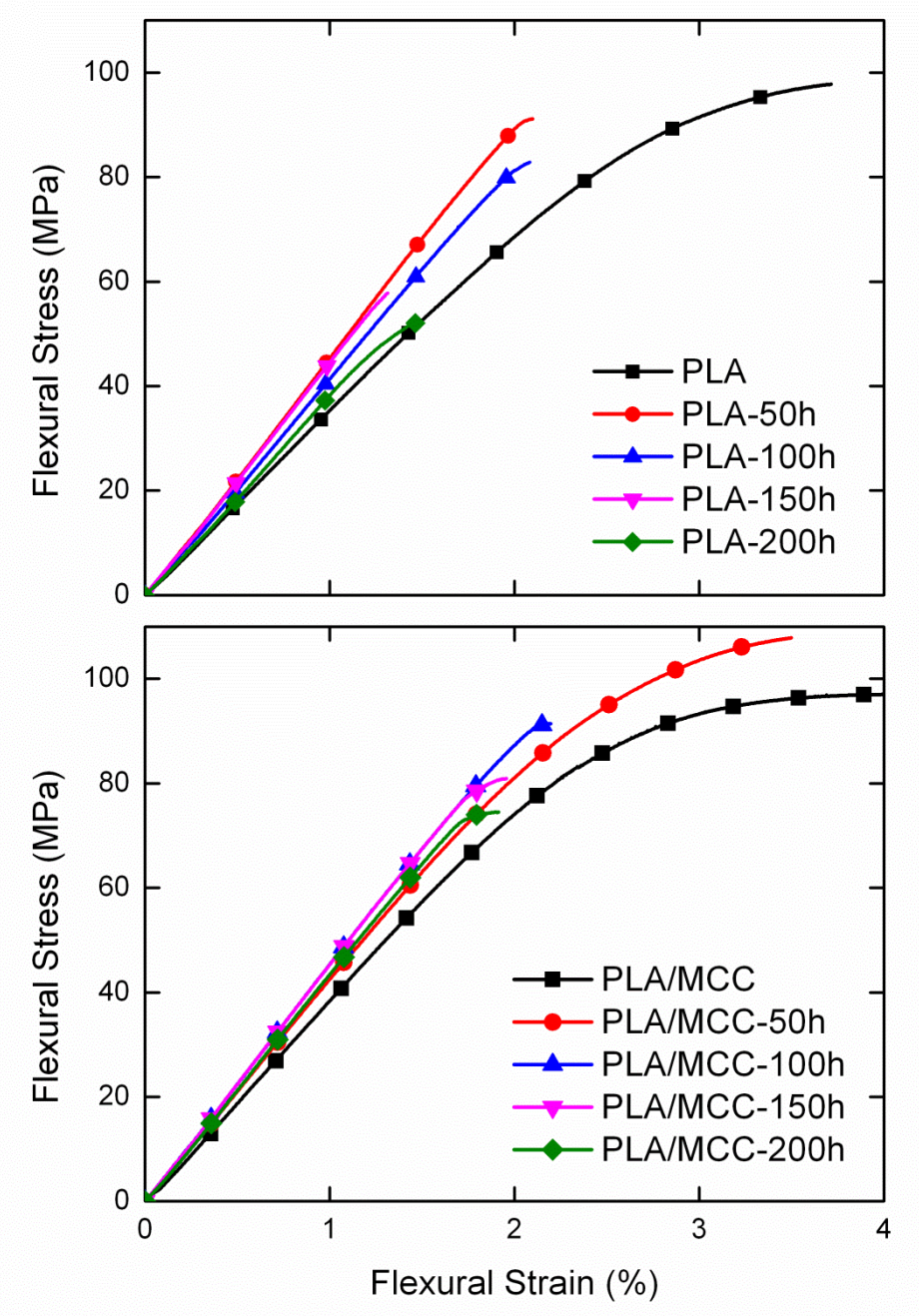

Figure 3.14 Flexural stress-strain curves of the neat PLA and its MCC biocomposite specimens before and after each accelerated weathering period

Table 3.6 Tensile Modulus (E), Flexural Modulus (E_{Flex}), Tensile Strength (σ_{TS}) and Flexural Strength (σ_{Flex}) of the neat PLA and its 3 wt% MCC biocomposite specimens before and after each accelerated weathering period

Specimens	E **(GPa)**	E_{Flex} **(GPa)**	σ_{TS} **(MPa)**	σ_{Flex} **(MPa)**
PLA	2.85±0.08	3.60±0.07	58.6±1.4	97.9±1.3
PLA-50h	2.89±0.16	4.58±0.09	51.6±1.1	93.0±1.9
PLA-100h	2.86±0.18	4.51±0.01	39.1±0.6	82.8±0.2
PLA-150h	2.73±0.09	4.21±0.04	29.5±1.2	57.7±2.7
PLA-200h	2.43±0.13	4.12±0.13	22.8±1.5	52.3±0.6
PLA/MCC	2.72±0.04	4.02±0.10	57.5±2.0	98.3±0.8
PLA/MCC-50h	2.98±0.10	4.59±0.07	64.3±1.0	107.6±1.5
PLA/MCC-100h	2.86±0.19	4.53±0.09	59.1±1.6	91.5±0.6
PLA/MCC-150h	2.69±0.11	4.38±0.07	51.0±0.3	83.7±9.4
PLA/MCC-200h	2.61±0.28	4.27±0.09	43.7±3.1	75.0±6.8

However, accelerated weathering beyond 50 h, chemical degradation due to photolysis, photo-oxidation and hydrolysis was more dominant than the stiffening action of the crystallinity. Therefore, both elastic modulus values (E and E_{Flex}) decreased gradually. For example, after 200 h, compared to the highest values of 50 h weathering, the decreases in E_{Flex} values were 10% for PLA, and 7% for PLA/MCC specimens. On the other hand, E_{Flex} values after 200 h were still more than the E_{Flex} values of the unweathered PLA and PLA/MCC specimens.

In terms of strength (both σ_{TS} and σ_{Flex}), Table 3.6 and Figure 3.15(a) show that increase in the crystallinity was not sufficient to keep the strength values of the unweathered neat PLA specimen. Severe actions of chain scission resulted in the gradual decreases of strength values after each accelerated weathering period. At the end of 200 h total accelerated weathering, σ_{TS} of neat PLA decreased 61%, while this decrease in σ_{Flex} was 47%.

In the specimen of PLA/MCC biocomposite, Table 3.6 and Figure 3.15(b) this time show that after 50 h accelerated weathering, there are certain level of increases in the values of strength; such as 12% in σ_{TS} and 10% in σ_{Flex}, respectively. These increases were not just benefits of higher crystallinity, but also due to the additional composite strengthening mechanisms That is, "decrease of mobility" of PLA chains and "load transfer" from the PLA matrix to MCC reinforcements. However, beyond 50 h accelerated weathering, decrease of M_w of the PLA matrix was dominant leading to gradual decrease in the strength values. At the end of 200 h weathering, compared to unweathered PLA/MCC biocomposite, both σ_{TS} and σ_{Flex} decreased 24%.

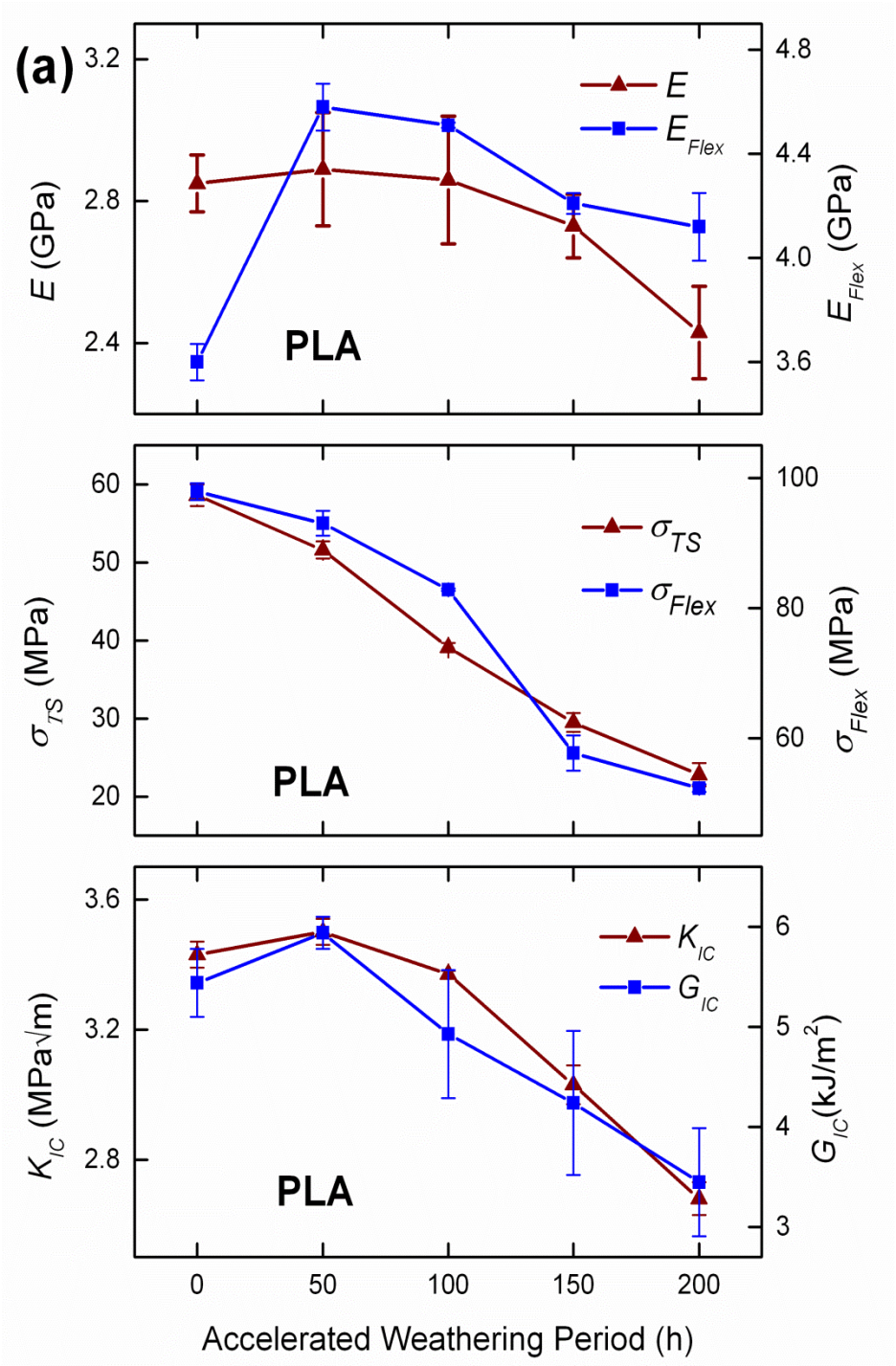

Figure 3.15 Effects of each accelerated weathering period on the mechanical properties of the specimens: (a) neat PLA, (b) PLA/MCC biocomposite

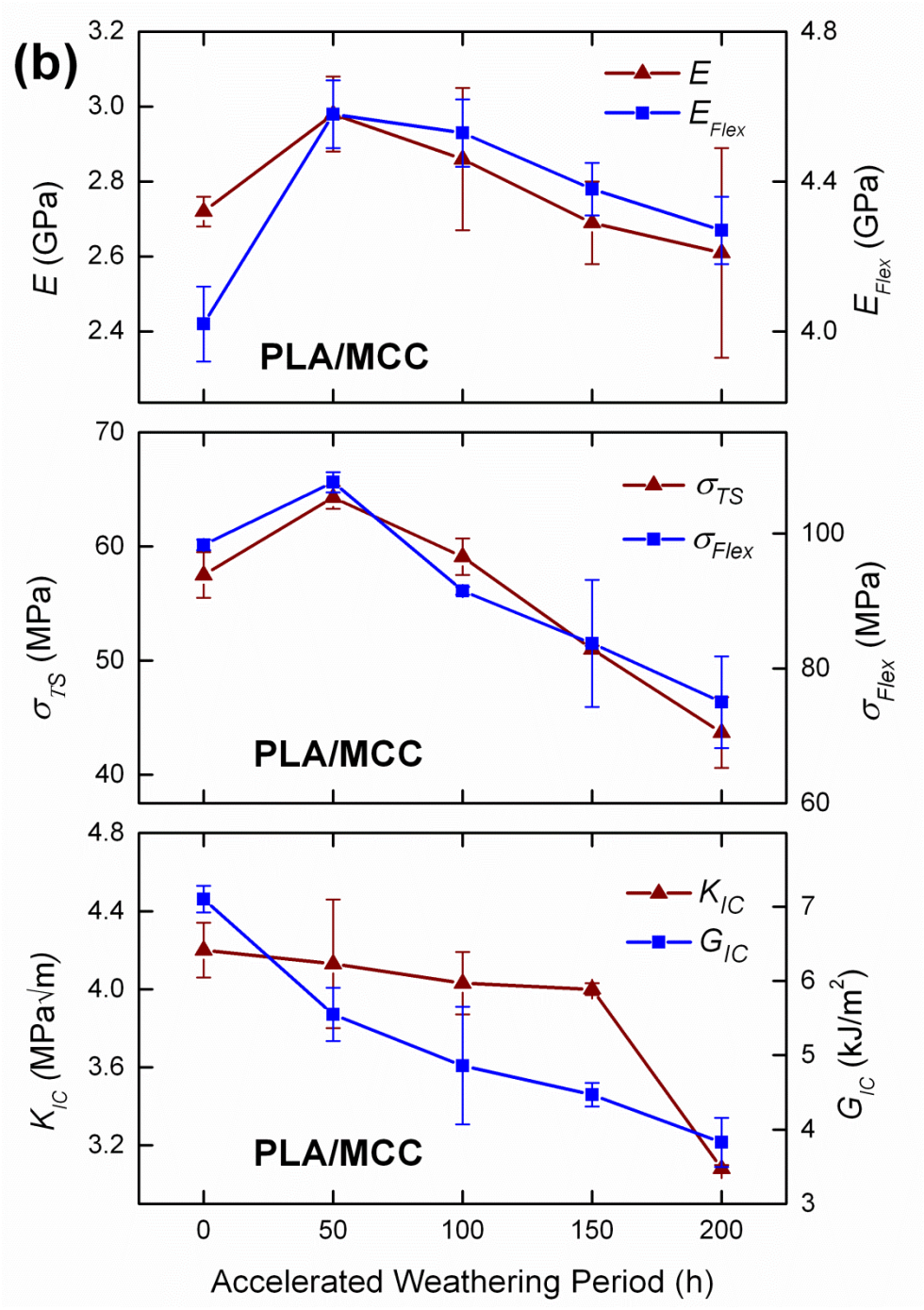

Figure 3.15 (Continued)

Changes in ductility of the neat PLA and its 3 wt% MCC biocomposite specimens was evaluated by comparing the "%final strain at break" (ε_f) values. These data were determined from their tensile stress-strain curves given in Figure 3.13, and tabulated in Table 3.7. It is clearly seen that ε_f values of each specimen drop successively with increasing accelerated weathering period; the drop after 200 h weathering in PLA is 69%, while in PLA/MCC it is 49%. Decreases in the ductility of the specimens, that is decreases in the ability of the specimens to have permanent plastic deformation up to fracture, are again due to the deteriorated molecular weight of the PLA matrix.

Table 3.7 Tensile Strain at Break (ε_f) and Fracture Toughness (K_{IC} and G_{IC}) of the neat PLA and its 3 wt% MCC biocomposite specimens before and after each accelerated weathering period

Specimens	ε_f **(%)**	K_{IC} **(MPa$\sqrt{m}$)**	G_{IC} **(kJ/m^2)**
PLA	3.48±0.25	3.43±0.04	5.44±0.34
PLA-50h	2.39±0.19	3.50±0.04	5.94±0.16
PLA-100h	1.51±0.15	3.37±0.01	4.93±0.64
PLA-150h	1.18±0.10	3.03±0.06	4.24±0.72
PLA-200h	1.08±0.09	2.68±0.05	3.45±0.54
PLA/MCC	6.03±1.70	4.20±0.14	7.10±0.18
PLA/MCC-50h	5.47±0.27	4.13±0.33	5.55±0.36
PLA/MCC-100h	4.69±0.29	4.03±0.16	4.86±0.79
PLA/MCC-150h	3.26±0.30	4.00±0.03	4.47±0.16
PLA/MCC-200h	3.05±0.05	3.08±0.02	3.83±0.33

Changes in the toughness of the PLA and PLA/MCC specimens were investigated by comparing their fracture toughness values in terms of "Critical Stress Intensity Factor (K_{IC})" and "Critical Strain Energy Release Rate (G_{IC})"; as given in Table 3.7 and Figure 3.15. It is known that K_{IC} and G_{IC} values indicate the ability of the specimens to hinder initiation and growth of cracks leading to fracture.

For the neat PLA specimen, Table 3.7 and Figure 3.15 show that, except very slight increases in the values after 50 h accelerated weathering (due to the higher crystallinity), fracture toughness values all decreased with increasing accelerated weathering period. After 200 h total accelerated weathering, decreases in the K_{IC} and G_{IC} values of neat PLA were 22% and 37%, respectively.

For the PLA/MCC biocomposite specimen, decreases in these fracture toughness values started even in the 50 h weathering period. Because, in this specimen, the chemical degradation was not only in the PLA matrix material, but also in the chemical interactions between the matrix and MCC interface, which prevented certain composite toughening mechanisms, such as "crack deflection". In this biocomposite specimen; decreases in K_{IC} and G_{IC} values after total 200 h accelerated weathering were 27% and 46%, respectively.

Finally, in order to reveal benefits of using PLA/MCC biocomposite rather than neat PLA, all the mechanical properties of these two specimens after total 200 h of accelerated weathering period are tabulated in Table 3.8. Note that benefits of using PLA/MCC-200h biocomposite specimen compared to PLA-200h specimen are tabulated in terms of "Δ benefit" (i.e. increase in the values) and also "% benefit" (i.e. percent increase in the values).

Table 3.8 Comparison of the mechanical properties of the PLA-200h and PLA/MCC-200h specimens with benefits of the biocomposite specimen in terms of "Δ benefit" (increase in the values) and "% benefit" (percent increase in the values)

Mechanical Properties	**PLA-200h**	**PLA/MCC-200h**	**Δ benefit**	**% benefit**
Tensile Modulus E (GPa)	2.43	2.61	0.28	11.5
Flexural Modulus E_{Flex} (GPa)	4.12	4.27	0.15	3.6
Tensile Strength σ_{TS} (MPa)	22.80	43.70	20.90	91.7
Flexural Strength σ_{Flex} (MPa)	52.30	75.00	22.70	43.4
Tensile Strain at Break ε_f (%)	1.08	3.05	2.97	275.0
Fracture Toughness K_{IC} (MPa$\sqrt{m}$)	2.68	3.08	0.40	14.9
Fracture Toughness G_{IC} (kJ/m^2)	3.45	3.83	0.38	11.0

It can be concluded that, according to the data given in Table 3.8, for the outdoor applications in terms of mechanical properties, use of PLA with only 3 wt% MCC is extremely beneficial compared to use of neat PLA. For instance, due to the reinforcing actions of MCC, tensile modulus E is more than 11% beneficial, tensile strength σ_{TS} is more than 91% beneficial, strain at break ductility ε_f is more than 2.7 times beneficial, and K_{IC} fracture toughness is 15% more beneficial.

3.2.6 Changes in Thermal Properties

Changes in the thermal properties of the neat PLA and its 3 wt% MCC biocomposite specimens before and after each accelerated weathering period were examined first by DSC analyses and then TGA. Figure 3.16 shows DSC thermograms of each specimen during first heating profile, while Table 3.9 tabulates important transition temperatures: "glass transition, crystallization, melting" (T_g , T_c , T_m), "enthalpies of melting and crystallization" (ΔH_m and ΔH_c), and also "percent crystallinity" (X_C) of the specimens. X_C is determined by using ΔH_m, ΔH_c and $\Delta H_m°$ which is the melting enthalpy of 100% crystalline PLA determined as 93 J/g in the literature [67].

Figure 3.16 and Table 3.9 indicate that there were almost no changes in the glass transition and melting temperatures of the PLA matrix. The most considerable change during weathering periods in the first heating DSC thermograms was the loss of exothermic cold crystallization (ΔH_c) peaks. Due to the very fast cooling rate of injection molding, crystallinity amount (X_C) of the neat PLA and the matrix of the biocomposite specimens before weathering were both around 16%. However, during accelerated weathering, UV irradiation cycles at 70°C lead to more energy and time for the conformational mobility of PLA chains to crystallize even more. Therefore, as seen in Table 3.9, X_C of each specimen during weathering reached to around 30%, i.e. an increase of almost two times.

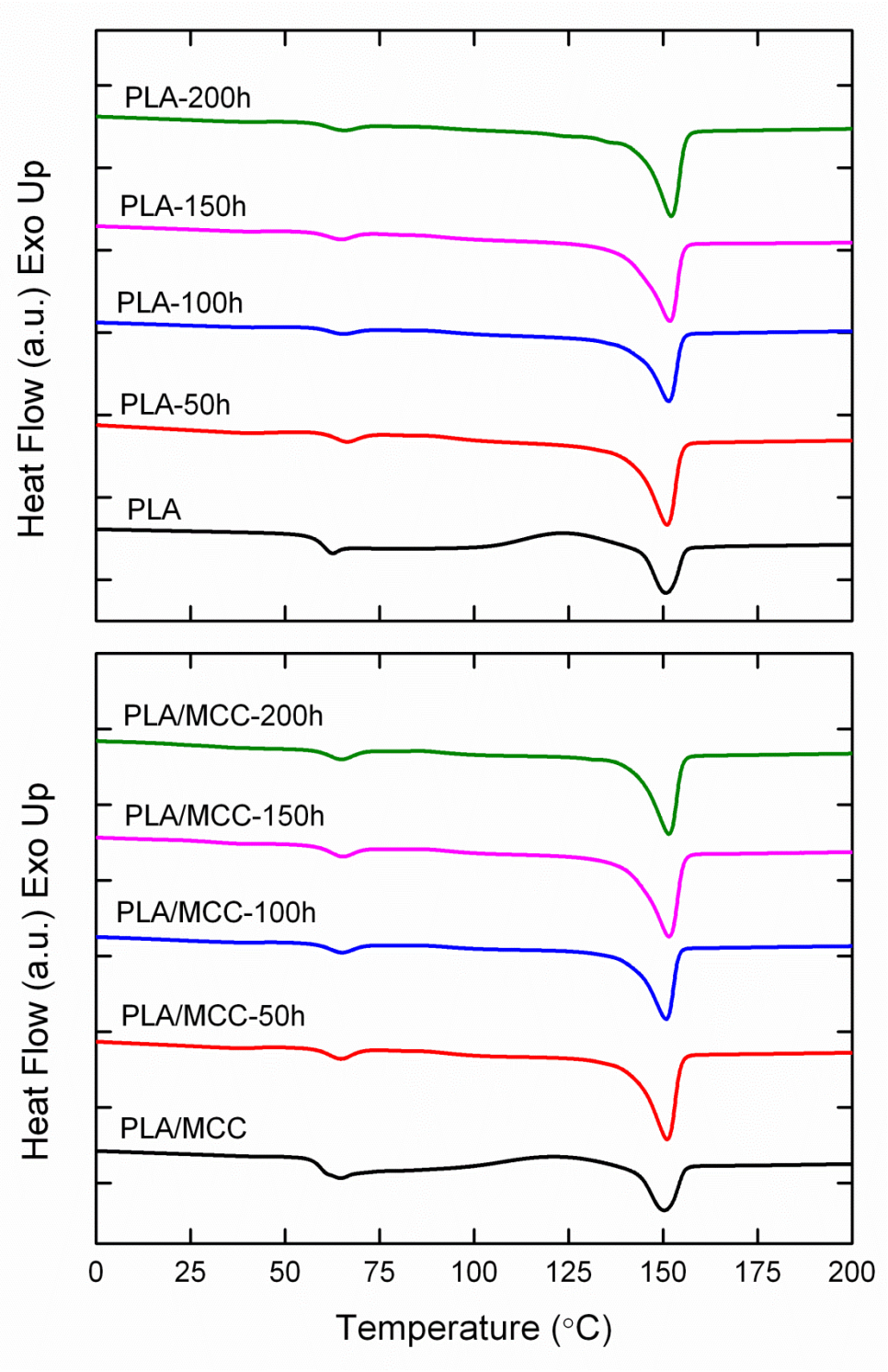

Figure 3.16 First heating DSC thermograms of the neat PLA and its MCC biocomposite specimens before and after each accelerated weathering period

Table 3.9 Transition temperatures (T_g, T_c, T_m), enthalpies (ΔH_m, ΔH_c) and crystallinity percent (X_C) of the neat PLA and its 3 wt% MCC biocomposite specimens before and after each accelerated weathering period obtained during first heating DSC profile

Specimens	T_g **(°C)**	T_c **(°C)**	T_m **(°C)**	ΔH_m **(J/g)**	ΔH_c **(J/g)**	X_C **(%)**
PLA	65	120	151	16.2	1.2	16.1
PLA-50h	66	-	151	30.5	-	32.8
PLA-100h	65	-	151	28.5	-	30.6
PLA-150h	65	-	151	28.2	-	30.3
PLA-200h	65	-	152	27.9	-	30.0
PLA/MCC	65	124	151	15.8	0.9	16.5
PLA/MCC-50h	65	-	151	29.3	-	32.5
PLA/MCC-100h	65	-	151	27.9	-	30.9
PLA/MCC-150h	65	-	152	26.6	-	29.5
PLA/MCC-200h	64	-	152	25.8	-	28.6

Note that another reason for the increased crystallinity during accelerated weathering would be chain scission (i.e. decrease of M_w) actions of photolysis and hydrolysis. Since shorter PLA chains would be more mobile, then the conformational requirement for the ordered crystalline structure would be easier.

Secondly, thermal degradation behavior of the PLA and PLA/MCC biocomposite specimens before and after each accelerated weathering period were investigated by TGA. Figure 3.17 gives thermogravimetric curves, while thermal degradation temperatures determined for each specimen are tabulated in Table 3.10. In this table, $T_{5\%}$, $T_{10\%}$ and $T_{25\%}$ represent thermal degradation temperatures of the specimens at 5, 10 and 25 wt% mass losses, while T_{max} represents the temperature at maximum mass loss.

It is seen in Table 3.10 that there were no significant drops in the thermal degradation temperatures of each specimen during each accelerated weathering period, which was due to the increased crystallinity of the PLA matrix as discussed above. There were only slight decreases (4-5^{o}C) in the onset temperatures of thermal degradation, i.e. in the values of $T_{5\%}$ and $T_{10\%}$.

Table 3.10 Thermal degradation temperatures ($T_{5\%}$, $T_{10\%}$,$T_{25\%}$) of the neat PLA and its 3 wt% MCC biocomposite specimens at 5, 10 and 25 wt% mass losses and the maximum mass loss temperature (T_{max}) before and after each accelerated weathering period

Specimens	$T_{5\%}$ **(°C)**	$T_{10\%}$ **(°C)**	$T_{25\%}$ **(°C)**	T_{max} **(°C)**
PLA	330	340	352	367
PLA-50h	321	333	347	365
PLA-100h	327	339	352	367
PLA-150h	326	339	352	367
PLA-200h	326	338	352	367
PLA/MCC	332	342	353	366
PLA/MCC-50h	329	340	351	365
PLA/MCC-100h	325	337	349	364
PLA/MCC-150h	326	338	351	365
PLA/MCC-200h	326	337	350	364

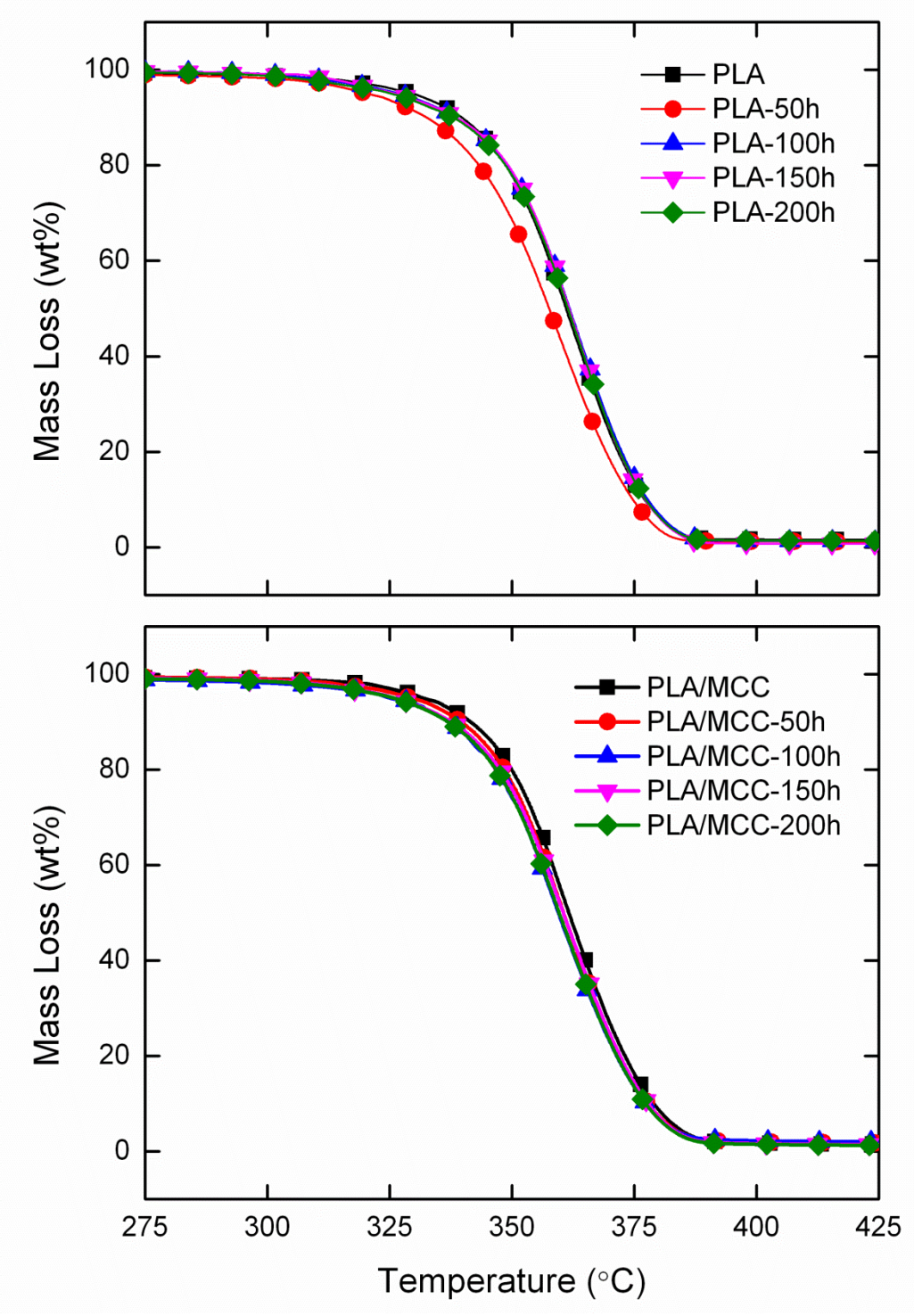

Figure 3.17 Thermogravimetric curves of the neat PLA and its MCC biocomposite specimens before and after each accelerated weathering period

CHAPTER 4

CONCLUSIONS

The main conclusions drawn from the two different parts of this thesis can be summarized as follows:

(i) Effects of MCC Content and MA Compatibilization

- Infrared spectroscopy revealed that the possibility of hydrogen bond formation between the surfaces of cellulose (i.e. hydroxyl groups) and the functional groups of PLA structure (i.e. carbonyl groups of the backbone, hydroxyl and carboxyl groups of the chain terminals) is rather weak. On the other hand, after maleic anhydride (MA) copolymer compatibilization; hydrogen bond type chemical interaction could occur between the hydrogen of the hydroxyl groups of the cellulose surfaces and the oxygen of the carbonyl groups of the MA structure.

- Morphological analyses via SEM indicated that there was no significant distribution problem when microcrystalline cellulose (MCC) content was 1 and 3 wt%, while slight level of agglomeration occurred with 5 and 7 wt% MCC. Use of PLA-g-MA copolymer compatibilization improved not only the distribution uniformity of MCCs, but also decreased the level of their "debonding" and "pulled-out" from the PLA matrix.

- Mechanical tests pointed out that elastic modulus and strength of PLA were not improved by the MCC fillers under tensile loading; only slight improvements can be achieved under bending loading. On the other hand, due to the efficient toughening mechanisms, significant levels of improvements were observed in

the ductility and fracture toughness values. For instance, use of only 3 wt% MCC resulted in 78% increase in %strain at break (ε_f) value and 31% increase in G_{IC} fracture toughness value. After MA compatibilization, these increases were as much as 82% and 55%, respectively.

- Thermal analyses via DSC and TGA indicated that use of MCC resulted in no significant changes in the transition temperatures and thermal degradation temperatures of PLA.

(ii) Effects of Accelerated Weathering

- XRD diffractograms indicated that due to the very fast cooling rate during injection molding, neat PLA and the matrix of MCC biocomposite specimens have mainly amorphous structures. On the other hand, very sharp XRD peaks of the α crystal phase of PLA were observed, indicating the higher crystallinity of the weathered specimens. Because, UV irradiation cycles at 70^{o}C provided sufficient energy and time for the PLA chains to crystallize.

- Photographic images and CIELAB color space parameters showed that changes in the color mainly take place between the unweathered specimens and 50 h accelerated weathering specimens. Neat PLA specimen transformed from colorless (transparent amorphous structure) into white; while glossy creamy color of PLA/MCC turned into pale cream. Further accelerated weathering periods resulted in only very slight changes.

- SLS spectrometry revealed that the level of chain scission in the PLA matrix after each accelerated weathering period was significant. Decrease in the molecular weight (M_w) of the PLA matrix due to the chemical degradation via photolysis, photo-oxidation and hydrolysis was from $3.7x10^5$ down to $0.8x10^5$ after 200 h;

leading to certain level of reductions in the mechanical properties of the specimens.

- Mechanical tests pointed out that higher crystallinity in the weathered specimens prevented drop in the elastic modulus values. However, strength, ductility and toughness of the specimens decreased substantially due to their deteriorated chemical structure with much lower M_w. For instance, at the end of 200 h total accelerated weathering, decreases in the tensile strength of PLA and PLA/MCC were 61% and 24%, respectively; in strain at break ductility 69% and 49%, respectively; and in G_{IC} fracture toughness 37% and 46%, respectively.

- After comparing the mechanical properties of the neat PLA and PLA/MCC biocomposite specimens having 200 h of accelerated weathering, it was concluded that; for the outdoor applications use of PLA/MCC biocomposite (with only 3 wt% MCC) was extremely beneficial compared to using neat PLA. For instance, due to the reinforcing actions of MCC, tensile strength was more than 91% beneficial, while ductility was more than 2.7 times beneficial.

- Except the increased crystallinity during accelerated weathering, DSC and TGA thermal analyses showed that there were no significant changes in the transition temperatures and thermal degradation temperatures of the neat PLA and PLA/MCC biocomposite specimens

REFERENCES

[1] K. M. Nampoothri, N.R. Nair and R. P. John, *"An overview of the recent developments in polylactide (PLA) research"*, **Bioresource Technology**, 101, 8493-8501 (2010)

[2] E. Petinakis, L. Yu, G. Simon and K. Dean, "*Natural Fibre Bio-Composites Incorporating Poly(Lactic Acid). In Fiber Reinforced Composites – The Technology Applied for Concrete Repair"*, **InTech,** 1st ed., pp. 41-59 (2013)

[3] D. Henton, P. Gruber, J. Lunt and J. Randall, *"Polylactic Acid Technology. In Natural Fibers, Biopolymers, and Biocomposites"*, **Florida: CRC Press,** 1st ed., pp. 527-577 (2005)

[4] R. L. Crawford, "*Lignin biodegradation and transformation*", **New York: John Wiley and Sons** (1981)

[5] M. Poletto, V. Pistor and A. J. Zattera, *"Structural Characteristics and Thermal Properties of Native Cellulose. In Cellulose-Fundamentals Aspects"*, **InTech**, 1st ed., pp. 45-68 (2013)

[6] R. J. Moon, A. Martini, J. Nairn, J. Simonsen and J. Youngblood, *"Cellulose nanomaterials review: structure, properties and nanocomposites"*, **Chemical Society Reviews**, 40, 3941-3994 (2011)

[7] A Sarkar and S. Perez, *A database of polysaccharide 3D Structures*, **Centre de Recherches sur les Macromolécules Végétales (CERMAV-CNRS)** (2012)

[8] R. J. Moon, "*McGraw-Hill Yearbook in Science&Technology*", **McGraw-Hill**, 225-228 (2008)

[9] *Genomics: GTL Roadmap: Systems Biology for Energy and Environment*", **U.S. Department of Energy Office of Science**, 204 (2005)

[10] A. Dufresne, *"Nanocellulose: a new ageless bionanomaterial"*, **Materials Today**, 16 (6), 220-227 (2013)

[11] M. E. Malainine, A. Dufresne, D. Dupeyre, M. Mahrouz, R. Vuong and M. R. Vignon, "*Structure and morphology of cladodes and spines of Opuntia ficus-indica. Cellulose extraction and characterisation",* **Carbohydrate Polymers**, 51(1), 77-83 (2003)

[12] R. K. Johnson, A. Zink-Sharp, S. H. Renneckar and W. G. Glasser, *"A new bio-based nanocomposite: fibrillated TEMPO-oxidized celluloses in hydroxypropylcellulose matrix",* **Cellulose,** 16(2), 227–238 (2009)

[13] Y. Habibi, A. L. Goffin, N. Schiltz, E. Duquesne, P. Dubois and A. Dufresne, *"Bionanocomposites based on poly(ε-caprolactone)-grafted cellulose nanocrystals by ring-opening polymerization",* **Journal of Materials Chemistry**, 18, 5002-5010 (2008)

[14] M. N. Angles and A. Dufresne, *"Plasticized Starch/Tunicin Whiskers Nanocomposites. 1. Structural Analysis"*, **Macromolecules**, 33, 8344-8353 (2010)

[15] O. Faruk, A. K. Bledzki, H. P. Fink and M. Sain, *"Biocomposites Reinforced with Natural Fibers: 2000-2010",* **Progress in Polymer Science**, 37, 1552-1596 (2012)

[16] H. Tsuji, Y. Echizen and Y. Nishimura, *"Photodegradation of biodegradable polyesters: A comprehensive study on poly(L-lactide) and poly(ε-caprolactone)",* **Polymer Degradation and Stability,** 91, 1128-1137 (2006)

[17] A.V. Janorkar, A. T. Metters and D. E. Hirt, *"Degradation of poly(L-lactide) films under ultraviolet-induced photografting and sterilization conditions",* **Journal of Applied Polymer Science**, 106, 1042-1047 (2007)

[18] W. L. Tham, B. T. Poh, Z. A. Mohd Ishak and W. S. Chow, *"Water absorption kinetics and hygrothermal aging of poly(lactic acid) containing halloysite nanoclay and maleated rubber"*, **Journal of Polymer and Environments**, 23, 242-250 (2015)

[19] S. Yıldız, B. Karaağaç and G. Ozkoc, *"Toughening of Poly(lactic acid) with Silicone Rubber"*, **Polymer Engineering and Science**, 54(9), 2029-2036 (2014)

[20] C. Zhang, W. Wang, Y. Huang, Y. Pan, L. Jiang, Y. Dan, Y. Luo and Z. Peng, *"Thermal, mechanical and rheological properties of polylactide toughened by epoxidized natural rubber"*, **Materials and Design**, **2013**. 45, 198-205 (2013)

[21] N. Bitinis, R. Verdejo, P. Cassagnau and M.A. Lopez-Manchado, "*Structure and properties of polylactide/natural rubber blends"*, **Materials Chemistry and Physics,** 129, 823-831 (2011)

[22] R. Jaratrotkamjorn, C. Khaokong and V. Tanrattanakul, *"Toughness Enhancement of Poly (lactic acid) by Melt Blending with Natural Rubber"*, **Journal of Applied Polymer Science**, 124, 5027-5036 (2012)

[23] J. J. Han and H. X. Huang, *"Preparation and Characterization of Biodegradable Polylactide/Thermoplastic Polyurethane Elastomer Blends"*, **Journal of Applied Polymer Science,** 120, 3217-3223 (2011)

[24] F. Feng and L. Ye, *"Morphologies and Mechanical Properties of Polylactide/Thermoplastic Polyurethane Elastomer Blends"*, **Journal of Applied Polymer Science,** 119, 2778-2783 (2011)

[25] H. Hong, J.Wei, Y. Yuan, F. P. Chen, J. Wang, X. Qu and C. H. Liu, *"A Novel Composite Coupled Hardness with Flexibleness-Polylactic Acid Toughen with Thermoplastic Polyurethane"*, **Journal of Applied Polymer Science**, 121, 855-861 (2011)

[26] M. Jonoobi, J. Harun, A. P. Mathew and K. Oksman, *"Mechanical properties of cellulose nanofiber (CNF) reinforced polylactic acid (PLA) prepared by twin screw extrusion"*, **Composites Science and Technology,** 70, 1742-1747 (2010)

[27] D. Cho, J. M. Seo, H. S. Lee, C. W. Cho, S. O. Han and W. H.Park, *"Property improvement of natural fiber-reinforced green composites by water treatment"*, **Advanced Composite Materials,** 16(4), 299-314 (2007)

[28] S. Ochi, *"Mechanical properties of kenaf fibers and kenaf/PLA composites"*, **Mechanics of Materials,** 40, 446-452 (2008)

[29] M. S. Huda, L. T. Drzal, A. K. Mohanty and M. Misra, *"Effect of fiber surface-treatments on the properties of laminated biocomposites from poly (lactic acid) (PLA) and kenaf fibers"*, **Composites Science and Technology,** 68, 424-432 (2008)

[30] G. Ben, Y. Kihara, K. Nakamori and Y. Aoki, *"Examination of heat resistant tensile properties and molding conditions of green composites composed of kenaf fibers and PLA resin"*, **Advanced Composite Materials,** 16(4), 361-376 (2007)

[31] K. Oksman, M. Skrifvars and J. F. Selin, *"Natural fibres as reinforcement in polylactic acid (PLA) composites"*, **Composites Science and Technology,** 63, 1317-1324 (2003)

[32] S. Wong, R. A. Shanks and A. Hodzic, *"Mechanical Behaviour and Fracture Toughness of Poly (L-lactic acid) –Natural Fiber Composites Modified with Hyperbranched Polymers"*, **Macromolecular Materials and Engineering,** 289, 447-456 (2004)

[33] E. Bodros, I. Pillin, N. Montrelay and C. Baley, *"Could biopolymers reinforced by randomly scattered flax fibre be used in structural applications?",* **Composites Science and Technology,** 67, 462-470 (2007)

[34] R. A. Shanks, A. Hodzic and D. Ridderhof, *"Composites of Poly(lactic acid) with Flax Fibers Modified by Interstitial Polymerization",* **Journal of Applied Polymer Science,** 101, 3620-3629 (2006)

[35] R. Tokoro, D. M. Vu, K. Okubo, T. Tanaka, T. Fuji and T. Fujiura, *"How to improve mechanical properties of polylactic acid with bamboo fibers"*, **Journal of Material Science**, 43, 775-787 (2008)

[36] K. Okubo, T. Fujii and N. Yamashaita, *"Improvement of Interfacial Adhesion in Bamboo Polymer Composite Enhanced with Micro-Fibrillated Cellulose",* **The Japan Society of Mechanical Engineers International Journal**, 48(4), 199-204 (2005)

[37] S. H. Lee and S. Wang, *"Biodegradable polymers/bamboo fiber biocomposite with bio-based coupling agent",* **Composites: Part A**, 37, 80-91 (2006)

[38] K. Okubo, T. Fujii and E. T. Thostenson, *"Multi-scale hybrid biocomposite: Processing and mechanical characterization of bamboo fiber reinforced PLA with microfibrillated cellulose"*, **Composites: Part A**, 40, 469-475 (2009)

[39] R. Hu and J. K. Lim, *"Fabrication and Mechanical Properties of Completely Biodegradable Hemp Fiber Reinforced Polylactic Acid Composites"*, **Journal of Composite Materials**, 41(13), 1655-1669 (2007)

[40] R. Masirek, Z. Kulinski, D. Chionna, E. Piorkowska and M. Pracella, *"Composites of Poly(L-lactide) with Hemp Fibers: Morphology and Thermal and Mechanical Properties",* **Journal of Applied Polymer Science,** 105, 255-268 (2007)

[41] O .A. Khondker, U. S. Ishiaku, A. Nakai and H. Hamada, *"A novel processing technique for thermoplastic manufacturing of unidirectional composites reinforced with jute yarns"*, **Composites: Part A**, 37, 2274-2284 (2006)

[42] J. K. Pandey, A. N. Nakagaito and H. Takagi, *"Fabrication and Applications of Cellulose Nanaoparticle-Based Polymer Composites",* **Polymer Engineering and Science.** 2013.

[43] A. P. Mathew, K. Oksman and M. Sain, *"Mechanical Properties of Biodegradable Composites from Poly Lactic Acid (PLA) and Microcrystalline Cellulose (MCC)"*, **Journal of Applied Polymer Science** 97, 2014-2025 (2005)

[44] M. K. Mohamad Haafiz, A. Hassan, Z. Zakaria, I. M. Inuwa, M.S. Islam and M. Jawaid, *"Properties of polylactic acid composites reinforced with oil palm biomass microcrystalline cellulose",* **Carbohydrate Polymers,** 98, 139-145 (2013)

[45] L. Xiao, Y. Mai, F. He, L. Yu, L. Zhang, H. Tang and G. Yang, *"Bio-based green composites with high performance from poly(lactic acid) and surface-modified microcrystalline cellulose"*, **Journal of Materials Chemistry,** 22, 15732-15739 (2012)

[46] T. Mukherjee, M. Sani, N. Kao, R. K. Gupta, N. Quazi and S. Bhattacharya, *"Improved dispersion of cellulose microcrystals in polylactic acid (PLA) based composites applying surface acetylation"*, **Chemical Engineering Science,** 101, 655-662 (2013)

[47] P. Stloukal, V. Verney, S. Commereuc, J. Rychly, L. Matisova-Rychla, V. Pis and M. Koutny, *"Assessment of the interrelation between photooxidation and biodegradation of selected polyesters after artificial weathering"*, **Chemosphere,** 88, 1214-1219 (2012)

[48] A. Copinet, C. Bertrand, S. Govindin, V. Coma and Y. Couturier, *"Effects of ultraviolet light (315 nm), temperature and relative humidity on the degradation of polylactic acid plastic films"*, **Chemosphere,** 55, 763-773 (2004)

[49] S. Sztajnowski, I. Krucinska, K. Sulak, M. Puchalski, H. Wrzosek and J. Bilska, *"Effects of the artificial weathering of biodegradable spun-bonded PLA nonwovens in respect to their application in agriculture"*, **Fibres & Textiles in Eastern Europe**, 20, 6B(96), 89-95 (2012)

[50] H. Shinzawa, M. Nishida, T. Tanaka and W. Kanematsu, *"Accelerated weathering-induced degradation of poly(lactic acid) fiber studied by near-infrared (NIR) hyperspectral imaging"*, **Applied Spectroscopy**, 66, 470-4 (2012)

[51] M. Deroine, A. L. Duigou, Y. M. Corre, Y. M. L. Gac, P. Davies, G. Cesar and S. Bruzaud, *"Accelerated aging of polylactide in aqueous environments: Comparative study between distilled water and seawater"*, **Polymer Degradation and Stability**, 108, 319-329 (2014)

[52] E. Hablot, S. Dharmalingam, D. G. Hayes, L. C. Wadsworth, C. Blazy and R. Narayan, *"Effect of simulated weathering on physicochemical properties and inherent biodegradation of PLA/PHA nonowen mulches"*, **Journal of Polymer and Environments**, 22, 417-429 (2014)

[53] I. Moura, G. Botelho and A. V. Machado, *"Characteriation of EVA/PLA blends when exposed to different environments"*, **Journal of Polymer and Environments**, 22, 148-157 (2014)

[54] I. Spiridon, O. M. Paduraru, M. F. Zaltariov and R. N. Darie, *"Influence of keratin on polylactic acid/chitosan composite properties. Behavior upon accelerated weathering"*, **Industrial & Engineering Chemistry Research**, 52, 9822-33 (2013)

[55] W. Grigsby, J. Bridson, C. Lomas and J. A. Elliot, *"Esterification of condensed tannins and their impact on the properties of poly(lactic acid)"*, **Polymers**, 5, 344-60 (2013)

[56] R. Acioli-Moura and S. X. Sun, *"Thermal degradation and physical aging of poly(lactic acid) and its blends with starch"*, **Polymer Engineering and Science**, 48(4), 829-836 (2008)

[57] G. H. Yew, W. S. Chow, Z. A. Mohd Ishak and A. M. Mohd Yusof, *"Natural weathering of poly (lactic acid): Effects of rice starch and epoxidized natural rubber"*, **Journal of Elastomers and Plastics**, 41, 369-82 (2009)

[58] B. S. Ndazi and S. Karlsson, *"Characterization of hydrolytic degradation of polylactic acid/rice hulls biocomposites in water at different temperatures"*, **eXPRESS Polymer Letters**, 5, 119-31 (2011)

[59] I. Spiridion, K. Leluk, A. M. Resmerita and R. N. Darie, *"Evaluation of PLA-lignin bioplastics properties before and after accelerated weathering"*, **Composites: Part B**, 69, 342-349 (2015)

[60] M. S. Islam, K. L. Pickering and N. J. Foreman, *"Influence of accelerated ageing on the physico-mechanical properties of alkali-treated industrial hemp fibre reinforced poly(lactic acid) (PLA) biocomposites"*, **Polymer Degradation and Stability**, 95, 59-65 (2010)

[61] R. N. Darie, R. Bodirlau, C. A. Teaca, J. Macyszyn, M. Kozlowski and I. Spiridon, *"Influence of accelerated weathering on the properties of polypropylene/polylactic acid/eucalyptus wood biocomposites"*, **International Journal of Polymer Analysis and Characterization**, 18, 315-327 (2013)

[62] C. Kaynak and Y. Meyva, *"Use of maleic anhydride compatibilization to improve toughness and other properties of polylactide blended with thermoplastic elastomers"*, **Polymers for Advanced Technologies,** 25, 1622-1632 (2014)

[63] G. H. Yew, A. M. Mohd Yusof, Z. A. Mohd Ishak and U. S. Ishiaku, *"Water absorption and enzymatic degradation of poly(lactic acid)/rice starch composites"*, **Polymer Degradation and Stability,** 90, 488-500 (2005)

[64] P. Qu, Y. Gao, G. F. Wu and L. P. Zhang, *"Nanocomposites of Poly(lactic acid) Reinforced with Cellulose Nanofibrils"*, **Bioresources,** 5(3), 1811-1823 (2010)

[65] S.W. Hwang, S. B. Lee, C. K. Lee, J. Y. Lee, J. K. Shim, S. E. M. Selke, H. Soto-Valdez, L. Matuana, M. Rubino and R. Auras, *"Grafting of maleic anhydride on poly(L-lactic acid) Effects of physical and mechanical properties"*, **Polymer Testing,** 31, 333-344 (2012)

[66] H. F. Li, H. Li, X. Zhong, X. Li, M. E. Gibril, Y. Zhang, K. Han and M. Yu, *"Study on the chemical modification of Cellulose in Ionic Liquid with Maleic Anhydride"*, ***Advanced Materials Research*****,** 581-582, 287-291 (2012)

[67] H. Osman, H. Ismail and M. Mustapha, *"Effects of Maleic Anhydride Polypropylene on Tensile, Water Absorption, and Morphological Properties of Recycled Newspaper Filled Polypropylene/Natural Rubber Composites"*, **Journal of Composite Materials,** 44, 1477-1491 (2010)

[68] E. W. Fischer, H. J. Sterzel and G. Wegner, *"Investigation of structure of solution grown crystals of lactide copolymers by means of chemical reactions"*, **Colloid and Polymer Science,** 251, 980-990 (1973)

[69] J. Zhang, K. Tashiro, H. Tsuji and A. J. Domb, *"Disorder-to-disorder phase transition and multiple melting behavior of poly(l-lactide) investigated by simultaneous measurements of WAXD and DSC"*, **Macromolecules**, 41, 1352-1357 (2008)

[70] J. Zhang, K. Tashiro, A. J. Domb and H. Tsuji, *"Confirmation of disorder a form of poly(l-lactic acid) by X-ray fiber pattern and polarized IR/Raman spectra measured for uniaxially-oriented samples"*, **Macromolecular Symposia**, 242, 274-278 (2006)

[71] I. Kaygusuz and C. Kaynak, *"Influences of Halloysite Nanotubes on Crystallisation Behaviour of Polylactide"*, **Plastics, Rubber and Composites: Macromolecular Engineering**, 44 (2), 41-49 (2015)